NASA CR-134540

HIGH PRESSURE COMBUSTION OF LIQUID FUELS

by

G. S. Canada

Mechanical Engineering Department
The Pennsylvania State University
University Park, Pennsylvania

prepared for

NATIONAL AERONAUTICS AND SPACE ADMINISTRATION

NASA Lewis Research Center
Contract NGR 39-009-077
Richard J. Priem, Program Manager and Technical Monitor

1. Report No. NASA CR-134540	2. Government Accession No.	3. Recipient's Catalog No.
4. Title and Subtitle High Pressure Combustion of Liquid Fuels		5. Report Date January, 1974 6. Performing Organization Code
7. Author(s) G. S. Canada		8. Performing Organization Report No.
9. Performing Organization Name and Address Mechanical Engineering Department The Pennsylvania State University University Park, Pennsylvania 16802		10. Work Unit No. 11. Contract or Grant No. NGR 39-009-077
12. Sponsoring Agency Name and Address National Aeronautics and Space Administration Washington, D.C. 20546		13. Type of Report and Period Covered Contractor Report 14. Sponsoring Agency Code

15. Supplementary Notes

Project Manager, Richard J. Priem, Chemical Propulsion Division
NASA Lewis Research Center, Cleveland, Ohio

16. Abstract

Measurements were made of the burning rates and liquid surface temperatures for a number of alcohol and n-paraffin fuels under natural and forced convection conditions. Porous spheres ranging in size from 0.64-1.9 cm O.D. were employed to simulate the fuel droplets. The natural convection cold gas tests considered the combustion in air of methanol, ethanol, propanol-1, n-pentane, n-heptane, and n-decane droplets at pressures up to 78 atmospheres. The pressure levels of the natural convection tests were high enough so that near critical combustion was observed for methanol and ethanol vaporization rates and liquid surface temperature measurements were made of droplets burning in a simulated combustion chamber environment. Ambient oxygen molar concentrations included 13%, 9.5% and pure evaporation.

Fuels used in the forced convection atmospheric tests included those listed above for the natural convection tests. The ambient gas temperature ranged from 600 to 1500°K and the Reynolds number varied from 30 to 300. The high pressure forced convection tests employed ethanol and n-heptane as fuels over a pressure range of one to 40 atmospheres. The ambient gas temperature was 1145°K for the two combustion cases and 1255°K for the evaporation case. The Reynolds number range was from 70 to 672.

Due to the high pressures of the natural and forced convection tests, the phase equilibrium models of the analysis included both low and high pressure versions, with the latter allowing for real gas effects and the solubility of the combustion gases in the liquid phase. The burning rate predictions of the various theories were similar and in fair agreement with the data. The greatest differences between the two theories lies in the predicted critical burning conditions. The low pressure theory predicts a significantly lower pressure for critical combustion, at a given ambient oxygen concentration, than the high pressure theory. Furthermore, the low pressure theory predicted higher liquid surface temperatures at all pressures for critical combustion than the high pressure theory.

17. Key Words (Suggested by Author(s))	18. Distribution Statement
Liquid fuel combustion High pressure combustion	Unclassified - Unlimited

19. Security Classif. (of this report)	20. Security Classif. (of this page)	21. No. of Pages	22. Price*
Unclassified	Unclassified	146	$3.00

* For sale by the National Technical Information Service, Springfield, Virginia 22151

FOREWARD

This report summarizes a portion of the work done on NASA Grant NGR 39-009-077. The study was under the direction of G. M. Faeth, Associate Professor of Mechanical Engineering.

TABLE OF CONTENTS

Page

Page

Page

LIST OF TABLES (CONTINUED)

LIST OF FIGURES

LIST OF FIGURES (CONTINUED)

NOMENCLATURE

Symbol	Description
a'	Weighted specific heat parameters, Equation (B.15)
a°	Parameter, Equation (2.52)
a°_{ij}	Parameter, Equation (C.4)
a_d	Droplet absorptivity
A_i	Specific heat constant, Equation (2.21)
$\bar{A}$	Parameter, Equation (C.15)
b'	Weighted specific heat parameter, Equation (B.16)
b°	Parameter, Equation (2.52)
b°_i	Parameter, Equation (C.6)
B_i	Specific heat constant, Equation (2.21)
$\bar{B}$	Parameter, Equation (C.16)
C	Molar density
$\bar{C}$	Parameter, Equation (C.17)
C_p	Specific heat
$C_1 \ldots C_{24}$	Constants in property equations, Appendix D
D	Binary diffusivity
$\bar{D}$	Parameter, Equation (C.18)
d	Sphere diameter
e_f	Emissivity
f	Fugacity
g	Acceleration due to gravity
h	Enthalpy
H_i	Heat of vaporization of species i
k_{ij}	Binary interaction parameter

L	Enthalpy rise of vaporization
$\dot{m}$	Mass burning rate
M	Molecular weight
$\dot{n}$	Molar flow rate in the inner region
$\dot{n}_f$	Molar flow rate in the outer region
N_i	Molar flux of species i per unit area
P	Pressure
P_c	Critical pressure of pure fuel
P_{cij}	Parameter, Equation (C.7)
Pr	Prandtl number ($Pr = Cp\ \mu/\lambda$)
P_R	Reduced pressure ($P_r = P/Pc$)
P_v	Vapor pressure
Q_ℓ	Standard heat of reaction at T_ℓ
$\dot{Q}_R$	Radiant heat flux
r	Radial distance
R	Universal gas constant
Re	Reynolds number ($Re = \rho V_\infty d/\mu$)
Sc	Schmidt number ($\mu/\rho\mathcal{D}$)
T	Temperature
T_c	Critical temperature of pure fuel
T_{cij}	Parameter, Equation (C.10)
Tr	Reduced temperature ($T_R = T/T_c$)
V	Molar volume
$\bar{V}$	Partial molar volume
V_{cij}	Parameter, Equation (C.8)
V_∞	Velocity
W_i	Chemical symbol for species i

X	Mole fraction
Z	Compressibility factor
Z_{cij}	Parameter, Equation (C.9)
α	Stoichiometry parameter, Equation (2.10)
γ	Parameter, Equation (2.35)
ε	Mole flux fraction
η, η'	Parameters, Equations (2.28, 2.36)
θ	Parameter, Equation (D.11)
λ	Thermal conductivity
μ	Viscosity
ν	Kinematic viscosity
ξ	Parameter, Equation (2.26)
ρ	Mass density
σ	Stefan-Boltzmann constant
ϕ, ϕ'	Parameters, Equations (2.24, 2.33)
χ	Parameter, Equation (2.22)
ω	Accentric factor
Ω_{ai}	Dimensionless constant, Equation (C.4)
Ω_{ai}	Dimensionless constant, Equation (C.6)

Subscripts

A	Region A
B	Region B
f	Flame surface
F	Fuel vapor
i	Inner region
ℓ	Conditions at liquid surface

N	Oxidizer component
o	Outer region
O	Oxygen species
P	Product species
1	Fuel component
∞	Ambient conditions
+	Outer side of a surface
-	Inner side of a surface

Superscripts

L	Liquid
V	Vapor

SUMMARY

This report discusses activities under NASA Contract NGR 39-009-077, involving a theoretical and experimental study of high pressure fuel droplet combustion. The investigation was divided into two phases, as follows:

1. Droplet combustion at elevated pressures (1-100 atm) in air maintained at room temperature. The droplet was in a natural convection environment with Grashoff numbers in the range 10^4-10^8 (based on approach conditions.)
2. Droplet evaporation and combustion at elevated pressures (1-40 atm) in a high temperature (600-1500° K) flowing combustion gas environment which simulates actual combustion chamber conditions. The ambient oxygen concentration of the droplet was varied in the range 0-13% (molar) with forced convection evaluated over the Reynolds number range 10-800 (based on approach conditions).

Porous spheres were used to simulate fuel droplets in order to determine burning rates and liquid surface temperatures under steady conditions. The fuels considered in the tests included methanol, ethanol, propanol-1, n-pentane, n-heptane and n-decane.

The theory used for comparison with the experimental results was based upon an extension of the variable property, variable specific heat model of droplet combustion proposed by Goldsmith and Penner. This approach has the advantage of postulating realistic property variations for the fuels considered in the tests. Constant specific heat and constant property versions of the theory were also compared with the experimental results. The effect of natural or forced convection was

treated by means of a multiplicative correction based upon the Grashoff or Reynolds number evaluated at approach conditions. Phase equilibrium at the liquid surface was determined by both the conventional approach typically used at low pressures, as well as a high pressure version which allows for phenomena which become important as the thermodynamic critical point of the liquid phase is approached (solubility of ambient gases in the liquid phase, etc.). The phase equilibrium calculations of the high pressure theory employed a modified Redlick-Kwong equation of state with mixing rules for multicomponent mixtures.

The conclusions of the study are as follows:

1. Both the low and high pressure versions of the theories gave essentially the same burning rate predictions over the range of pressures for which they overlap. The greatest difference between the theories is that the low pressure model predicts a significantly lower pressure for the liquid surface to reach its thermodynamic critical point for given ambient conditions.
2. The various property treatments; variable property-variable specific heat, variable property-constant specific heat and constant property models gave similar predictions as long as any assumed constant property was evaluated at an average condition.
3. Discrepancies between theoretical and experimental burning rates were similar to those encountered for atmospheric pressure tests. The theories modelled the effect of variations in temperature, pressure, ambient oxygen concentration, droplet dia-

meter and convection conditions reasonably well. The representation of the effect of fuel type was less satisfactory with the theory giving good predictions in some cases and errors up to 50% in other instances.

4. At pressures up to 20 atm, liquid surface temperatures were in good agreement with the low pressure version of the theory. At higher pressures the surface temperatures tended to approach the surface temperature predictions of the high pressure theory in most instances.

5. The experiments gave evidence of the liquid surface reaching its thermodynamic critical point for the combustion of methanol and ethanol at pressures in the range 80-100 atm. This pressure range was in agreement with the critical combustion predictions of both theories.

6. A major advantage of the high pressure model is that it provides a more satisfying physical description of conditions at the liquid surface as the thermodynamic critical point is approached. With the high pressure model, the composition of the gas and liquid phases approach one another with increasing pressure, becoming identical at the critical point. This provides a smooth transition into the compressed gas combustion regime at high ambient pressures, rather than the artificial composition discontinuity that is implicit in the low pressure model near the critical combustion condition.

CHAPTER I

INTRODUCTION

1.1 General Statement of the Problem

Many important combustion devices such as the combustion chamber of diesel engines, gas turbines, liquid propellant rocket engines, and industrial furnaces involve the introduction of the liquid fuel into the combustion space in the form of a spray. The heterogeneous combustion of a liquid fuel spray is a complex phenomenon and a realistic description of spray combustion requires a knowledge of the mechanism of evaporation and combustion of individual fuel droplets. Therefore, an understanding of the behavior of fuel droplets in a hot, oxidizing gas is useful to the rational design of efficient combustion systems for these applications.

The combustion of droplets has been the subject of numerous investigations, with particular emphasis in recent years on high-pressure combustion. High pressure combustion, especially in the vicinity of the critical point of the fuel, gives rise to a number of problems not encountered with processes at low pressures. If the critical temperature of the droplet is approached, phenomena such as fuel stripping from the drop may become important due to reduced surface tension. If stripping is absent, the droplet becomes a puff of gas when the critical condition is exceeded and burns in an unsteady diffusion flame. Any of these instances give rise to conditions where the droplet combustion process is no longer vaporization controlled, as at low pressures.

A number of models have been developed to describe the combustion process at high pressures, but the experimental investigations to date have not considered a wide enough range of conditions to provide a stringent test of high pressure theoretical predictions.

In addition, most of the high pressure research to date has focussed on a quasi-steady analysis of droplet combustion in essentially a quiescent gas environment. In studies that considered the effect of convection, the ambient gas temperatures were generally not high enough to realistically simulate actual high pressure combustion. More importantly, previous studies of high pressure droplet combustion did not provide steady state burning rate data, giving rise to uncertainties in the interpretation of the data. The present investigation of high pressure droplet combustion under free and forced convection conditions was undertaken to provide fundamental data and further insight into this problem, which is of great practical importance. The investigation concentrated on temperature and pressure levels high enough to simulate an actual high pressure combustion process.

1.2 Previous Related Studies

1.2.1 Experimental Techniques in Droplet Vaporization

Past experimental investigations on the vaporization and combustion of liquids have employed three basic techniques. These include the suspended droplet technique, falling droplet technique, and porous sphere technique.

The suspended droplet technique may be used to obtain the rate of change of droplet diameter or size as a function of time. The fuel droplets are usually suspended on stationary quartz fibers and the rate of combustion after ignition is observed photographically. The suspended droplet technique yields accurate results for the variation of the droplet diameter as a function of time. Some of the earliest experimental investigations of droplet combustion utilized this technique. [1, 2, 3, 4]

In the falling drop method, small freely falling fuel droplets are ignited and observed during burning, usually through photographic methods. This technique is particularly suitable for studies of very small droplets. In practice a single droplet or low density cloud of droplets is produced by a suitable generator, such as an electrostatic generator [5], ultrasonic atomiser, vibrating steel tube [6], or spinning disc atomiser [2, 7]. Usually, the droplets are allowed to fall under gravitational forces or are projected into a suitable hot environment where self-ignition occurs.

The porous or supporting sphere technique provides a method of studying the steady-state combustion of simulated droplet burning. The supporting sphere technique consists of supplying liquid fuel to the surface of a supporting, inert, solid sphere at a rate equal to its rate of combustion. Spalding [8] was one of the first investigators to use this method. In porous sphere studies the fuel is supplied internally to a stationary, non-reactive, porous sphere at a steady rate which is just sufficient to maintain a liquid film on the surface of the sphere during burning.

The porous sphere method is convenient in that different diameter support spheres may be used for a variety of experiments involving the steady-state combustion of fuel droplets. Most importantly, of the three basic droplet burning techniques only the porous sphere method is a truly steady-state process.

1.2.2 Droplet Evaporation

1.2.2.1 Low Pressure Investigations

Previous investigations on pure droplet evaporation mainly employed the free droplet and porous sphere techniques. Ingebo [9] considered nine pure liquids and a range of air-stream pressure, temperature, and velocity conditions in evaporation studies. He found that the droplet surface temperatures were approximately equal to the wet-bulb temperatures.

Investigations by Ranz and Marshall [10] confirmed the analogy between heat and mass transfer at low Reynolds number, and verified the simple expression for the Nusselt number at zero Reynolds number. Based upon their experimental findings, Ranz and Marshall developed a general correlation for the vaporization of spherical particles.

Studies by Borman, et al., [11] considered hexane, decane, and hexadecane drops vaporizing in air at various temperatures. The pressure range was from one to five atmospheres. Their experimental measurements of droplet temperatures and mass transfer rates compared favorably with theoretical predictions over the pressure and temperature range investigated.

1.2.2.2 High Pressure Investigations

Torda and Matlosz [12] performed a series of high-pressure vaporization experiments for n-pentane droplets. In these experiments, droplets were injected into and supported in a heated and pressurized test chamber containing nitrogen. The pressure range for the data was 200-1400 psia at a fixed temperature of 390°F. The flow field environment was essentially due to free convection. The attempts of these investigators to compare their theory with the experimental results were not particularly successful. These experiments involved pressures that were in excess of the critical pressures of the pure fuels under test.

The investigations by Savery and Borman [13] considered the histories of vaporizing n-heptane and Freon-13 droplets suspended in a heated air stream. The temperature range for their tests was between 100°F and 300°F and the pressure range was from 1.5 to 100 atmospheres. Comparisons were made between the measured equilibrium temperatures and vaporization rates, and analogous values predicted from a quasi-steady theory uncorrected for high pressure properties. A corrected version which included the effects of ambient gas solubility and other high pressure corrections to the thermodynamic properties was also considered in the comparison. Some of the conclusions of this investigation are:

1. The corrected theory gave good agreement with measured equilibrium temperatures and predicted vaporization rates (within 25% of the measured values) at low ambient temperatures.

2. The uncorrected theory gave good predictions of droplet equilibrium temperatures but underestimated the vaporization rates by as much as 80% at high pressures.
3. The mass transfer rates predicted by the corrected theory agreed to within 35% of the measured value at reduced pressures below 1.5. The predicted mass transfer rates become progressively lower as the pressure increases.
4. At moderate ambient gas temperatures and high pressures, the corrected and uncorrected theory predictions were lower by 10-15°F than the measured equilibrium temperatures.

More recently, Tarifa [14] considered theoretically the deviations from the quasi-steady theories for subcritical and supercritical droplet vaporization and combustion. He concludes that the corrections to the quasi-steady theory are of the order of the square root of the gas density to the liquid density.

Matlosz, Leipziger, and Torda [15] conducted an experimental and analytical study of the evaporation of n-hexane droplets in a nitrogen and argon gas environments. The ambient gas temperature was 540°K and the pressure range was from 6.8 to 102 atmospheres. In agreement with other investigators they found that the effects of non-ideal behavior of the gas phase was important at high pressures.

In a theoretical analysis of the vaporization (with and without combustion) of dodecane droplets in heated air at high pressures, Rosner [16] demonstrated certain inadequacies of the quasi-steady approximation. He concluded that the evaporation process for

isolated fuel droplet just below its critical temperature cannot be reasonably treated as quasi-steady even in cases where the boundary conditions for temperatures and compositions are strictly steady.

1.2.3 Combustion Under Natural Convection Conditions

1.2.3.1 Low Pressure Investigations

The earliest droplet combustion studies concentrated on the steady burning period of the droplet. Analytical studies by Godsave, Spalding, Hottel, et al., [1, 7, 8] gave predictions of burning rates that were in reasonable agreement with experimental results conducted at atmospheric pressure. [2, 3, 4, 7, 8] These studies were based upon a quasi-steady analysis that assumed:

1. Steady state conditions for fixed droplet sizes.
2. Temperature and concentration profiles in the gas phase adjust instantaneously to changes in the boundary condition at the droplet surface.
3. The regression rate or radial interface velocity of the droplet surface is small compared to the velocity of the vapor leaving the liquid surface.
4. Reaction rates at the flame zone are fast compared to the rates at which reactants are transported to the reaction zone.
5. Fuel and oxidizer combine in stoichiometric proportions at the flame surface.

In Godsave's analysis the temperature dependence of the physical properties was neglected and constant average values were employed. Goldsmith and Penner [17] eliminated some of the restrictive

assumptions of Godsave's analysis and extended and generalized his work through a variable property model for the steady burning of a fuel droplet in an oxidizing environment. This model included the use of integrated forms for the equations of conservation of mass and the conservation of energy. In addition, the model included the consideration of the temperature dependence of the fuel thermal conductivity and specific heat. While providing a reasonable correlation of Godsave's experimental results, Goldsmith and Penner were also able to formulate explicit expressions for the combustion temperature and the flame radius.

The experiments conducted by Goldsmith [3] to test the theory of the Goldsmith and Penner model considered the combustion of n-heptane and ethyl alcohol droplets in various ambient oxygen concentrations. The theory predicted flame temperatures much higher than those found experimentally due to the neglect of dissociation. The experimental burning rates compared reasonably well with the theory. The experimental range of this study, however, was too limited with regard to fuel types, pressure levels, etc. to provide a stringent test of the theory.

Bolt and Boyle [18] obtained the burning rate coefficients for droplets burning in a spray but made no measurements of the ambient conditions such as temperature and oxygen concentrations. Wood, et al., [5] passed droplets through a methane flame and obtained burning rate coefficients at 1500°C for a series of fuels under various oxygen concentrations, using various drop sizes. They found that the burning rate coefficients varied with initial droplet radius and that radiative heat transfer had little effect on the results.

Faeth and Lazar [19] considered a wide range of bipropellant fuel droplets burning in ... ustion gas environment. This study considered an ambient temp... re range of 1660-2530°K and oxygen mass fractions of 0-.38. Som... their findings included the observation that all theoretical m... progressively overestimate the burnin, rate as the molecular w... the fuel is increased. They attributed this failure to ... composition in the region between the droplet surface and the ...dation zone. They found that the simplified diffusion flame theory gave reasonable agreement with experimental results.

Additional studies of low and high pressure convection testing may be found in a number of recent reviews [20, 21] on the combustion of liquid fuels.

1.2.3.2 High Pressure Investigations

While there has been a large number of combustion studies at atmospheric or relatively low pressures, there have been relatively few investigations at high pressures. The available high pressure studies have shown that certain assumptions of the quasi-steady analysis become questionable at very high pres...ures and particularly near the critical point. Williams [22] and Brzustowski [23] point out that the assumptions of negligible finite regression rates of the droplet surface and neglecting the transient adjustments of the boundary layer around the droplet to changing conditions at the droplet surface become suspect as the droplet liquid density approaches that of the gas mixture.

The experiments of Hall and Diedrichsen [2] considered the combustion of suspended droplets in air at pressures up to 20 atm. Since this data is presented as total droplet lifetime (which includes both heat-up and quasi-steady burning), the interpretation of the results is greatly complicated.

Brzustowski and Natarajan [24] considered the combustion of aniline droplets at high pressures in a convective flow field. They considered in their investigation a two-film model consisting of a spherical inner stagnant film through which diffusion and conduction occur and an outer film through which mass transfer occurs. The increase in burning rates with pressure which they observed can be explained by the effect of natural convection on the combustion process. Spalding [25] and Rosner [26] have considered the supercritical combustion of a fuel drop as a problem involving the transient diffusion of a dense gas pocket containing pure fuel vapor, under conditions of no convection. Spalding replaces the fuel droplet by a point source of fuel vapor, while Rosner considers the fuel vapor to be uniformly distributed in a finite-size spherical region. Neither of these theories, however, attempts to describe the details of the processes occurring in the immediate vicinity of the fuel droplet, nor do they define the lower limit of pressure at which they are applicable.

In a theoretical investigation of the transient combustion of a liquid fuel droplet which instantaneously reaches its thermodynamic critical state on introduction into a supercritical, hot, stagnant oxidizing environment, Polymeropoulos and Peskin [26] found that the total combustion time decreased with increasing ambient temperatures

ambient oxygen concentration. They also found that the flame zone is larger than that calculated using models which neglected the convection velocity.

Chervinsky [27] considered the combustion of liquid droplets under supercritical conditions using an analysis in the Von Mises-Prandtl plane. He reached essentially the same conclusions as in other studies [24, 28, 29] but also found that the burning time is dependent upon a temperature term, so that in the case of highly exothermic reactions, the burning times are less than those predicted by other theories.

1.2.4 Combustion Under Forced Convection Conditions

1.2.4.1 Low Pressure Investigations

Droplets burn in envelope flames in low velocity gas streams whereby the flame envelopes the leading half of the sphere. As the velocity increases the boundary layer thickness decreases and mass transfer rates increase, but above a critical stream velocity, termed the extinction or transition velocity, the flame on the leading half of the sphere is extinguished and a small flame is stabilized in the wake of the droplet. [21, 30, 31] Udelson [32] indicates a third regime of combustion in which the flame stabilizes in the boundary layer at the sides of the liquid sphere.

Several investigations [28, 33, 34] have focussed on the variation of the extinction velocity (U_c) with droplet diameter (d_ℓ). Recent studies [34, 35] have indicated experimentally that the extinction velocity is proportional to the square root of the droplet diameter.

There have been few theoretical or experimental investigations of the structure of droplet flames burning under different combustion conditions in forced convection. Gollahalli and Brzustowski [35] found that the burning rate decreases by a factor of three when the envelope flame is transformed into a wake flame at a critical approach velocity and that envelope flames radiate much more than wake flames.

Investigations by Sjorgen [34] and Michael and El-Wakil [36] have indicated that in the case of hydrocarbon fuels the formation of soot in the wake of the flame may be a significant source of soot in spray combustion. Furthermore, this condition is dependent upon whether the droplet burns with an envelope or with a wake flame.

1.2.4.2 High Pressure Investigations

There have been very few theoretical and experimental investigations of high pressure, forced convection droplet combustion. Several studies [37, 38] have focussed upon the projecting of droplets into hot oxidizing environments. Gollahalli [39] studied the flame structure in the wakes of small porous spheres burning under forced convection conditions. The pressure range was from 1 to 30 atmospheres and the ambient air temperature was 300°K. He found that increasing the ambient pressure increases the soot concentration and the size of soot particles. Also the burning rate decreased by a factor of three when the envelope flame was transformed to a wake flame.

Sami and Ogasawara [40] considered the combustion of fuel droplets at pressures up to 16 atmospheres. The ambient air temperature was quite low ranging from 25 to 600°C. Their findings

included the observations that variations of ambient air temperature had little effect on the burning rate and that the burning rate decreased markedly when the air velocity exceeded the extinction velocity.

1.2.5 High Pressure Phase Equilibrium Investigations

Manrique [41] conducted a theoretical study of the vaporization of carbon dioxide droplets in a high pressure nitrogen atmosphere. His theoretical model considered both steady state and transient vaporization cases, which included non-ideal effects associated with high pressure mixtures, ambient gas solubility in the liquid phase, variation of thermophysical properties in the boundary layer and the effects of total pressure on the vapor pressure and enthalpy of vaporization. The ambient temperature range was 375-1600°K and the pressure range was 70-120 atmospheres. Some of the conclusions of this work indicate:

1. A vaporizing droplet can reach and exceed its thermodynamic critical temperature, thus becoming a dense mass of vapor, at supercritical pressure, by an intrinsically unsteady process.
2. All nonideal effects usually neglected in low pressure vaporization models are important in the critical region.
3. Reasonable estimates of vaporization times over a wide range of temperatures and pressures can be obtained with the low pressure model provided the effects of ambient gas solubility and the effects of total pressure on the vapor pressure and enthalpy of vaporization are accounted for at high density conditions.

The work by Lazar and Faeth [42] and Lazar [43] considered bipropellant droplet combustion in the critical pressure range. These tests were conducted under zero gravity conditions. The fuels considered included n-octane and n-decane supported droplets burning in air at pressures up to 2000 psia. The theoretical results considered the conventional low-pressure treatment of phase equilibrium at the droplet surface as well as high pressure models which allowed for real gas effects as well as finite ambient gas solubility. Some of their findings and major conclusions are as follows:

1. High pressure corrections and solubility effects should be considered in estimating droplet conditions at high pressure as well as in estimations of the pressures required for supercritical combustion. A good approximation for combustion in air can be obtained by assuming that the gas at the droplet surface is a binary mixture of fuel and nitrogen due to the predominance of nitrogen in the system.
2. The common unity Lewis number assumption will not yield useful predictions of droplet conditions at high pressures.
3. Conditions were found where water should condense on burning n-paraffin drops. This occurred for steady burning at pressures greater than 1 atm for paraffins up to n-pentane. Condensation can also occur for the heavier hydrocarbons during heat-up, at sufficiently low droplet temperatures.

1.3 Specific Statement of the Problem

The preceding discussion has indicated that there are certain important aspects of high pressure combustion that have not been fully explored. While the results of Manrique, Savery and Borman, et al., [13, 41] have demonstrated the importance of high pressure effects on the mechanism of evaporation, the combustion of fuel droplets was not considered. Other studies [11, 12, 41] also failed to consider this aspect of the problem. The investigations of Lazar and Faeth [42] provided combustion rate data at high pressures in a convection free environment. However, the burning rates obtained were unsteady state and the ambient temperature of the air around the droplet was low.

Investigations [39, 40] that considered the effect of forced convection on pressurized combustion did not consider realistic ambient pressure or ambient temperature levels. This aspect of the problem is of great importance when attempting to model an actual spray combustion process.

Therefore, the present investigation was undertaken with the following specific objectives:

1. To compare the theoretical predictions of the various high pressure models, when modified to include variable properties, ambient gas solubility, and the separate determination of the concentrations of the various gas phase species with experimental results for hydrocarbon and alcohol droplets burning in a high pressure, cold air environment under essentially natural convection conditions. Comparisons are made between the theoretical

and experimental burning rates and liquid surface temperatures. Real gas effects are considered and emphasis is placed on the prediction of the pressures required for the droplets to reach a critical combustion condition.

2. To compare the high pressure theoretical burning rate and liquid surface temperature predictions, using the above modifications, with experimental results for fuel droplets burning at high pressures in hot combustion gases of variable oxygen concentrations under forced convection.

3. To determine experimental evaporation rates and liquid surface temperatures of fuel droplets, in the absence of combustion, in hot gases under forced convection and to compare the results with the theoretical predictions of the various high pressure models.

The preliminary stage of the investigation consisted of developing a high pressure combustion apparatus capable of carrying out the experimental objectives. The investigation is in two parts; the first aspect of the investigation considered the high-pressure, steady-state combustion of liquid fuels in a cold air, natural convection environment at pressures up to 100 atmospheres. The experimental results were compared with droplet combustion theories which both neglected and considered real gas effects. The fuel droplets were simulated by porous spheres. Sphere sizes ranged from 0.63-1.9 cm outside diameter. Fuels considered in this portion of the investigation included methanol, ethanol, propanol-1, n-pentane,

n-heptane, and n-decane. The ambient gas temperature was maintained around 300°K. A discussion of this phase of the investigation is presented in Section 4.2.

The second aspect of the investigation considered the combustion and evaporation of fuels in a hot combustion gas environment under forced convection. The hot combustion gases were provided by a swirl-stabilized burner. The atmospheric tests which provided baseline data for the subsequent high pressure vaporization experiment employed methanol, ethanol, propanol-1, n-pentane, n-heptane, and n-decane as test fuels. The ambient air temperature of these experiments ranged from 600°K to 1530°K and over a Reynolds number range of 30 to 300.

For the high pressure tests, the fuels included ethanol and n-heptane. The pressure range was from one to 40 atmospheres and the ambient gas temperature was maintained around 1150°K for the combustion tests and around 1255°K for the pure evaporative tests. The Reynolds range for these tests was from 70 to 672.

CHAPTER II

THEORETICAL CONSIDERATIONS

2.1 Description of the General Model

The theoretical objective of this investigation was to compare the predictions of the various high pressure models with respect to their ability to accurately predict bipropellant droplet vaporization characteristics at high ambient temperatures and pressures. Major emphasis was placed upon the prediction of steady burning rates, liquid surface temperatures, and critical burning states under variable oxygen concentrations. The present theory is similar in many respects to that of References [42 and 43] for high pressure droplet combustion. The major point of difference involves the different boundary conditions at the liquid surface for the present porous sphere combustion case as opposed to steady droplet combustion, and a correction to the burning rate for convection effects. These considerations are discussed in Sections 2.2.3 and 2.3, respectively.

The theory may be divided into a gas phase model of the combustion process and a phase equilibrium model for conditions at the liquid surface. The solution to the theoretical combustion problem involves the solution of the conservation equations for diffusion of heat and mass.

The physical model for analyzing quasi-steady bipropellant droplet combustion has been developed by Spalding, Goldsmith and Penner, et al., [1, 5, and 8). A sketch of this model is shown in Figure 1. The present experiment differs from these investigations in

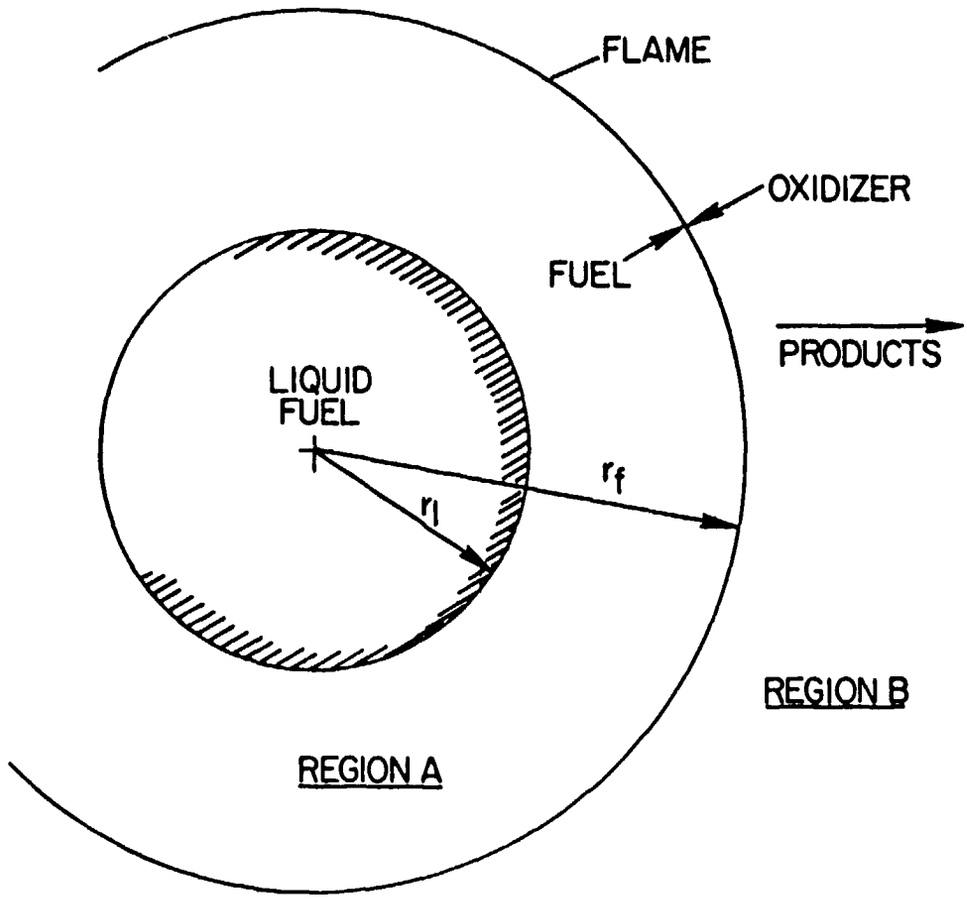

Figure 1 Model of the Burning of a Fuel Droplet in an Oxidizing Atmosphere

that truly steady-state conditions prevail. A major simplification to the theory, therefore, is that all transient phenomena (finite radius regression rate, time required to attain steady droplet temperature, etc.) associated with the combustion process do not have to be considered.

The gas phase analysis involved extending the variable property, steady burning solution of Goldsmith and Penner [8] since the property variations in this approach are particularly suited to the present vaporization conditions. This extension included the consideration of the effect of dissolved gas evaporation, separate determination of the concentrations of the various gas phase species and allowance for variable specific heats of all species. The analysis is cast on a molar basis in order to facilitate matching the gas phase solution with the phase equilibrium solution at the droplet surface.

The basic analysis, therefore, assumes spherical symmetry and neglects convection effects. The analysis of droplet combustion based upon the assumption of spherical symmetry with a multiplicative correction for convection effects has been demonstrated by many investigators [44, 45, 46 and 47] as an approach that gives good agreement with experimental results. The treatment of the combustion problem under the previously stated assumptions is presented in the following sections of this chapter.

2.2 Gas Phase Model

2.2.1 Description

Referring to Figure 1, it is assumed that reaction is confined to a spherically symmetric, infinitely thin flame surface where fuel and

oxidizer combine in stoichiometric proportions. This assumption provides a useful limit when the reaction rates are fast in comparison to the diffusion rates. [23]

The total gas pressure is taken to be constant throughout the boundary layer and body forces are neglected. Faeth [48] considers this problem and defines the limits under which this approximation is valid for droplet combustion. For the conditions of the present investigation, consideration of the momentum equation in Appendix A.1 indicates that the pressure variation across the boundary layer is negligible. Thermal diffusion is neglected in the gas phase analysis. Williams [44] indicates that thermal diffusion is usually negligible in comparison with the ordinary concentration gradient diffusion. Therefore, only concentration diffusion is considered in the gas phase analysis.

The influence of compressibility effects on transport properties in the boundary layer is neglected and the ideal gas equation is employed to compute the molar density in the gas phase. Compressibility effects are small except near the droplet surface due to the high temperature of most of the gas phase.

The effect of thermal radiation on the combustion process is neglected in the analysis. In the present investigation only radiation from the envelope flame is of interest due to the construction of the experimental apparatus. The effect of radiation on the combustion of porous spheres is examined in Appendix A.2. In addition to the above assumptions the concentration dependence of the thermal conductivity is neglected and the binary diffusivities of all

species are taken to be the same, although different values of each of these properties can be employed inside (Region A, Figure 1) and outside (Region B) the flame. The use of equal binary diffusivities in multicomponent mixtures is a common assumption employed in the analysis of diffusional processes for burning fuel droplets. [44, 49]

The usual unity Lewis number assumption was not employed in the analysis since earlier studies [42] have shown that the value of the Lewis number has a strong influence on conditions at the liquid surface. The effect of property variations on the combustion process is examined in Chapter IV.

In the present experiment the liquid fuel was pumped to the center of the sphere from a storage vessel at atmospheric pressure. It is appropriate, therefore, to assume that the liquid entering the sphere has a negligible dissolved gas concentration due to the low solubility of gases in the test fuels at low pressures. Under this assumption, the liquid phase flux of dissolved gas is zero, and the fuel is the only component with a finite molar flux inside the flame surface.

The formulation of the problem under the above assumptions results in the following unknowns:

1. Burning rate, $\dot{n}_f$
2. Temperature of the flame, T_f
3. Liquid surface temperature, T_ℓ
4. Flame radius, r_f
5. Species mole fractions at the droplet surface, $X_{i\ell}$
6. Species concentrations in Region B

In the following sections of this chapter, and in Appendix B the appropriate transport equations were solved to determine these parameters for steady droplet burning conditions.

2.2.2 Conservation Equations

For a spherically symmetric system (Figure 1) the governing equations for the spherical shells defined by Region A and Region B, under the previously stated assumptions, for a multicomponent system are:

$$\frac{d}{dr}(r^2 N_i) = 0 \qquad i=1, \ldots, N \text{ (Mass)} \tag{2.1}$$

$$\frac{d}{dr}\left[r^2 \sum_{i=1}^{N} N_i h_i - r^2 \lambda \frac{dT}{dr}\right] = 0 \quad \text{(Energy)} \tag{2.2}$$

$$N_i = -CD \frac{dX_i}{dr} + X_i \sum_{j=1}^{N} N_j, \qquad i=1, \ldots, N \text{ (Species)} \tag{2.3}$$

where N_i is the molar flux per unit area of species i.

In the following the fuel is denoted as component 1 (absent in Region B) and the oxidizer, component N (absent in Region A).

The overall burning rate can be shown to be a constant by multiplying Equation (2.1) by 4π, summing over all species, and integrating; this yields

$$4\pi r_\ell^2 \sum_{i=1}^{N-1} N_i = \text{Constant} = \dot{n} \tag{2.4}$$

The mole flux fractions in Region A, ε_i, are defined as

$$\varepsilon_i = \frac{N_i}{\sum_{i=1}^{N-1} N_i} \tag{2.5}$$

Since the fuel is the only component diffusing in Region A, for the porous sphere case, $\varepsilon_1=1$ and $\varepsilon_i=0$ (i=2, ..., N-1) in Region A.

Considering the energy equation

$$\frac{d}{dr}\left[r^2(h-h_\ell)_1 - 4\pi r^2\lambda \frac{dT}{dr}\right] = 0$$

Integrating between r_ℓ and r for $r < r_f$ leads to

$$\left[\dot{n}(h-h_\ell)_1 - 4\pi r^2\lambda_A \frac{dT}{dr}\right]_r = \left[\dot{n}(h-h_\ell)_1 - 4\pi r^2\lambda_A \frac{dT}{dr}\right]_{r_\ell^+} \qquad (2.6)$$

The right hand side of Equation (2.6) may be evaluated through consideration of conservation of energy at the droplet interface. Under the steady burning assumption all of the energy reaching the droplet surface goes into the heat of vaporization of the fuel. The rate of energy transport is

$$4\pi r^2\lambda_A \frac{dT}{dr}\bigg|_{r_\ell^+} = \dot{n}L_1 \qquad (2.7)$$

Two cases may be considered theoretically:

1. For droplet burning, L, is the heat of vaporization for all gas phase components and
$$L = \sum_{i=1}^{N-1} \nu_i L_i$$
2. For porous spheres, the present case under investigation only the fuel is gasified and the quantity L_1 must include any liquid phase enthalpy rise of the fuel as well as the heat of vaporization.

Therefore, the equation for conservation of energy for steady burning in Region A becomes:

$$\dot{n}(h-h_\ell + L)_1 = 4\pi r^2\lambda_A \frac{dT}{dr} \qquad (2.8)$$

Employing the definition of ε_i given by Equation (2.5) and substituting this quantity into Equation (2.3), the conservation of species for Region A becomes

$$\dot{n}[X_{i\ell}-1] - 4\pi r^2 (CD)_A \frac{dX_i}{dr}, \qquad i=1, \ldots, N-1 \tag{2.9}$$

The determination of the mole flux fractions in Region B is made by considering the combustion process at the flame surface. The stoichiometry of the reaction (where W_i denotes the chemical symbol of species i) at the flame surface is taken as follows

$$W_1 \rightarrow \sum_{i=2}^{N} \alpha_i W_i \tag{2.10}$$

The total molar flux in Region B can be shown to be a constant through the use of the continuity equation. This leads to

$$\dot{n}_f = 4\pi r_f^2 \sum_{i=2}^{N} N_{if} \tag{2.11}$$

Therefore, for the outer region

$$\dot{n}_o = \sum_{i=2}^{N} \dot{n}_i = \dot{n}_1 \sum_{i=2}^{N} \alpha_i \tag{2.12}$$

and

$$\frac{\dot{n}_i}{\dot{n}_o} = \varepsilon_i = \frac{\alpha_i}{\sum_{j=2}^{N} \alpha_j} \qquad i=2, \ldots, N \tag{2.13}$$

Writing the conservation of energy across the flame surface

$$\left\{\dot{n}(h-h_\ell)_1 - 4\pi r^2 \lambda \frac{dT}{dr}\right\}_{f^-} = \left\{\dot{n}_f \sum_{i=2}^{N} \varepsilon_i h_i - 4\pi r^2 \lambda \frac{dT}{dr}\right\}_{f^+} \tag{2.14}$$

The left hand side of the above equation is constant in Region A and may be evaluated at the droplet surface.

For Region B conservation of energy (which must account for the heat of reaction) leads to

$$\dot{n}\{\sum_{i=2}^{N} \alpha_i (h-h_\ell)_i - Q_\ell + L\} = 4\pi r^2 \lambda_B \frac{dT}{dr} \tag{2.15}$$

where

$$Q_\ell = h_{1\ell} - \sum_{i=2}^{N} \alpha_i h_{i\ell} \tag{2.16}$$

is the heat of reaction at T_ℓ for gaseous reactants and products.

The conservation of species in Region B becomes

$$\dot{n}\{\sum_{i=2}^{N} \alpha_i X_i - \alpha_i\} = 4\pi r^2 (CD)_B \frac{dX_i}{dr} \tag{2.17}$$

2.2.3 Boundary Conditions

The boundary conditions on Equation (2.8) and (2.9) in Region A are as follows:

$$\begin{aligned} &r = r_\ell, \quad T = T_\ell, \quad X_i = X_{i\ell} \quad (i=1, \ldots, N-1) \\ &r = r_f, \quad T = T_f, \quad X_1 = 0, \quad x_i = x_{if} \quad (i=2, \ldots, N) \end{aligned} \tag{2.18}$$

In Region B the boundary conditions assume the form:

$$\begin{aligned} &r = r_f, \quad T = T_f, \quad X_i = X_{if}, \quad (i=2, \ldots, N-1), \quad X_N = 0 \\ &r = r_\infty, \quad T = T_\infty, \quad X_i = X_{i\infty} \quad (i=2, \ldots, N) \end{aligned} \tag{2.19}$$

The steady burning equations of conservation of species and energy, Equations (2.8), (2.9), (2.15) and (2.17) and the boundary conditions, Equations (2.18) and (2.19), can be integrated upon substitution of the relationships for the physical properties contained in these expressions.

For the most general case the following relations were adopted for the thermal conductivity and the specific heat:

$$\lambda = \lambda_\ell (T/T_\ell) \tag{2.20}$$

$$C_{Pi} = A_i + B_i T, \quad i=1, \ldots, N \tag{2.21}$$

The quantity

$$\chi_i = (\lambda/CD)_i \tag{2.22}$$

is only a weak function of temperature and is assumed to have a constant average value in each field.

The detailed solution of the steady burning equations using the above property relations is discussed in Appendix B. The results for the solution of the unknowns given in Section 2.2.1 are presented in the following.

The most general solution of the equations consider both variable properties and variable specific heats in the gas phase using the property variations given by Equations (2.20), (2.21) and (2.22). In the following the fuel is denoted as component 1 and oxygen is denoted as component N.

The gas phase solution in the region inside the flame gives the following expression for the fuel mole fraction at the liquid surface. There are three branches to the solution:

$$X_{1\ell} = 1 - \left[\frac{\left(A_1 + B_1T_f + \xi\right)\left(A_1 + B_1T_\ell - \xi\right)}{\left(A_1 + B_1T_f - \xi\right)\left(A_1 + B_1T_\ell + \xi\right)}\right]^{\chi_A/\xi}, \qquad \xi^2 > 0 \tag{2.23}$$

$$X_{1\ell} = 1 - \exp\left[\frac{2\chi_A}{\phi}\left[\tan^{-1}\frac{(A_1 + B_1T_\ell)}{\phi} - \tan^{-1}\left(\frac{A_1 + B_1T_f}{\phi}\right)\right]\right] \qquad \phi^2 > 0 \tag{2.24}$$

$$X_{1\ell} = 1 - \exp\left[\frac{2\lambda_F B_1(T_\ell - T_f)}{(A_1 + B_1T_\ell)(A_1 + B_1T_f)}\right], \qquad \phi^2 = 0 \tag{2.25}$$

where

$$\chi_A = (\lambda/CD)_A$$

and

$$\xi^2 = -\phi^2 = A_1^2 - 2B_1\left[L_1 - A_1T_\ell - \frac{B_1}{2}T_\ell^2\right] \tag{2.26}$$

The mole fractions of the remaining species at the liquid surface are given in terms of the composition of the flame

$$X_{i\ell} = X_{if}(1-X_{1\ell}), \qquad i=2, \ldots, N-1 \tag{2.27}$$

The solution in the region inside the flame yields an expression for the burning rate in terms of properties in the flame. There are again three branches to the solution as follows:

$$\frac{\dot{n}T_\ell B_1}{4\pi r_\ell \lambda_{A\ell}}\left(1 - \frac{r_\ell}{r_f}\right) = \ell n\left[\frac{L_1 + \frac{B_1}{2}(T_f^2 - T_\ell^2) + A_1(T_f - T_\ell)}{L_1}\right] + \eta \tag{2.28}$$

where η is given by

$$\eta = \ell n\left[\frac{(A_1 + B_1T_f + \xi)(A_1 + B_1T_\ell - \xi)}{(A_1 + B_1T_f - \xi)(A_1 + B_1T_\ell + \xi)}\right], \qquad \xi^2 > 0 \tag{2.29}$$

or

$$\eta = \frac{-2A_1}{\phi}\left[\tan^{-1}\left(\frac{A_1 + B_1T_f}{\phi}\right) - \tan^{-1}\left(\frac{A_1 + B_1T_\ell}{\phi}\right)\right], \qquad \phi^2 > 0 \tag{2.30}$$

or

$$\eta = \frac{-2A_1B_1(T_f - T_\ell)}{(A_1 + B_1T_f)(A_1 + B_1T_\ell)}, \qquad \xi^2 = 0 \tag{2.31}$$

The flame temperature is related to the ambient oxygen concentration as follows:

$$\frac{\alpha_N}{\alpha_N - \alpha' X_{N\infty}} = \left[\frac{(b'T_\infty + a' + \gamma)(b'T_f + a' - \gamma)}{(b'T_\infty + a' - \gamma)(b'T_f + a' + \gamma)}\right]^{X_B/\gamma\alpha'}, \qquad \gamma^2 > 0 \tag{2.32}$$

$$\ell n\left(\frac{\alpha_N}{\alpha_N - \alpha' X_{N\infty}}\right) = \frac{2\alpha' X_B}{\phi'}\exp\left[\tan^{-1}\left(\frac{a' + b'T_f}{\phi'}\right) - \tan^{-1}\left(\frac{a' + b'T_\infty}{\phi'}\right)\right], \qquad \phi'^2 > 0 \tag{2.33}$$

$$\ell n \frac{\alpha_N}{\alpha_N - \alpha' X_{N\infty}} = \frac{2\alpha' X_B b'(T_f - T_\infty)}{(a' + b'T_f)(a' + b'T_\infty)}, \qquad \phi'^2 = 0 \tag{2.34}$$

where

$$\gamma^2 = -\phi'^2 = a'^2 - 2b'(L_1 - Q_\ell - a'T_\ell - \frac{b'}{2} T_\ell^2) \tag{2.35}$$

An expression for the combustion radius is obtained by integrating the energy equation and applying the boundary conditions of Equation (2.19). The results are as follows:

$$\frac{1}{r_f} = \frac{4\pi\lambda_B}{\dot{n} T_\ell b'} \left[\ell n \left(\frac{(T_\infty - T_\ell)a' + \frac{b'}{2}(T_\infty^2 - T_\ell^2) - Q_\ell + L_1}{(T_f - T_\ell)a' + \frac{b'}{2}(T_f^2 - T_\ell^2) - Q_\ell + L_1} \right) + \eta' \right] \tag{2.36}$$

where

$$\eta' = \frac{a'}{\gamma} \ell n \left[\frac{(a' + b'T_f - \gamma)}{(a' + B'T_f + \gamma)} \quad \frac{(a' + b'T_\infty + \gamma)}{(a' + b'T_\infty - \gamma)} \right] \qquad \gamma^2 > 0 \tag{2.37}$$

and

$$\eta' = \frac{2a'}{\phi'} \left[\tan^{-1} \left(\frac{(a' + b'T_f)}{\phi'} \right) - \tan^{-1} \left(\frac{(a' + b'T_\infty)}{\phi'} \right) \right], \qquad \phi'^2 > 0 \tag{2.38}$$

and

$$\eta' = \frac{2a'b'(T_f - T_\infty)}{(a' + b'T_f)(a' + b'T_\infty)}, \qquad \gamma^2 = 0 \tag{2.39}$$

Another useful approximation is the case when B_i=0, since fuel is absent in the outer region and B_i in Equation (2.21) is small for the nonfuel species. The most significant difference between the solutions for the variable specific heat case and the constant specific heat case is the absence of three separate solutions for the constant specific heat case. A separate solution is presented in Appendix B.2 since the solution for finite B_i does not reduce conveniently to this case. The resulting expressions for liquid phase mole fractions, burning rate, flame temperature, and flame

radius, respectively, are as follows:

$$X_{1\ell} = 1 - \left[\frac{L_1}{L_1 + A_1(T_f - T_\ell)}\right]^{1/A_1\chi_A} \tag{2.40}$$

Equation (2.25) is unchanged for this case and remains

$$X_{1\ell} = X_{1f}(1 - X_{1\ell}), \qquad i=2, \ldots, N-1 \tag{2.41}$$

The expression for the burning rate is

$$\frac{\dot{n}a'^2 T_\ell}{4\pi r_f \lambda_{B\ell}} = a'(T_\infty - T_f) - (L_1 - Q_\ell - a'T_\ell)\ \ell n\left[\frac{a'(T_\infty - T_\ell) - Q_\ell + L_1}{a'(T_f - T_\ell) - Q_\ell + L_1}\right] \tag{2.42}$$

The expression for the combustion temperature is

$$\frac{1}{\alpha'}\ \ell n\left(\frac{\alpha_N}{\alpha_N - X_{N\infty}\alpha'}\right) = \frac{\chi_B}{a'}\ \ell n\left[\frac{a'(T_f - T_\ell) - Q_\ell + L_1}{a'(T_\infty - T_\ell) - Q_\ell + L_1}\right] \tag{2.43}$$

and the combustion radius is given as

$$\frac{\dot{n}T_\ell A_1}{4\pi r_\ell \lambda_{A\ell}}\left(1 - \frac{r_\ell}{r_f}\right) = A_1(T_f - T_\ell) - (L_1 - A_1 T_\ell)\ \ell n\left[1 + \frac{A_1}{L_1}(T_f - T_\ell)\right] \tag{2.44}$$

The third approximation neglects all temperature dependence for all properties. This solution corresponds to the usual low pressure, constant property model of droplet combustion.

The expressions for the liquid phase mole fractions are

$$X_{1\ell} = 1 - \left[1 + \frac{C_{PF}(T_f - T_\ell)}{L_1}\right]^{-\lambda/CDC_{PF}} \tag{2.45}$$

$$x_{2\ell} = (1 - X_{1\ell}) \tag{2.46}$$

The expressions for the burning rate, combustion temperature and combustion radius, respectively, are:

$$\frac{\dot{n}}{4\pi\lambda_A}\left(\frac{1}{r_\ell}-\frac{1}{r_f}\right)=\frac{1}{C_{PF}}\ell n\left[1+\frac{C_{PF}(T_f-T_\ell)}{L_1}\right] \tag{2.47}$$

$$\ell n\left[\frac{a'(T_f-T_\ell)-Q_s+L_1}{a'(T_\infty-T_\ell)-Q_s+L_1}\right]=\frac{a'}{\alpha'}\left[\frac{CD_N}{\lambda_B}\ell n\frac{\alpha_N}{\alpha_N-\alpha' X_{N\infty}}\right] \tag{2.48}$$

$$\frac{1}{r_f}=\frac{4\pi\lambda_B}{C_{Po}\dot{n}}\ell n\left[\frac{a'(T_\infty-T_\ell)-Q_s+L_1}{a'(T_f-T_\ell)-Q_s+L_1}\right] \tag{2.49}$$

The calculations proceeded by guessing a value for the liquid surface temperature T_ℓ, at a given total pressure, and then computing L_1 and $X_{1\ell}$ (the fuel mole fraction at the liquid surface) from the phase equilibrium analysis. These values were then employed to compute a value for $X_{1\ell}$ from the gas phase analysis given previously and in Appendix B. The final solution was obtained by varying T_ℓ until the two values of $X_{1\ell}$ matched.

2.3 Convection Correction

Since heat and mass transfer are increased by the effects of convection, a low limit for the burning rate will be obtained if the analysis is made for a droplet burning in a still atmosphere (stagnant film approximation). In the gas phase model, therefore, the effect of convection is treated by the use of a multiplicative correction of the burning rate predicted in the absence of convection. Since the experiment considers both natural and forced convection, the correlations employed are different in each case.

One aspect of the investigation deals with high-pressure droplet combustion under natural convection conditions with air being admitted into the combustion chamber at essentially ambient

temperature. For these conditions, using the definition of the Grashoff number as suggested by Spalding [50] for burning spheres, the convection correlation assumes the form

$$\dot{n}/\dot{n}_o = 1 + 0.221\ Pr^{1/3}\ (d^3g/\nu^2)^{1/4} \qquad (2.50)$$

The properties used in this correlation were taken at the ambient conditions of the burning sphere.

The second portion of the experimental program deals with high pressure droplet combustion in a forced convection flow of hot combustion gases. Therefore, it is necessary to correct the theoretical burning rate constant for the flow of burner gas past the test droplet. For steady droplet evaporation or combustion umerous investigators [45, 46, and 47] have suggested a convection correlation of the form

$$\dot{n}/\dot{n}_o = 1 + f(Re, Pr, Sc)$$

when $\dot{n}_o$ is the evaporation rate at no-flow. The specific correlation that will be used is

$$\dot{n}/\dot{n}_o = 1 + 0.278\ Re^{1/2}\ Pr^{1/3}(1 + 1.237\ Re^{-1}\ Pr^{-4/3})^{-1/2} \qquad (2.51)$$

This expression has the advantage of asymptotically approaching the mathematically rigorous results of Fendell, et al., [46] for small Peclet number as well as agreeing with the data of Frössling [47], Yuge [49], and Allender [50] for $10 < Re < 800$. Ambient gas properties are used for computing the non-dimensional quantities appearing in the above correlation.

2.4 Phase Equilibrium Analysis

The determination of steady state condition requires that the gas phase solution given in Appendix B be matched with the boundary conditions at the droplet surface. The evaluation of these boundary conditions requires a consideration of the thermodynamics of phase equilibrium at the vapor-liquid interface of the droplet. Three models were employed for computing phase equilibrium at the droplet surface, a low pressure model and two phase equilibrium models appropriate for use at high pressures. A discussion of these models is presented in the following sections of this chapter.

2.4.1 Low Pressure Theory

At low pressures it is usually a good approximation to neglect solubility effects and take the fuel mole fraction at the droplet surface, $X_{1\ell}$, as the vapor pressure of the pure fuel at the liquid temperature divided by the total pressure. Brzustowski [23] has shown that this approximation is valid for total pressures up to 1/10 of the critical pressure of the pure fuel. As the critical pressure is approached, high pressure effects cast doubt on the validity of the low pressure approximation.

For the low pressure model, the heat of vaporization, L_1, was determined by summing the compressed enthalpy change at T_o, the heat of vaporization at T_o, and the ideal gas enthalpy rise between T_o and T_ℓ. In this case the ideal gas enthalpy rise was computed by integrating actual specific heat correlations between T_o and T_ℓ as opposed to the linearized specific heat correlations employed in the gas phase analysis.

The enthalpy deviations were obtained from the tables of Lydersen, et al., presented in Reference [52]. The enthalpy deviations were determined between saturated vapor and the ideal gas states at T_o and T_ℓ.

2.4.2 High Pressure Theory

The two high pressure theories considered solubility and other high pressure effects through the use of a modified Redlich-Kwong equation of state. In an evaluation of the various methods for computing phase behavior, Lazar [43] found that this equation gave the most satisfactory agreement with experimental data for binary mixtures of a paraffin hydrocarbon with carbon dioxide or nitrogen. The Redlich-Kwong equation of state has the form

$$P = \frac{RT}{V-b^o} - \frac{a^o}{T^{0.5}V(V+b^o)} \tag{2.52}$$

A vapor phase and a liquid phase are in equilibrium when both are at the same temperature and pressure and when the fugacity of any component in the vapor phase is equal to that of the liquid phase, i.e.,

$$f_{iv} = f_{i\ell}, \qquad i=1, \ldots, N \tag{2.53}$$

The fugacity of a component in a mixture is related to the volumetric properties of the mixture through the relation

$$RT \ln(f_i/X_iP) = \int_0^P (\bar{V}_i - RT/P)\, dP \tag{2.54}$$

The various component fugacities can be determined by substituting the Redlich-Kwong equation of state, using the mixing

rules of Prausnitz and Chueh (Appendix C), into Equation (2.27) and integrating. The dimensionless constants Ω_a and Ω_b required by this thermodynamic model are obtained by setting the first and second isothermal derivatives of pressure with respect to volume equal to zero at the critical point. The numerical values of the constants then become 0.4278 and 0.0867, respectively. For temperatures far removed from the critical region Prausnitz and Chueh [51] suggest that it is more appropriate to obtain Ω_a and Ω_b by fitting the equation to the volumetric data of the saturated liquid and vapor.

The binary interaction constants, k_{ij}, are characteristic of the i-j interaction for each binary pair present in the system. This constant varies between zero and one and increases with increasing molecular weight of the hydrocarbon component in systems containing hydrocarbons with nitrogen and carbon dioxide. The binary interaction parameters, k_{ij}, required by the theory are listed in Reference [42] for the paraffins and the combustion product gases. For the alcohols the k_{ij} values were taken to be the same as the hydrocarbon homomorph of the fuel. The values for the alcohols determined in this manner are listed in Table 1. The sensitivity of the final calculations to the effect of variation of the interaction parameters is discussed in Chapter IV.

For the high pressure theories, the terms comprising the enthalpy rise of vaporization are basically the same as those discussed previously for the low pressure theory. The major difference between the two theories lies in the computation of the enthalpy deviations. As opposed to the method used for the low pressure model,

Table 1

Alcohol Binary Interaction Parameters, k_{ij}

Substance	N_2	CO_2	H_2O
Methanol	.10	.08	.15
Ethanol	.15	.11	.20
Propanol-1	.20	.16	.25

Note: $k_{ij} = k_{ji}$ and $k_{ii} = 0$

the enthalpy deviations for the high pressure theories were computed directly from the Redlich-Kwong equation of state.

2.4.2.1 Binary Phase Equilibrium Analysis

For combustion in air the major gaseous species at the liquid surface are fuel vapor, nitrogen, carbon dioxide, and water vapor. Since nitrogen predominates the non-fuel gases in the system, a simplified version of the high pressure theory assumed that this system could be presented by a binary mixture of fuel and nitrogen.

2.4.2.2 Quaternary Phase Equilibrium Analysis

Previous studies [13,41, 42] have demonstrated the importance of gas solubility in the liquid phase during droplet combustion. In the combustion of most bipropellant fuels the principal species present in the gas phase include carbon dioxide, water vapor, fuel, and nitrogen. Therefore, the most completion version of the high pressure phase equilibrium analysis considered this quaternary system.

CHAPTER III

EXPERIMENTAL APPARATUS

3.1 Introduction

This chapter is divided into two major parts. The first part of the chapter describes the experimental apparatus and procedures that were used to obtain fuel burning rates and liquid surface temperature measurements for the cold air, natural convection tests. The second part of the chapter describes the apparatus and procedures used to obtain burning rate and liquid surface temperature data for the forced convection tests using the high-pressure swirl-stabilized burner.

3.2 Natural Convection Apparatus

3.2.1 Overall System Description

A sketch of the overall system is shown in Figure 2. The apparatus consists of a high pressure test chamber, gas flow system, fuel probe and fuel supply system, and instrumentation to measure gas and liquid surface temperatures.

The test chamber consists of a high pressure cylindrical vessel 66 cm long with an internal diameter of 13 cm. The chamber is of steel construction and is lined with firebrick. Observation of the burning fuel droplets is made through two quartz windows located at the test section.

The remainder of the systems comprising the experimental apparatus is described in detail in the following sections.

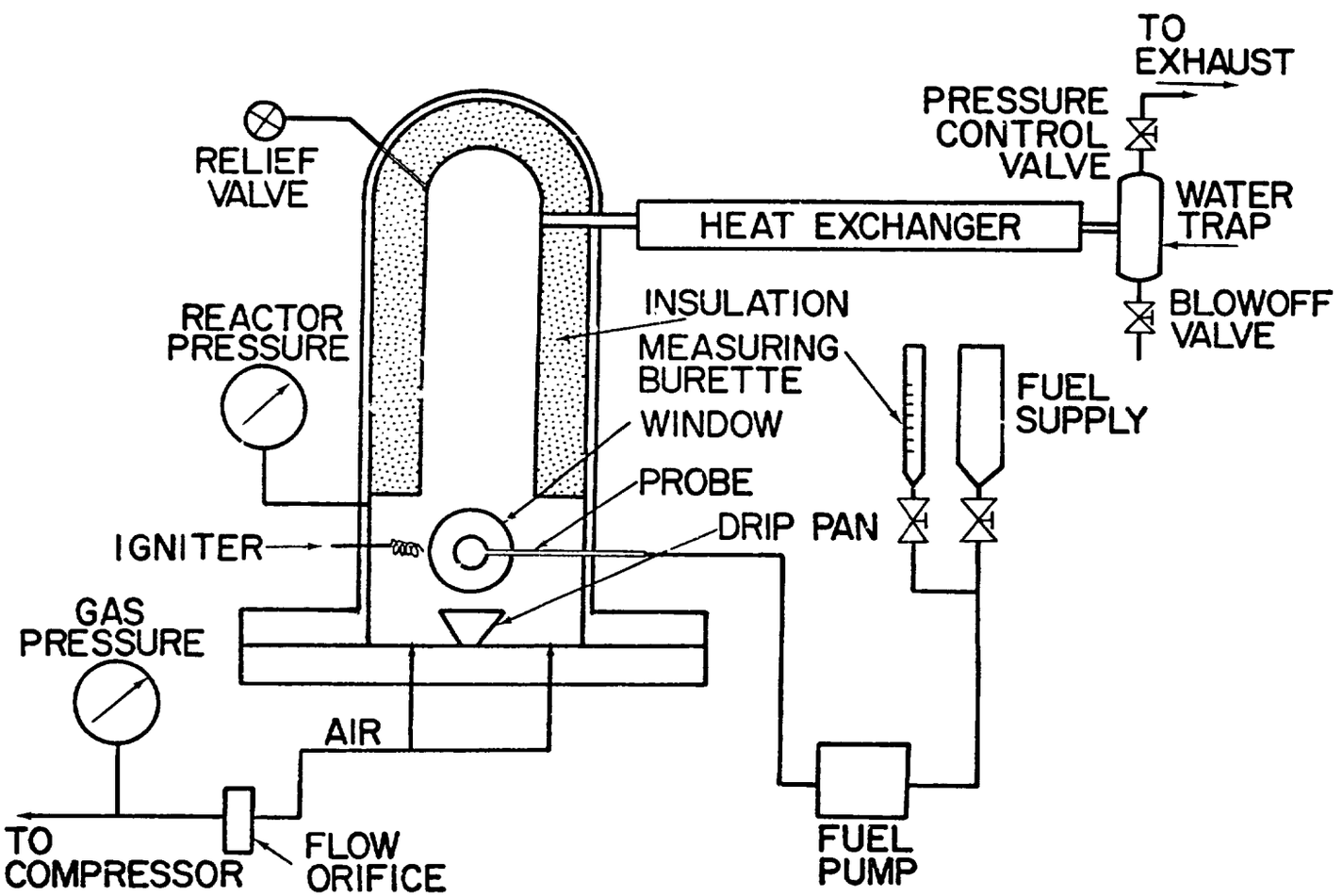

Figure 2 High Pressure Combustion Apparatus (Natural Convection)

3.2.2 Gas Flow System

Air for the combustion process is supplied by a 3000 psia compressor. The air flow is accurately controlled by a critical flow jeweled orifice system of the type described by Andersen and Friedman [52]. The orifices were calibrated using a Precision Scientific wet test meter.

A constant gas composition was maintained around the sphere by admitting the air through a multi-holed manifold at the bottom of the combustion chamber. The drift velocity of the air past the position of sphere was sufficiently low so that natural convection was the predominant flow effect.

The hot exhaust gases leaving the test chamber were cooled in a water cooled concentric tube heat exchanger. Water condensed in the heat exchanger was collected in a water trap and periodically blown off to a drain.

The reactor pressure was controlled by a stainless steel regulating valve located in the exhaust line. After passing through the regulating valve, the reactor gases were exhausted to the atmosphere.

The emergency pressure release system consisted of a rupture disc assembly set at 2000 psia. In addition, a one half inch stainless steel relief valve was used in conjunction with the rupture disc assembly.

3.2.3 Fuel Supply System

The fuel is pumped to the center of the sphere using a Whitey precision variable displacement pump. The pump is equipped with a 10 mm plunger and has a maximum discharge pressure of 5000 psia and a maximum delivery rate of 2200 milliliters per minute. The fuel flow rate is measured with a system of graduated burets at the pump inlet.

The porous spheres used in the combustion tests were made of alundum. The porous alundum spheres were obtained from the Norton Company. Because of irregularities in the manufacturing process, it was necessary to grind and sand the rough spheres to a smooth, spherical shape. Spheres having diameters of 0.64, 0.95 and 1.90 cm were employed in the testing. The tolerance on the sphere diameters was approximately $\pm$0.25 per cent.

A sketch of a fuel probe is shown in Figure 3. The fuel is fed to the center of the sphere through a stainless steel, water cooled hypodermic tube and forced radially outward and burned at the surface of the sphere. The smallest sphere size was limited by the outside diameter of the coolant water tube. The tube diameter was 0.20 cm for the 0.64 cm diameter sphere and 0.32 cm for the 0.95 and 1.90 cm diameter spheres, respectively.

Referring to Figure 3, the fuel is introduced through the center tube while coolant water passes through the second innermost tube and exits through the annulus formed by the second and third tubes. The inlet and outlet water coolant temperatures were continually monitored by means of thermocouples. For the natural

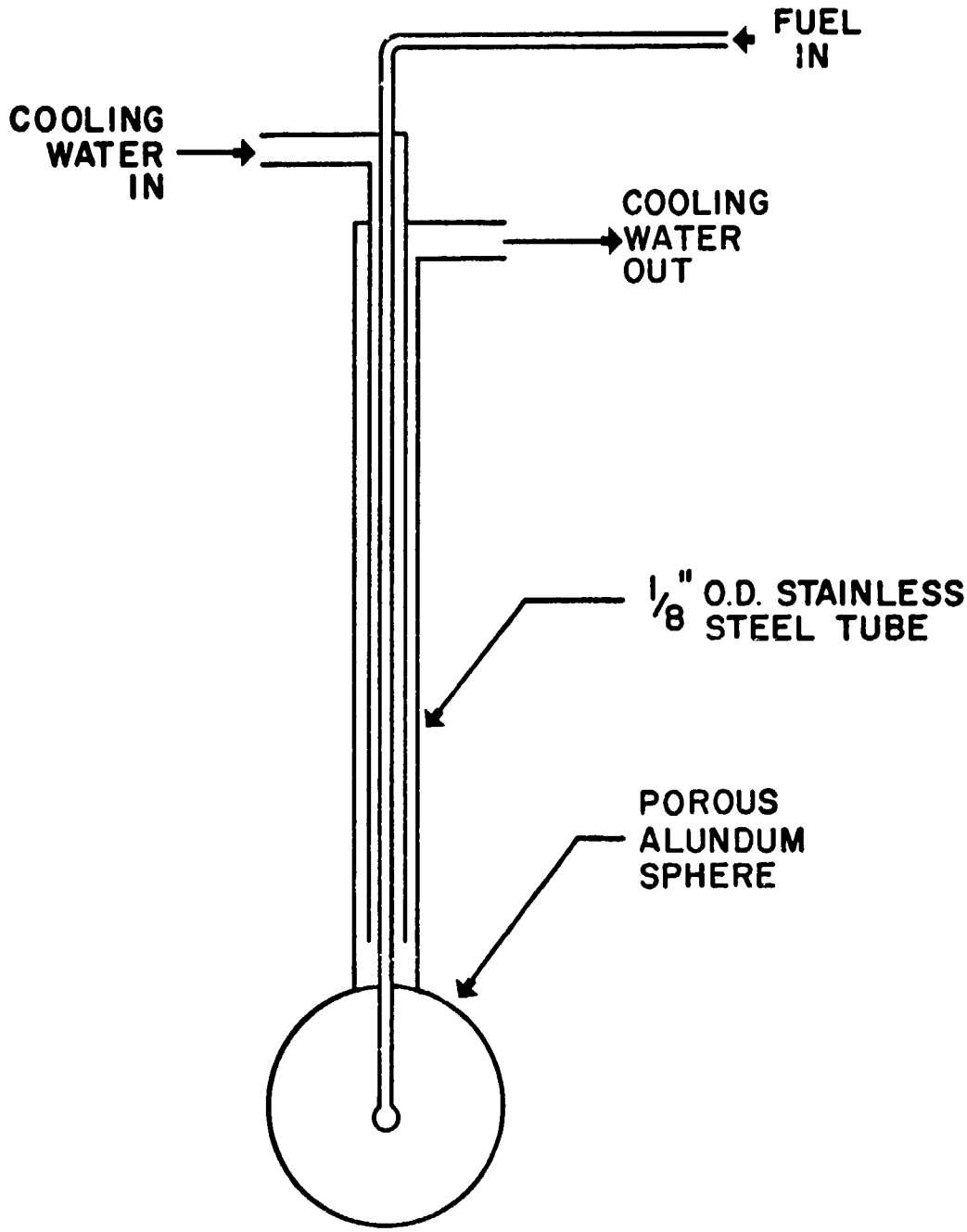

Figure 3 Porous Sphere Probe

convection combustion tests the coolant water temperature rise never exceeded 2 degrees F.

3.2.4 Instrumentation

3.2.4.1 Gas Temperature Measurement

Upstream stagnation air temperatures were measured using high pressure Omega chromel-alumel thermocouple probes. The output of the gas temperature and liquid surface temperature thermocouples was measured with a Leeds and Northrup Model 8686 millivolt potentiometer employing an ice bath reference junction. The constant temperature reference was provided by a Thermo-Electric Company "I-Cell." A series of thermocouples were also located within the combustion apparatus to measure the ambient air inlet temperature. This value was maintained around 300°K for the natural convection tests.

3.2.4.2 Liquid Surface Temperature Measurement

Liquid fuel temperatures at the surface of the sphere were made using two 0.0076 cm diameter chromel-alumel thermocouples. The thermocouples were mounted on the sphere such that the junctions of the thermocouples were flush with the sphere surface. The thermocouples were cemented in place with Saureisen high temperature cement and located approximately 60 degrees apart along the periphery of the sphere.

3.2.4.3 Dark Field Photography

A series of dark field photographs of the combustion process was taken using a 4 in. x 5 in. Super Graflex camera fitted

with a 135 mm Optar lens. The film used was Polaroid type 57 land film with an ASA rating of 5000. The droplet was photographed through one of the two observation windows.

3.2.5 Experimental Technique

3.2.5.1 Burning Rate Measurement

Burning rates were determined by measuring the length of time required for a given quantity of the fuel to be consumed. The liquid volume measurements were made with a graduated burette located at the inlet of the pump. The steady burning rate was determined as the flow rate when the surface of the sphere was fully wetted and not dripping. Liquid surface temperature measurements were also made at this condition. During adjustment to the steady burning condition, excess fuel dripping from the sphere was collected in a deadended tube at the bottom of the combustion apparatus. The drip tube was constructed in such a manner that there was no possibility of reignition of the fuel once it entered the tube. The liquid fuel was then periodically blown off to a drain.

Ignition was achieved by bringing a burning match in contact with the wetted sphere in the atmospheric baseline tests. The sphere was ignited by monentarily placing it in the vicinity of an electrically heated nichrome wire in the closed combustion chamber tests.

3.2.5.2 Operation of the Apparatus

The preliminary steps in the operation of the apparatus involved calibration of the thermocouple output with a millivolt potentiometer and focussing the camera for tests where dark field

photographs were taken. Ther thermocouple-potentiometer circuit was also checked before runs with an ice bath as reference. The fuel pump was then turned on and adjusted so that the sphere was fully wetted but not dripping. The reactor pressure was increased to 20 psia by admitting air through the manifold. The sphere was then brought momentarily in the vicinity of the ignitor wire until ignition was achieved. Upon ignition of the fuel probe, the ignitor was turned off and the sphere was repositioned by centering it in the observation window at the test section.

3.3 Forced Convection Apparatus

3.3.1 Overall System Description

A sketch of the high pressure combustion chamber with the burner is shown in Figure 4. The basic reactor vessel is similar to the one that was used for the cold gas natural convection tests. The reactor consists of a thick-walled cylindrical vessel 66 cm long with an inside diameter of 13 cm. The firebrick liner that was used for the natural convection tests was not used in the present forced convection apparatus. Observations are made through two quartz windows located at the droplet test section.

Other modifications to the basic apparatus included the installation of an internal stainless steel cooling coil. The cooling coil served to reduce radiation from the test chamber walls to the test droplet as well as maintaining the chamber walls at acceptable temperature levels when under pressure.

A 10,000 volt spark-ignition system was installed to ignite the burner gases. In addition, a pressurized nitrogen gas system

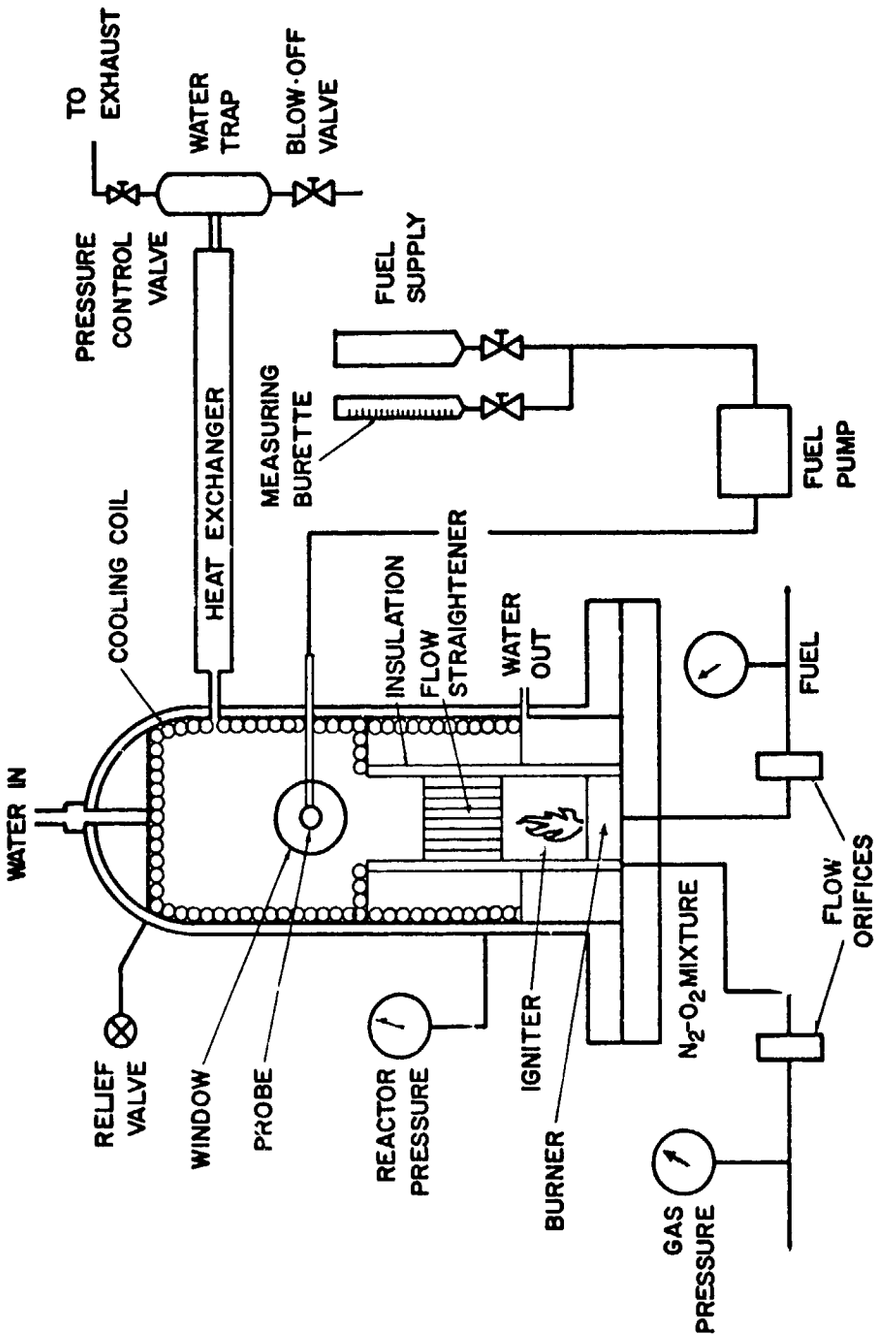

Figure 4 High Pressure Combustion Apparatus (Forced Convection)

heated by a 0.75 kilowatt electric heater was installed to remove condensate from the observation windows by directing a hot jet of nitrogen diluent against them. The fuel delivery and measuring system was the same as that described for the cold gas tests.

The basic fuel probe design is the same that was used for the natural convection tests. However, because of the hot combustion gas environment to which the probes were exposed, the internal configuration of the probe coolant lines was modified to allow for a greater volume flow rate of cooling water. The external diameter of the probe support was the same as for the natural convection tests. The maximum temperature rise of the coolant water was 3 degrees F.

All of the forced convection tests employed the 0.95 cm diameter sphere. Both alundum and sintered bronze spheres were used in the testing. Subsequent testing revealed no significant differences in test results employing the different sphere materials. The bulk of the testing was performed employing the alundum porous spheres.

3.3.2 Swirl-Stabilized Burner

A sketch of the high pressure burner is shown in Figure 5. A swirl-stabilized diffusion flame burner is used in the apparatus. The burner provides accurate composition control of the combustion gases, stable operation over a wide range of flow conditions, and the elimination of flashback. In earlier tests with premixed flat flame burners, flashback posed serious problems under pressurized testing conditions.

The burner used in the current tests employs a flame supplied with a mixture of carbon monoxide and air. Carbon monoxide was chosen

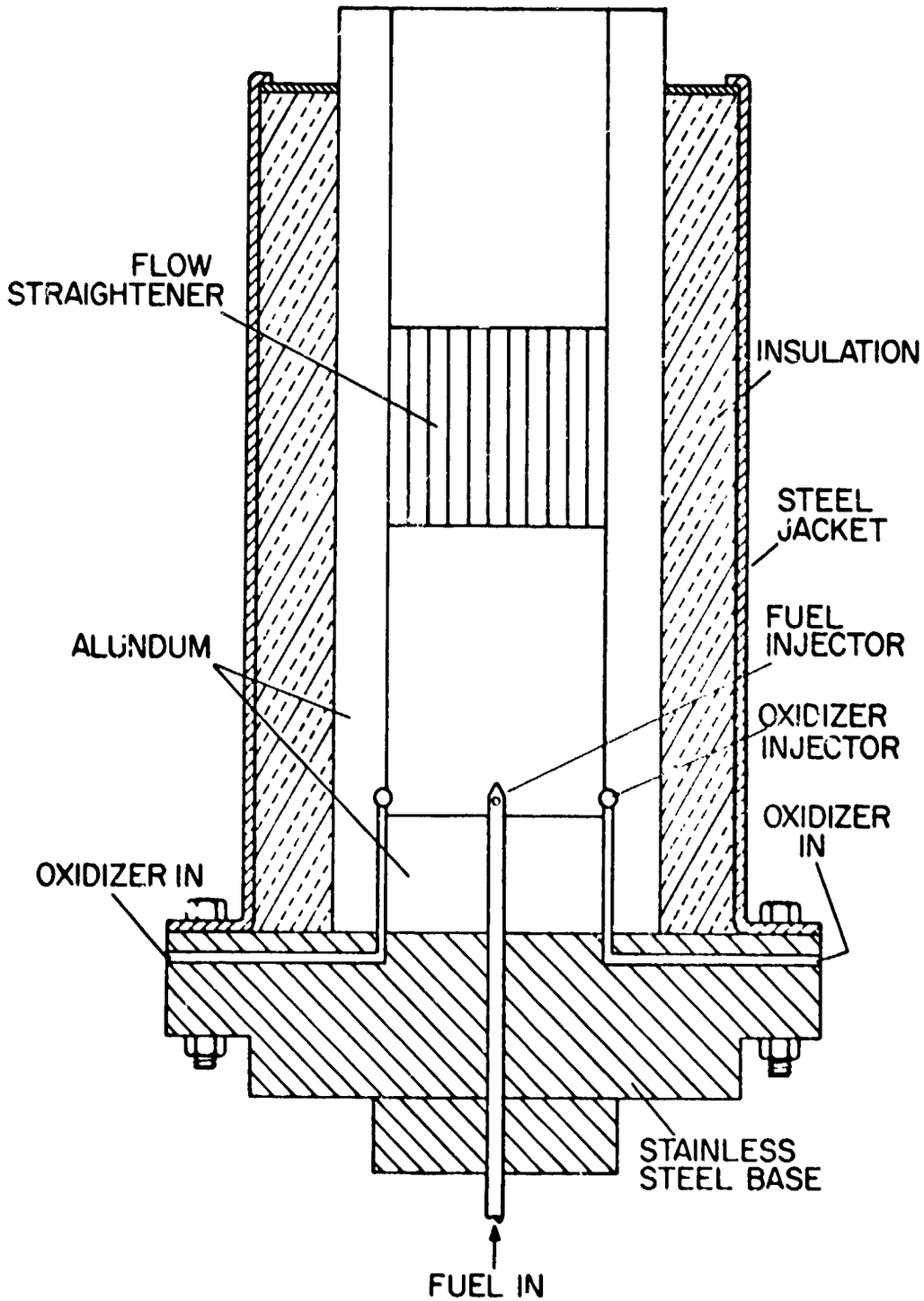

Figure 5 Diffusion Flame Burner (Swirl-Stabilized)

for a burner fuel since it is quite stable and reduces water vapor condensation within the apparatus. The carbon monoxide used in the high pressure burner tests was technical grade and was obtained from the Matheson Company.

The burner is constructed of Norton alundum ceramic tubing and type 316 stainless steel. The internal diameter of the burner test section is 5.08 cm. The burner wall consists of alundum tubing and alumina firebrick. Fuel is admitted through a multi-holed injector located in the center of the stainless steel burner base. The oxidizer is admitted through four tangential injectors located along the burner inner wall. A ceramic flow straightener was located in the burner passage and was designed such that the velocity and temperature profiles of the hot gases were uniform when the test section was reached. All gas flows through the burner were metered through a critical flow jeweled orifice system described in Section 3.2.2.

3.3.3 Instrumentation

3.3.3.1 Combustion Gas Temperature Measurements

Ambient gas temperatures at the test section were measured with a system of Pt-Pt-10% Rho fine wire thermocouples. The thermocouples were shielded, except for the last 0.63 cm, with a 0.079 cm O.D. ceramic insulator. The thermocouple measurements when corrected for radiation and conduction errors resulted in values that were approximately 35°K higher than the indicated readings. Ambient gas temperatures quoted in the investigation are average values for a given test condition.

To reduce oxidation and catalytic effects the gas temperature thermocouples were coated with silicone using a procedure outlined by Fristrom and Westenberg [53]. For the ambient gas temperature range of the present high pressure tests a silicone coating provided adequate protection for the thermocouples.

As a further check, the gas temperature and composition at the droplet location were computed from thermochemical calculations. Allowance was made for dissociation and heat loss through the burner walls.

3.3.3.2 Liquid Surface Temperature Measurements

Liquid surface temperature measurements were made in basically the same manner described in Section 3.1.4.2 for the natural convection tests. Because of the hot convective flow environment in which the sphere was placed, a third chromel-alumel thermocouple was located at the top of the sphere and flush with the surface to see if there were any significant variations in liquid surface temperature around the periphery of the sphere. In addition to this technique the sphere was rotated at intervals up to 360 degrees from its original position to provide a further check. Only minor variations were noted in the liquid surface temperatures. Consequently, only the two thermocouples located on the lower half of the sphere surface were used to obtain test results.

The two chromel-alumel thermocouples were located closer to the bottom stagnation point of the sphere (approximately 30 degrees apart) since preliminary testing with the burner revealed a tendency for the sphere to dry off at this point at high combustion gas flows

and at high ambient temperatures. Locating the thermocouples in this manner allowed this condition to be easily detected and corrected.

3.3.3.3 Operation of the Apparatus

Preliminary steps in the operating procedures included calibrating and checking the liquid surface temperature and combustion gas temperature thermocouples. The combustion chamber and burner were then purged with nitrogen. The burner ignition sequence consisted of activating the spark ignitor and then turning on the carbon monoxide-air mixture to the burner.

Following ignition the ignitor was turned off and the gas flows carefully adjusted. The burner combustion gas temperature and the probe and cooling coil water temperatures were continually monitored throughout the test. The fuel probe was ignited directly by the hot combustion gases. The recording of data followed essentially the same procedure as that used for the free convection tests.

CHAPTER IV

THEORETICAL AND EXPERIMENTAL RESULTS

4.1 Introduction

One of the major objectives of the present investigation was to determine bipropellant droplet vaporization characteristics under essentially combustion chamber conditions. Since convection has a dominant effect on the burning rate of fuel droplets, the experiment focussed on the combustion of fuel droplets under natural and forced convection conditions. The tests extended over a wide range of ambient pressures, ambient gas temperatures, Reynolds numbers, and ambient oxygen concentrations. Also, a wide range of fuels and droplet sizes was considered. This chapter is divided into two parts. The first section discusses the results of the natural convection tests, while the second section considers the results of forced convection tests in a combustion chamber environment.

4.2 Natural Convection Tests

4.2.1 Fuels and Range of the Tests

The objective of this part of the investigation was to study high pressure droplet combustion for a variety of fuels in a cold gas, natural convection environment. The experimental determination of both burning rates and liquid surface temperatures was considered in this effort. The experimental results were compared with droplet combustion theories which both neglected and considered real gas effects. The fuels used in the test consisted of three alcohols and three n-paraffins. The alochols included methanol, ethanol, propanol-1;

the n-paraffins included n-pentane, n-heptane, and n-decane. The pressure range varied from 1 to 51 atmospheres for the n-paraffin fuels and from 1 to 78 atmospheres for the alochols. Porous alundum spheres were used to simulate the fuel droplets. The sphere sizes included 0.63 cm, 0.95 cm, and 1.9 cm diameter spheres.

In addition to the determination of burning rates and liquid surface temperatures, a series of dark field photographs were taken. Methanol and ethanol were the fuels used in these tests. The sphere sizes employed were 0.63 cm, 0.95 cm, and 1.9 cm, in the pressure range from 1 to 35 atmospheres.

The experimental burning rate measurements and liquid surface temperature measurements reported in the following section of this chapter for the natural convection tests represent the average values for a series of separate runs. Typically, the values from the individual tests were within 2% of the average.

4.2.2 Observations

Envelope flames were observed during the natural convection tests with alcohols. The flames were blue over the forward portion of the sphere surface, turning to a yellowish flame over the rear half and in the wake. A photograph of a burning methanol droplet at 20 psia using the 0.95 cm sphere is shown in Figure 6. The same droplet burning at an ambient pressure of 310 psia is shown in Figure 7. At the higher pressure the envelope flame is very near the droplet surface and a luminous wake extends several sphere diameters above the probe.

The combustion flames of the n-paraffin fuels were very luminous. Sooting was a serious problem with all of the n-paraffin

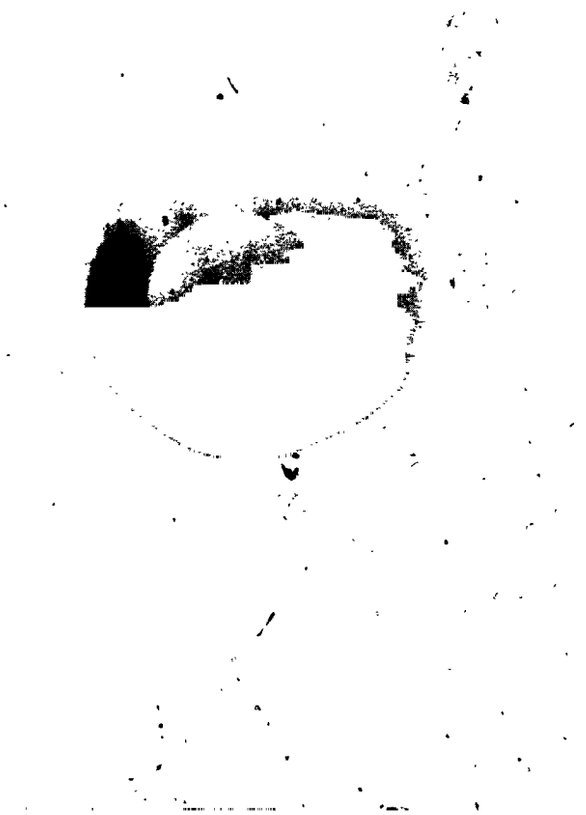

Figure 6 COMBUSTION OF METHANOL (P_{∞} = 1.36 ATM)

Figure 7 COMBUSTION OF METHANOL (P_{∞} = 21.1 ATM)

fuels. Methanol gave no indication of soot, and ethanol only began sooting at very high pressures (around 1100 psia). Propanol-1, on the other hand, exhibited sooting problems at much lower pressures (around 40 atmospheres).

Sooting was first observed around 7 atmospheres for decane and heptane and around 6 atmospheres for n-pentane. The upper limit for data acquisition due to sooting was approximately 52 atmospheres for n-pentane and n-heptane and around 32 atmospheres for n-decane, although the test range extended to 55 atmospheres.

4.2.3 Burning Rates

All the natural convection experimental results were obtained for combustion in air. The ambient air temperature and the fuel inlet temperature were both 300 K for these tests. The 0.95 cm diameter alundum sphere was used for the bulk of the burning rate measurements.

Figures 8 and 9 illustrate the burning rate results for the alcohols and paraffins, respectively. The theoretical results shown in Figures 8 and 9 were calculated using the variable property-variable specific heat gas phase analysis. The quaternary version is illustrated for the high-pressure theory.

The theoretical curves are terminated at high pressures when the critical burning condition is reached. For the low-pressure theory, critical burning was assumed to occur when the liquid surface temperature was equal to the critical temperature of the fuel. Critical burning for the high pressure theory formally occurs when the liquid surface reaches its critical mixing point for the conditions of

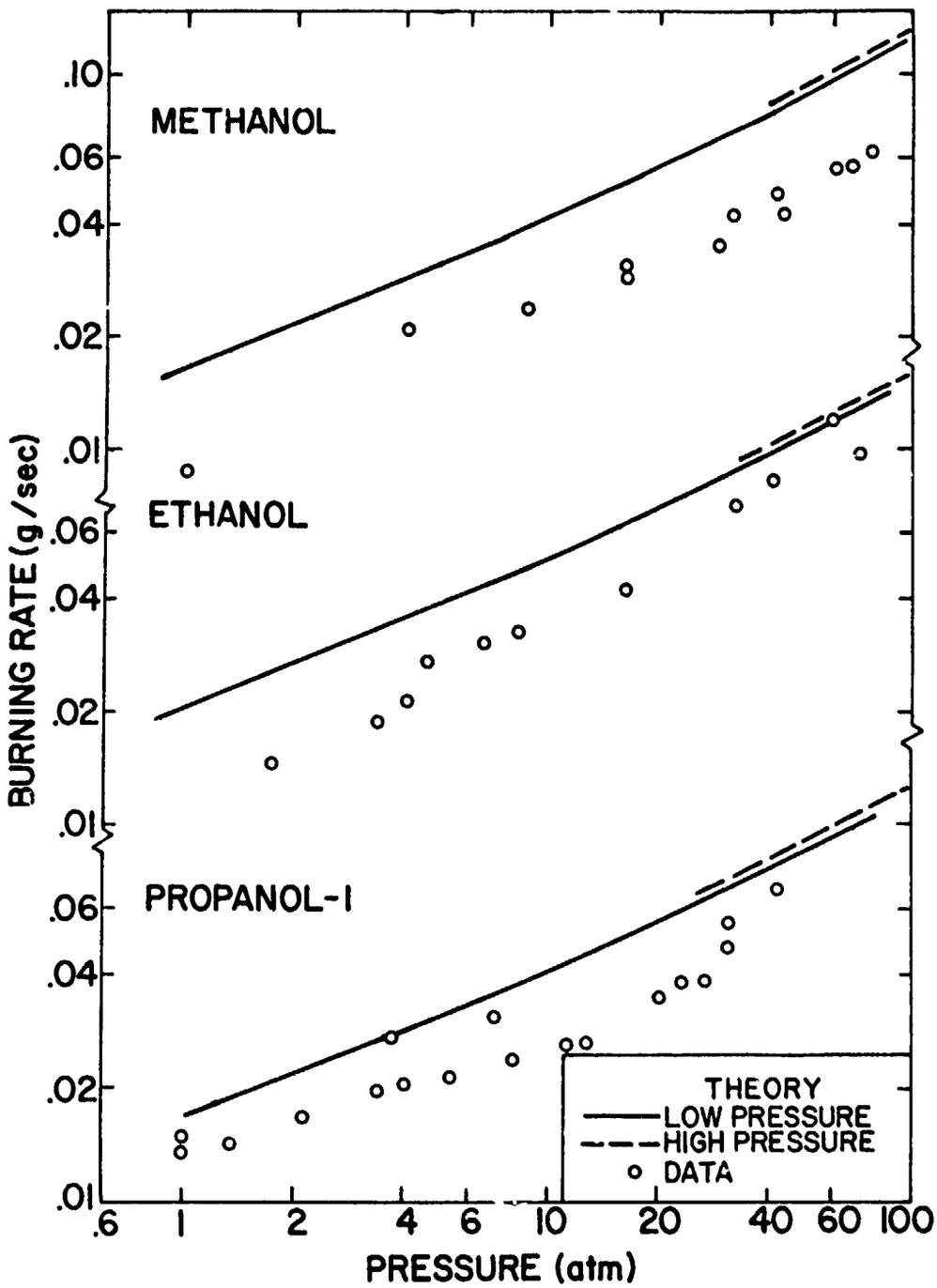

Figure 8 Experimental Burning Rates for Alcohols

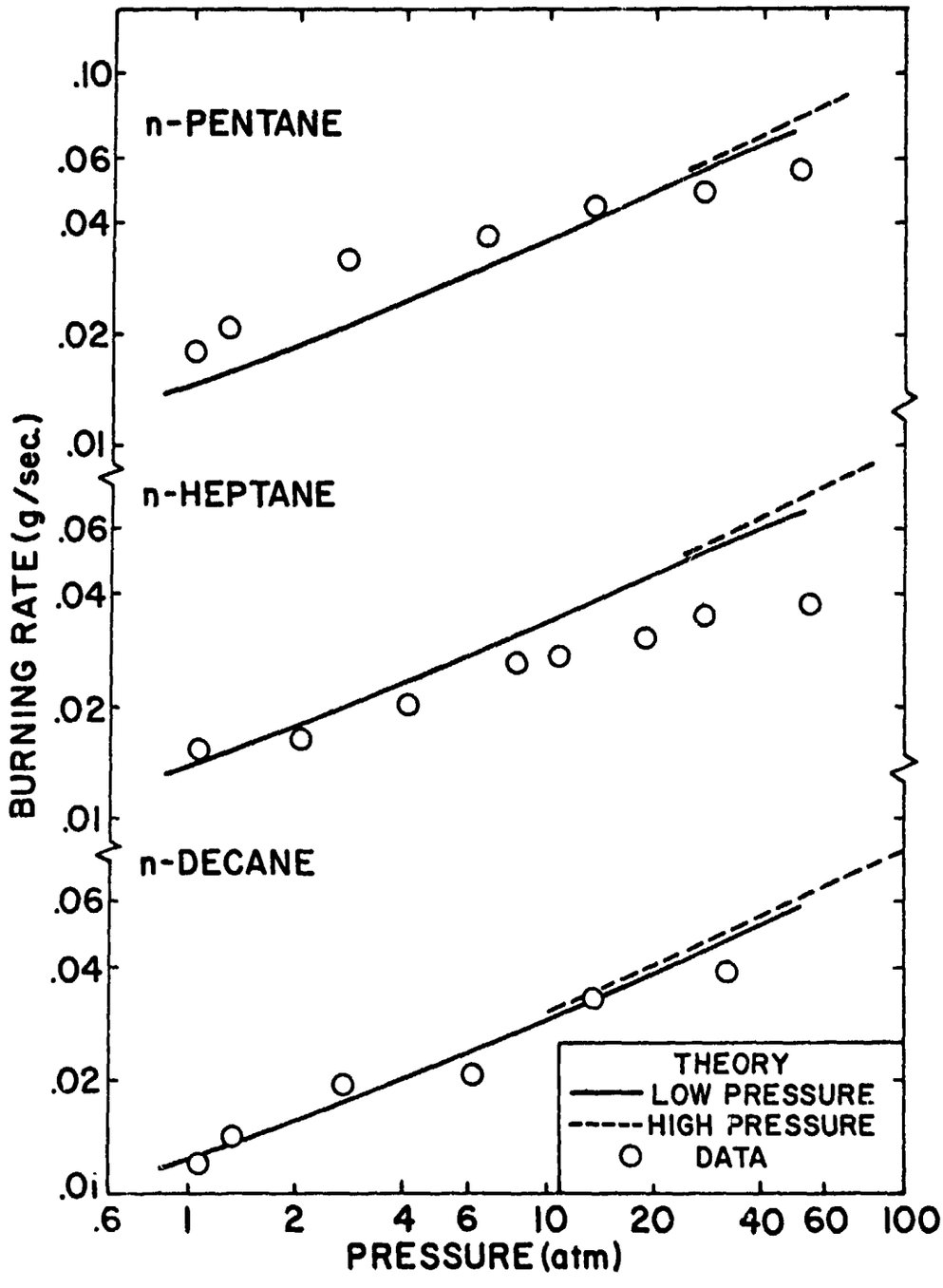

Figure 9 Experimental Burning Rates for N-Paraffins

the combustion process. The burning rate predictions of the two theories are almost identical, although the high pressure theory generally predicts a higher pressure for critical combustion.

The experimental results for methanol and ethanol (Figure 8) were terminated at high pressures due to difficulties in determining the burning rate. At pressures on the order of 80-100 atm, for these fuels, the flame zone would tend to move away from the sphere with increased fuel flow rates and clear evidence of fuel dripping could not be obtained. For both of these fuels vapor jets were observed rather than liquid drops, although methanol presented this problem at slightly higher pressures. This behavior probably indicates the onset of critical burning for these fuels, but the pressure at which this condition occurred could not be defined very precisely.

The burning rates for the remaining fuels in Figures 8 and 9 are terminated at high pressures due to the formation of soot. Ir these cases, carbon spots would form and grow on the surface of the sphere causing the test to be terminated at elevated pressures. The upper pressure limit for testing decreased with increasing molecular weight for the paraffin fuels tested.

The absolute agreement between the theoretical and experimental burning rates in Figures 8 and 9 is comparable to results obtained by Faeth and Lazar [19] in low pressure tests. In particular, the theory gives a reaonsably good indication of the rate of increase of the burning rate with increasing pressure.

The effect of varying sphere size is examined in Figure 10. The sphere sizes employed ranged from 0.63 cm-1.9 cm. For this plot,

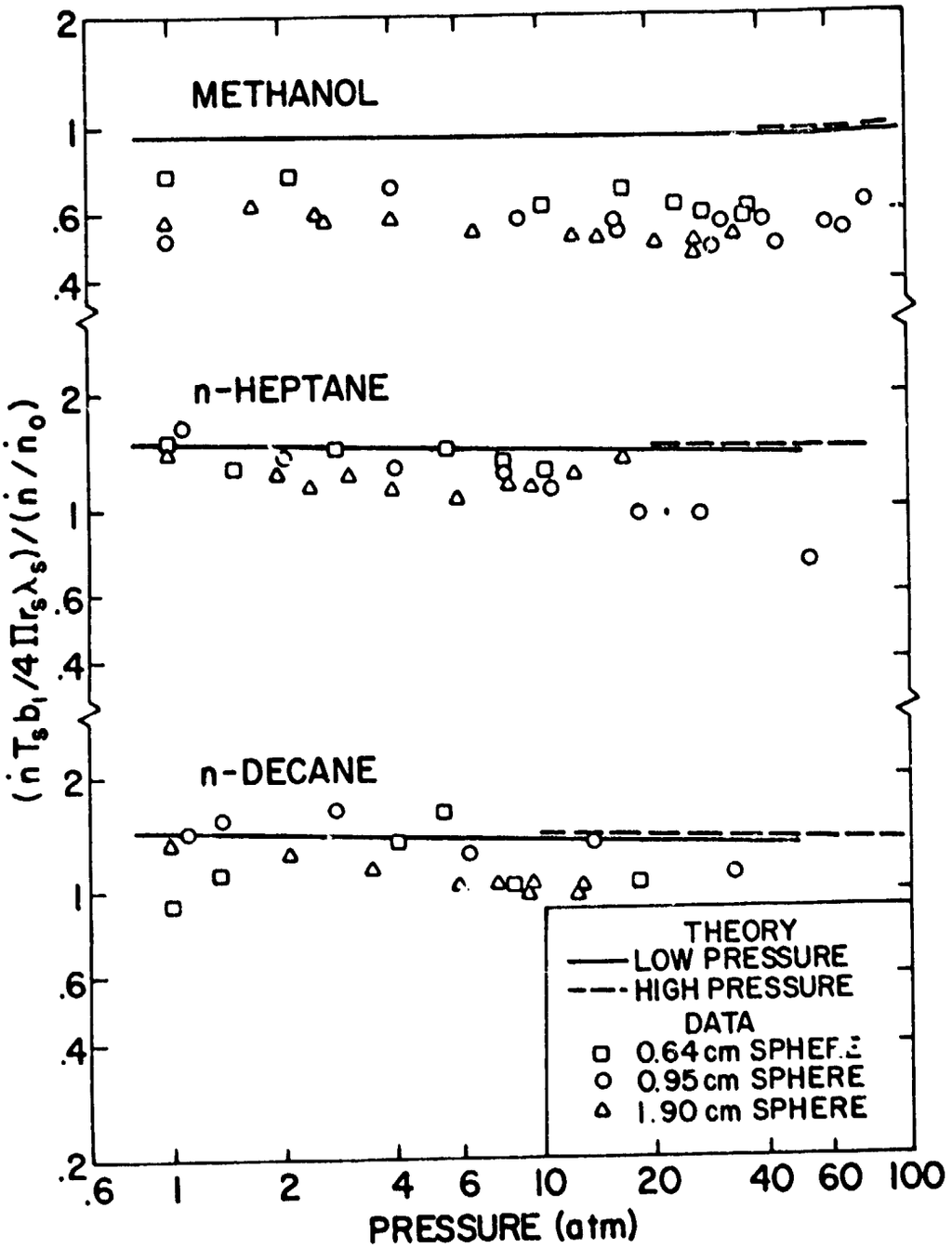

Figure 10 Burning Rates for Variable Sphere Size

the dimensionless burning rate, normalized by the convection correction is employed for the ordinate so that data for various sphere sizes should fall on a single curve.

The results shown in Figure 10 indicate that the normalized burning rate (which corresponds to the no-convection burning rate of the theory) is almost a constant up to the critical burning condition for the present porous sphere experiments. This is due to the fact that the no-convection burning rate is largely dependent upon the total enthalpy rise of vaporization, which does not change to a great degree with increasing pressure for porous spheres. For porous sphere combustion, the reduced heat of vaporization near the critical point is compensated by increases in the enthalpy rise required to bring the fuel from the inlet to the surface temperature.

The fact that the normalized burning rate is relatively constant indicates that the increase in burning rate with increasing pressure in Figures 8 and 9 is largely due to convection effects. The present experimental results represent a reasonably good test of the burning rate correction for natural convection, since the Grashoff number, based upon the Spalding [55] definition used in Equation (2.50), varies in the range 10^4-10^8.

4.2.4 Liquid Surface Temperatures

The liquid surface temperature results for the six fuels are illustrated in Figures 11 and 12. The boiling point curves and the surface temperature predictions of both the low-pressure and the quaternary high-pressure theories are shown on the figures along with the data.

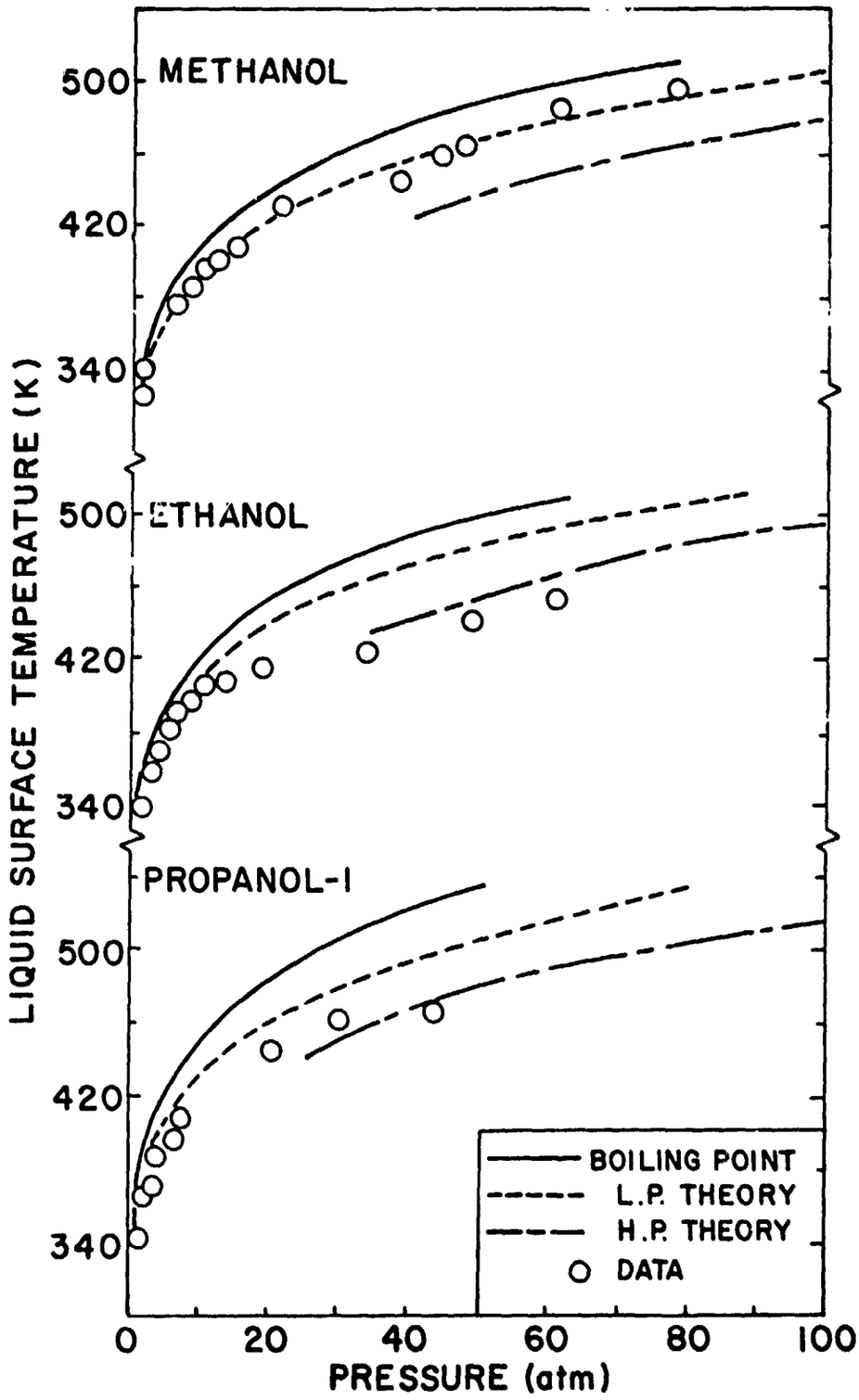

Figure 11 Liquid Surface Temperatures for Alcohols

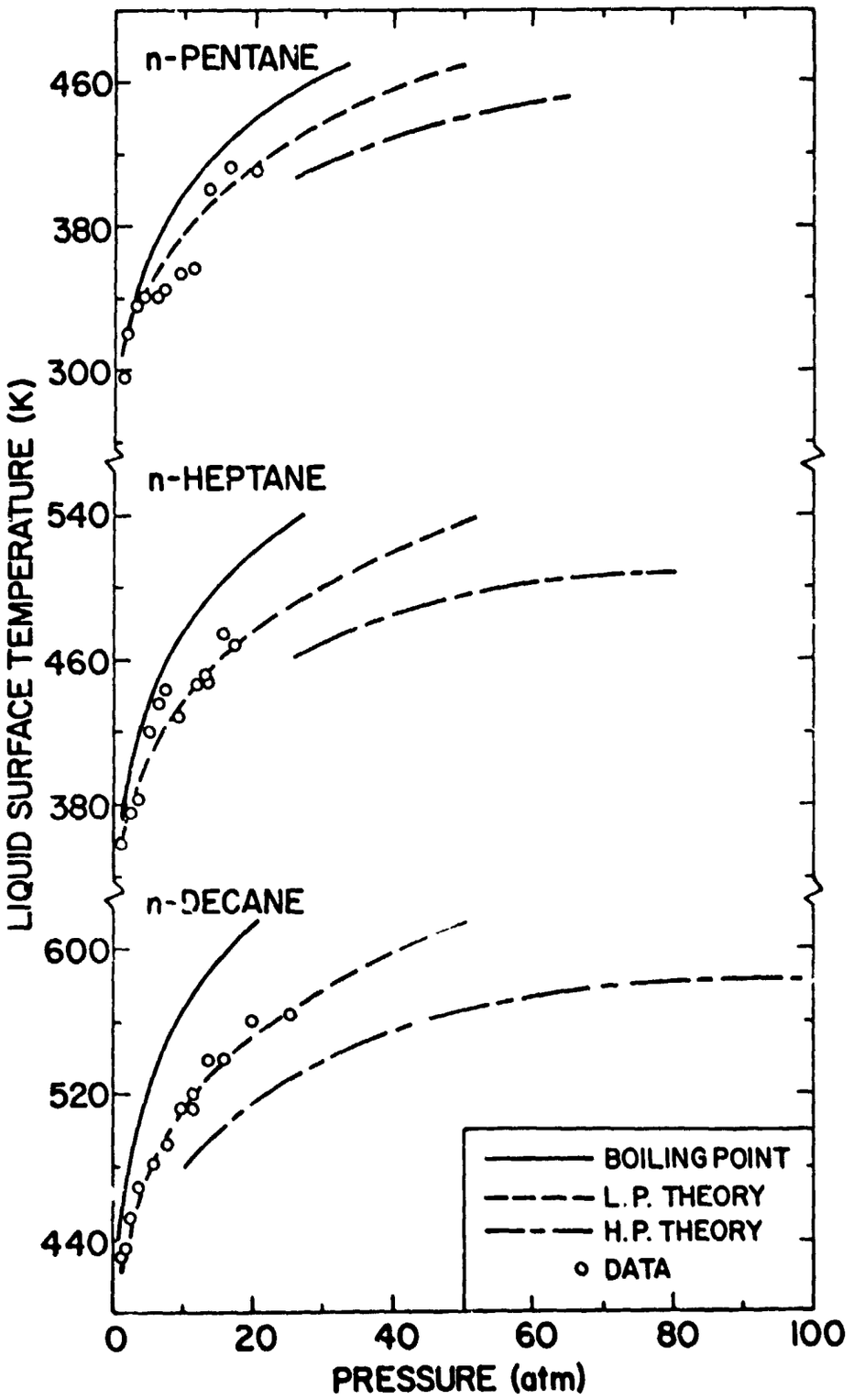

Figure 12 Liquid Surface Temperatures for N-Paraffins

The difference between the two theories is more obvious with regard to surface temperatures, than was the case for the burning rates, with the high pressure theory predicting the lowest surface temperature at a given pressure.

It is seen in Figure 11 that the data for ethanol and propanel-1 agrees reasonably well with the high pressure theory at high pressures. For methanol, however, the low pressure theory gives the best estimation of the data over the entire test range. The poorer high-pressure theoretical results for methanol could be due to the large quantities of water vapor in the combustion products of this fuel. Water is difficult to model precisely in the high-pressure phase equilibrium analysis, and materials with high water vapor concentrations in the products have generally shown poorer agreement with the high-pressure theory in the past. [56]

The experimental liquid temperature data for the paraffins shown in Figure 12, could not be extended to sufficiently high pressures to provide an adequate test of the high pressure theory due to the formation of soot. Over the available experimental range, the low pressure theory appears to be adequate for these materials.

4.2.5 Phase Equilibrium Results

Figure 13 illustrates computed gas and liquid phase compositions, at the liquid surface, for propanol-1 and n-heptane. These results pertain to porous sphere combustion in air, with a fuel inlet and ambient air temperature of 300°K. The gas phase composition remains relatively constant as the total pressure is increased for both fuels. In contrast, the liquid phase concentration of dissolved

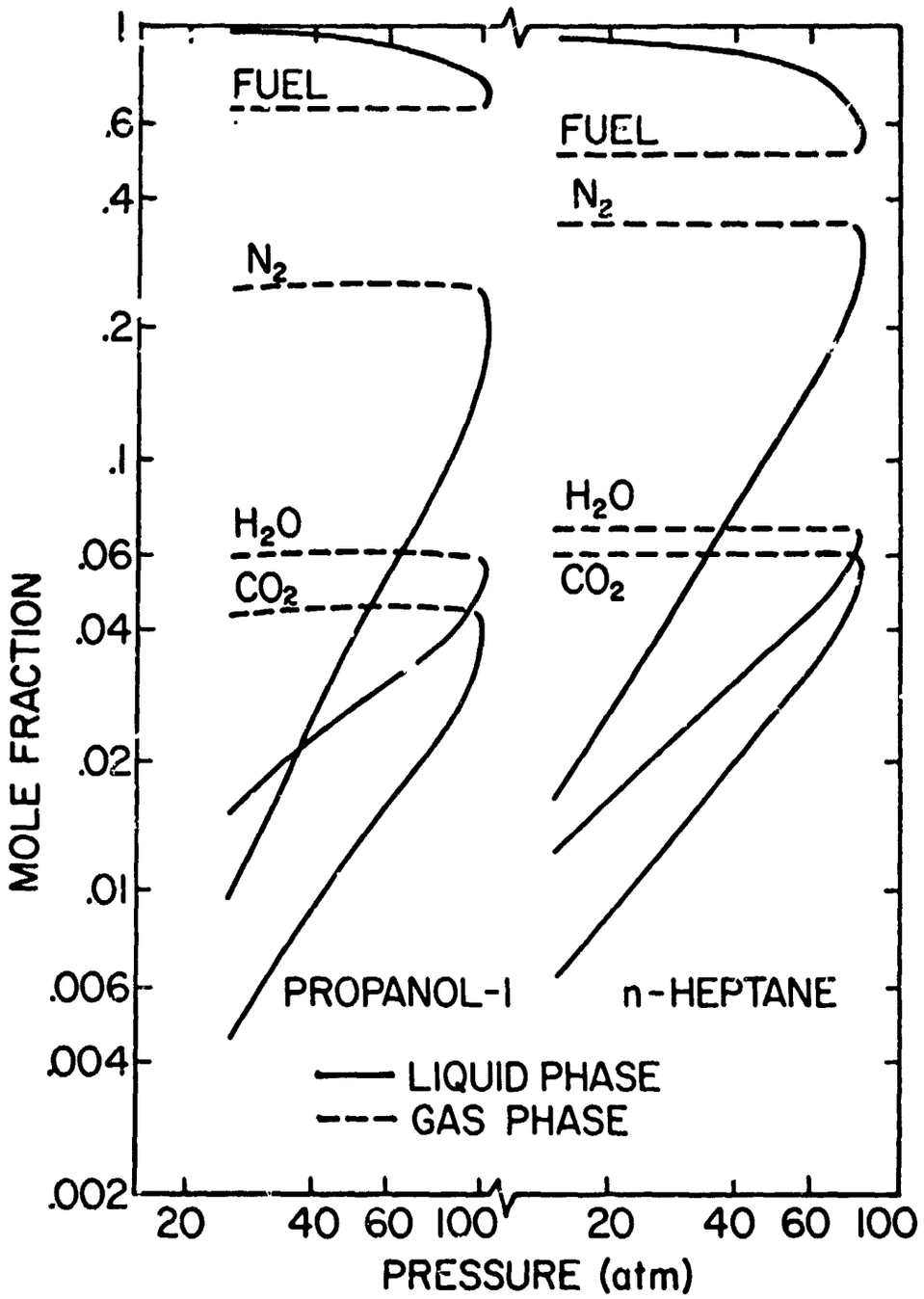

Figure 13 Predicted Liquid Surface Compositions for Porous-Sphere Combustion in Air, with Fuel Inlet and Ambient Temperature of 300°K

gas increases significantly with increasing pressure. The critical mixing point of the surface (the critical combustion condition) is indicated by the equality of the liquid and gas phase composition at this state. The dissolved gas concentration becomes quite large near the critical combustion condition for the present test conditions, reaching values as high as 60% for n-decane.

At pressures higher than the critical combustion condition, the process is similar to the porous sphere combustion of a gas. In this regime, no liquid surface would be observed and a range of fuel flow rates (subject to blow-off and quenching limits) could be accommodated by the sphere at a given pressure, as opposed to the single fuel flow rate possible for liquid fuel combustion at pressures below the critical combustion condition.

4.2.6 Discussion

The preceding theoretical results were obtained with the quaternary phase equilibrium model. The simplified binary model gave essentially the same results with regard to burning rates and liquid surface temperatures. In contrast to high pressure droplet combustion, however, there were significant differences between the critical porous sphere combustion pressures predicted by the two high-pressure theories. The critical combustion conditions for all three theories are compared with pure fuel critical properties in Table 2. In agreement with the experimental findings, both the low pressure and high pressure quaternary theories predict critical burning pressures on the order of 100 atm for methanol and ethanol. The theoretical indication that ethanol should experience critical burning at

Table 2

Predicted Critical Burning Conditions for Porous Sphere Combustion in Air*

Substance	CH_3OH	C_2H_5OH	C_3H_7OH	C_5H_{12}	C_7H_{16}	$C_{10}H_{22}$
Critical Properties						
Pressure	78.5	63.0	51.0	33.3	27.0	20.8
Temperature	513.2	516.0	540.7	469.5	540.2	619.0
Low Pressure Theory						
Total Pressure	109	88	78	48	52	51
Surface Temperature	513.2	516.0	540.7	469.5	540.2	619.0
Binary High Pressure Theory						
Total Pressure	168	125	125	82	108	125
Surface Temperature	489	496	516	450	512	590
Quaternary High Pressure Theory						
Total Pressure	114	100	102	65	80	108
Surface Temperature	486	494	514	449	510	583

*Fuel inlet and ambient air temperature of 300°K, pressure in atm, temperatures in K.

pressures somewhat below methanol is also in qualitative agreement with the fact that experimental difficulties in determining burning rates were encountered at somewhat lower pressures for ethanol, c.f. Figure 8.

All the previous theoretical results were obtained with the variable property--variable specific heat gas phase analysis, using the properties listed in Table 3. The use of the variable property-constant specific heat and constant property gas phase analysis gave essentially the same results, when the respective constant properties in each of these cases were evaluated at average conditions in each region. The effect of parametric variations of the k_{ij} and the gas phase properties listed in Table 1 was also examined. The value of χ_i had the greatest influence on the prediction of liquid surface temperatures and critical burning conditions. Quantitatively, the effect of variations of this parameter was similar to that encountered in earlier studies of high pressure combustion. [56, 57] Variations in the predicted burning rates were almost in direct proportion to variations in the value of λ_i, and were relatively insensitive to changes in χ_i.

4.3 Forced Convection Tests

4.3.1 Fuels and Range of the Tests

The objective of this part of the investigation was the determination of high pressure droplet burning and evaporation rates and liquid surface temperatures in a simulated combustion chamber environment. The experiment considered various gas flow velocities past the test droplet and various pressure levels to provide an evaluation of both the effects of forced convection and high pressure

Table 3

Properties Used in the Gas Phase Calculations

Material	A cal/mol K	B cal/gmol K^2	$\lambda_i \times 10^4$* cal/sec cm K	$\lambda_e \times 10^4$* cal/sec cm K	χ_i cal/gmol K	χ_e cal/gmol K	Q_s** K cal/gmol
Methanol	11.0	0.009	2.26	1.64	14.0	8.29	161.7
Ethanol	17.6	0.013	2.22	1.61	19.2	8.60	305.5
Propanol-1	22.0	0.019	2.17	1.59	21.8	8.20	452.2
n-Pentane	31.8	0.029	1.78	1.57	21.9	8.17	782.0
n-Heptane	44.1	0.040	1.72	1.57	23.6	8.17	1075.9
n-Decane	62.7	0.057	1.54	1.57	28.0	8.17	1516.6
CO_2	9.0	0.0025					
H_2O	7.9	0.0018					
N_2	6.9	0.0008					
O_2	7.1	0.0010					

*At 1000°K, λ from Equation (2) at any other temperature.

**At 298°K.

phenomena on droplet combustion. The experimental tests focussed upon droplet combustion and evaporation at atmospheric and high ambient pressures.

The tests at atmospheric pressure provided baseline data for the high pressure tests. Fuels considered in this phase of the investigation included methanol, ethanol, propanol-1, n-pentane, n-heptane, and n-decane. The ambient gas temperature range was from 600 to 1530°K and the ambient oxygen molar concentrations included 13%, 9.5% and pure evaporation. The Reynolds number range, based upon approach conditions, varied from 30 to 300. These baseline tests employed the swirl-stabilized burner described in Chapter III to provide the hot combustion gas environment around the test droplets. The 0.95 cm sphere was employed in the tests, using both alundum and sintered bronze spheres.

For the high pressure droplet tests, the fuels included ethanol and n-heptane. Three ambient molar oxygen concentrations were employed. These included molar concentrations of zero, 9.5 and 13 percent, respectively. The two combustion cases considered ambient oxygen concentrations of 9.5 and 13 percent and the ambient gas temperature was maintained around 1150°K. For the purely evaporative case the ambient gas temperature was maintained around 1260°K.

The Reynolds number range for the elevated pressure tests was from 70 to 672 and the pressure range was from one to 40 atmospheres. The tests employed a porous sphere having a 0.95 cm diameter. Both alundum and sintered bronze spheres were used, although the bulk of the measurements were made using the alundum spheres.

The experimental burning rate measurements and liquid surface temperature measurements reported in the remainder of this chapter for the atmospheric baseline and high pressure forced convection tests represent the average values for a series of separate runs performed at the same ambient gas temperatures and ambient pressures. The values obtained from the individual tests were within 3% of the average.

4.3.2 Observations

A pale blue flame was observed around the leading face of the sphere and close to the sphere surface for the combustion of the alcohols. The tail of the flame was yellowish and extended several diameters above the sphere. These characteristics are typical of an envelope flame. The combustion flames of the n-paraffins were almost completely yellow, and the flame of n-decane, in particular, was quite smoky.

For a finite ambient oxygen concentration, a well-defined luminous wake was present around the test droplet. With decreasing ambient oxygen concentration, the flame zone would move away from the droplet and the intensity of the luminosity would decrease. For negligible ambient oxygen concentration (evaporative case), a diffuse luminous wake was present at high ambient gas temperatures even though there was no flame resulting from exothermic reaction. This wake was probably due to radiation from hot carbon particles formed by decomposition of the fuel in the burner gases.

In agreement with the observations of other investigators [19], methanol did not exhibit a luminous wake at negligible ambient oxygen

concentrations and high ambient gas temperatures. This behavior may be attributed to the high resistance of methanol to the formation of carbon particles upon decomposition. The behavior of methanol was similar to the other fuels under oxidation conditions, however, although the flame luminosity was less intense.

At higher pressures the luminosity of the combustion flames for both ethanol and n-heptane increased dramatically with increasing ambient oxygen concentration. The rate of soot formation intensified with decreasing ambient oxygen concentration as the pressure was increased for the combustion cases employing n-heptane as a fuel.

In the open atmosphere baseline tests, side flames were observed at very high Reynolds numbers. These flames are characterized by the flame stabilizing along the sides of the sphere with the forward portion of the sphere extinguished. This phenomenon was not observed in the pressurized tests. No attempt was made to determine precisely when side flames occurred, since the determination of blow-off conditions was not an experimental objective. All measurements were made when the droplet burned with an envelope flame. There was no evidence of strictly wake flames, in which the flame resides totally in the downstream wake of the sphere, over the Reynolds number, ambient pressure and ambient gas temperature range of the tests.

4.3.3 Burning and Evaporation Rates

4.3.3.1 Atmospheric Pressure Baseline Test Results

Table 4 lists the computed properties of the ambient gas at the droplet test section for the most widely run test conditions.

The oxygen mole fraction in the ambient gases quoted in this table is an effective mole fraction based upon the concentrations of possible oxidizing species (O_2, O, NO) since the minor species (O, NO, etc.) are present only in very small concentrations at these gas temperatures.

Table 4

Properties of the Ambient Gas for the Test Conditions

$X_{O2\infty}$	T_∞ °K	CO	CO_2	N_2
0.130	1145	0.000	.132	.738
0.095	1145	0.000	.190	.715
0.000	1255	0.000	.348	.652

Plots of the experimental and theoretical burning rates versus ambient gas temperature at atmospheric pressure are shown for the alcohols in Figure 14, while Figure 15 gives similar results for the n-paraffins. The experimental results were corrected by the use of the multiplicative correction for forced convection given by Equation (2.51). The theoretical predictions were made using the variable property-variable specific heat low pressure model of Lazar and Faeth [42]. The theoretical burning rates tended to be lower than the measured rates for all fuels. The theory does predict the correct trends in vaporization rates with ambient gas temperature as may be

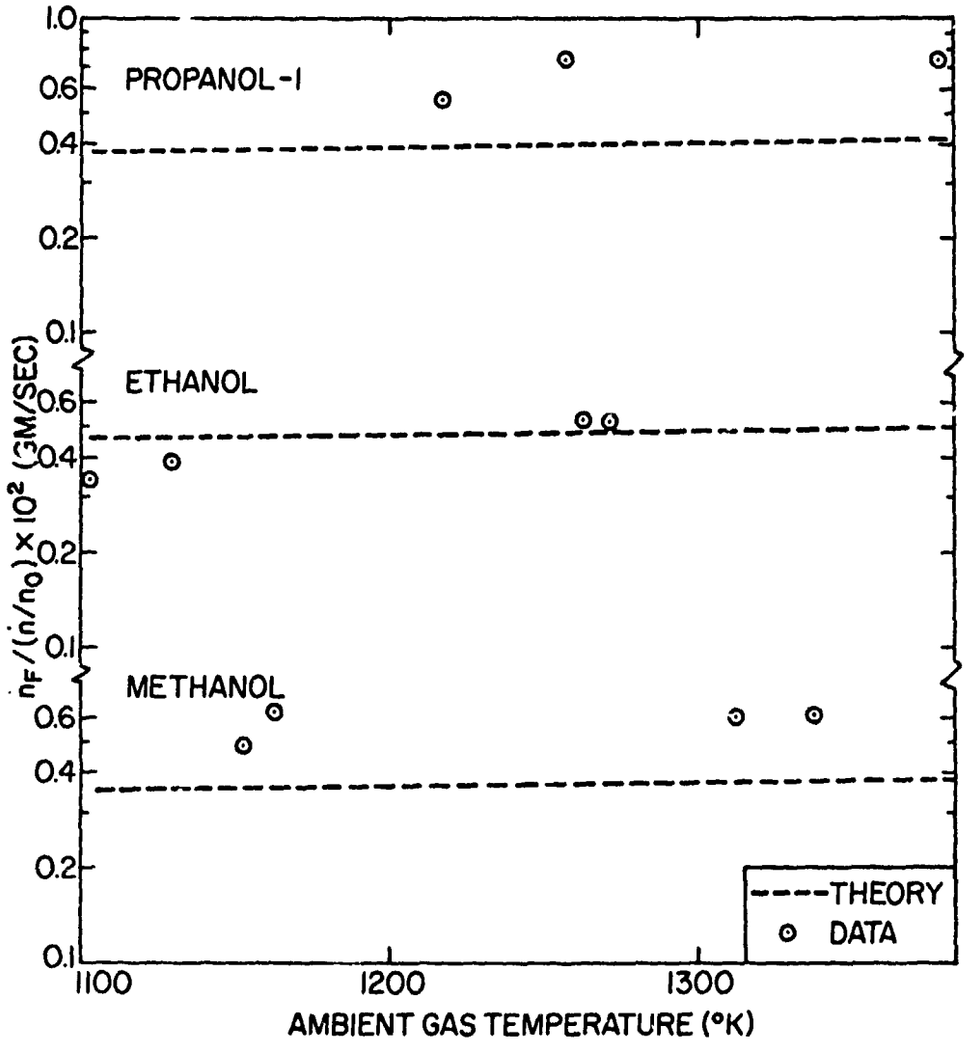

Figure 14 Atmospheric Pressure Burning Rates of the Alcohols, Ambient Oxygen Concentration 9.5% (Molar)

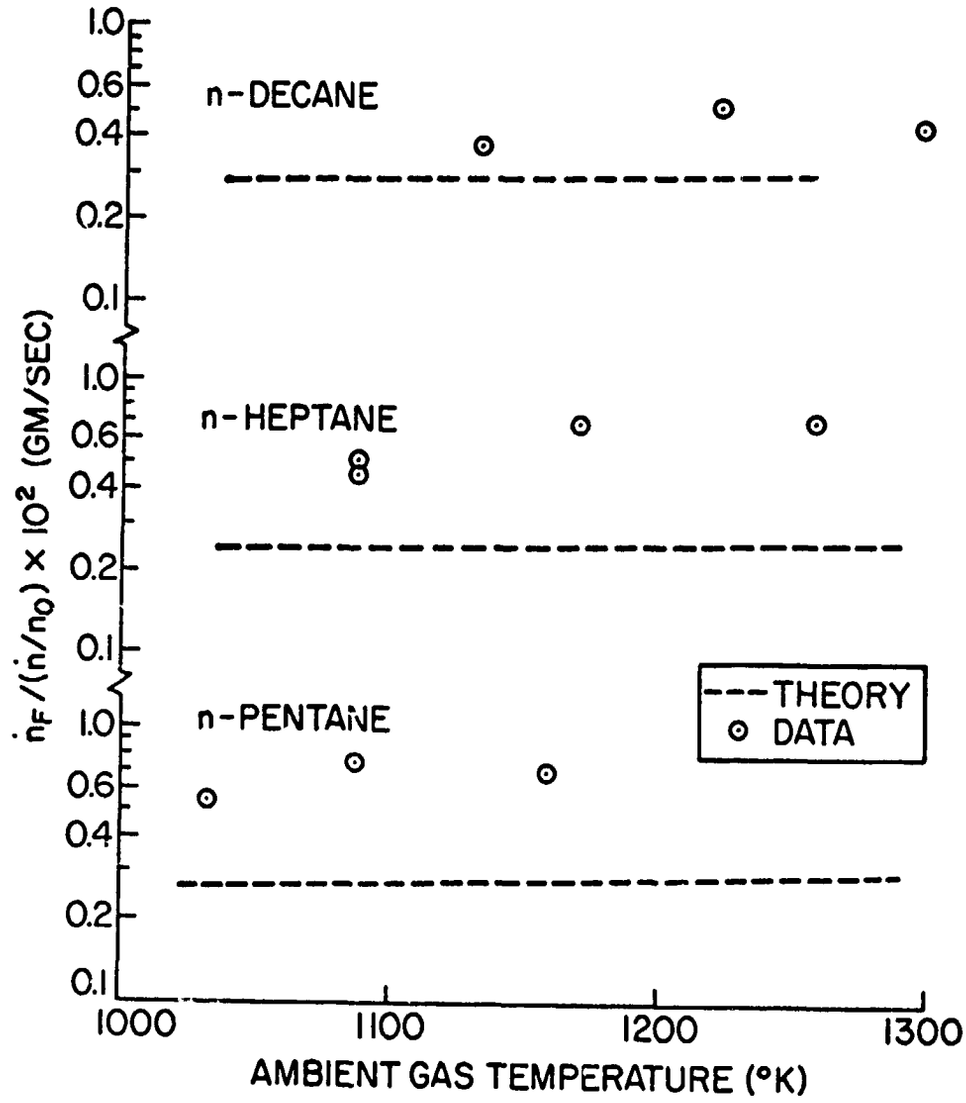

Figure 15 Atmospheric Pressure Burning Rates of the N-Paraffins, Ambient Oxygen Concentration 9.5% (Molar)

noted from the slopes of the curves. These tests results are in contrast to the burning rate measurements obtained for the high pressure, natural convection, cold gas tests discussed in the previous section. For these tests the theoretical predictions were found to be, on the average, higher than the observed burning rate. The experimental results did, however, confirm the theoretical prediction that ambient gas temperature has little effect on the burning rate.

Evaporation rates with zero oxygen concentration in the ambient gases are shown in Figures 16 and 17 for the different fuels. The theoretical predictions were lower than the experimental values over the entire test range. The evaporation rates followed a fairly linear increase with ambient gas temperature.

The evaporative case for methanol in Figure 18 is shown over a wider temperature range than the earlier results. From this plot it can be seen that the correct trend in evaporation rates is observed between theory and experiment and that there is fair agreement at the lower ambient gas temperatures. A consideration of the evaporation rates in Figures 16 and 17 reveals that an extrapolation of the experimental and theoretical results in these figures lead to the same general conclusion.

The behavior of the theoretical evaporation curves at various ambient gas temperatures is examined in Figure 19 for ethanol and n-heptane. The results are for vaporization rates from a 0.95 cm sphere at one atmosphere pressure. The results show that with decreasing ambient gas temperatures, the vaporization rates are quite sensitive to ambient oxygen concentration.

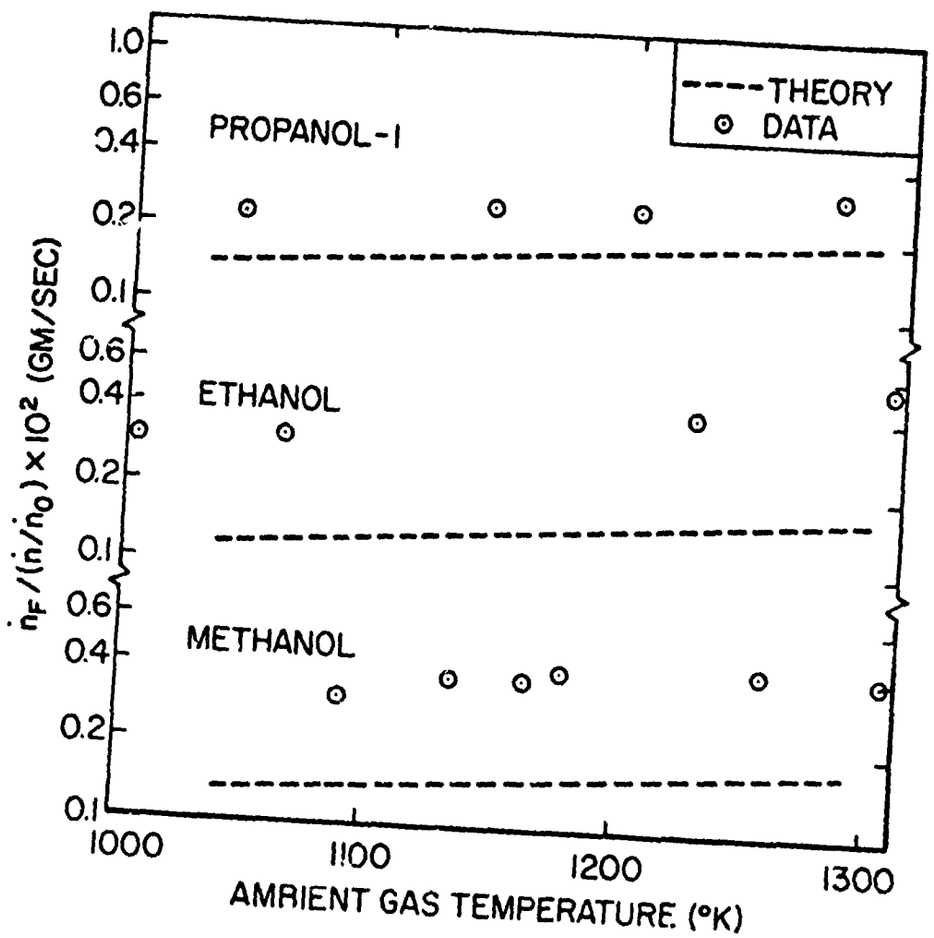

Figure 16 Atmospheric Pressure Evaporation Rates for Alcohols

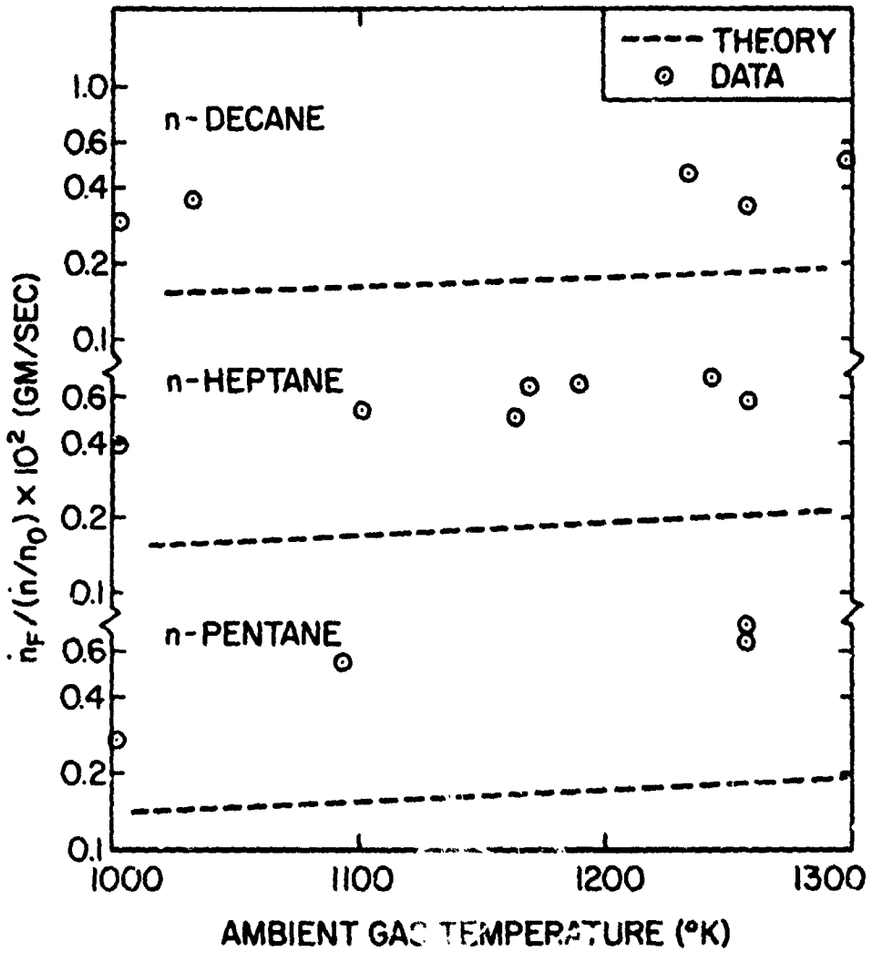

Figure 17 Atmospheric Pressure Evaporation Rates for N-Paraffins

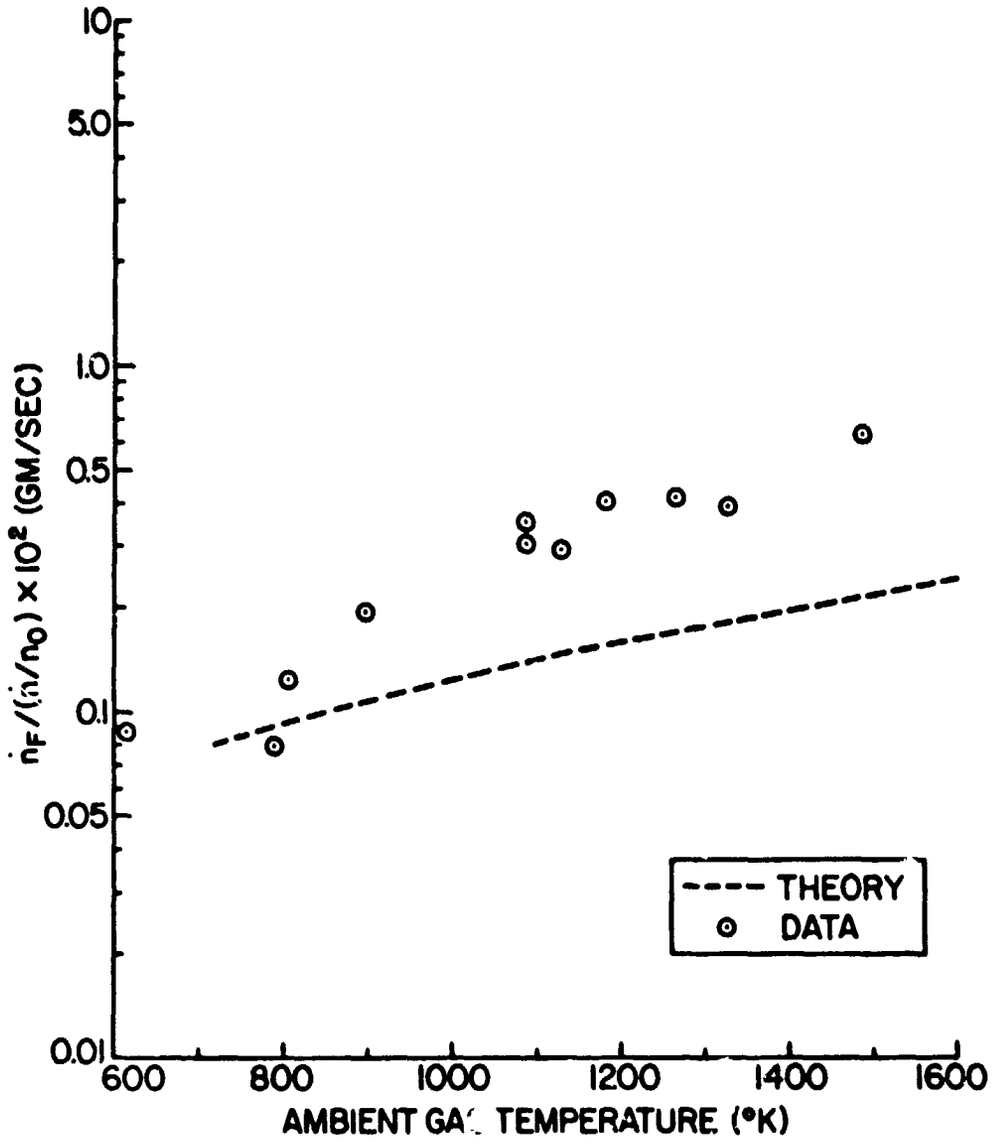

Figure 18 Methanol Evaporation Rates

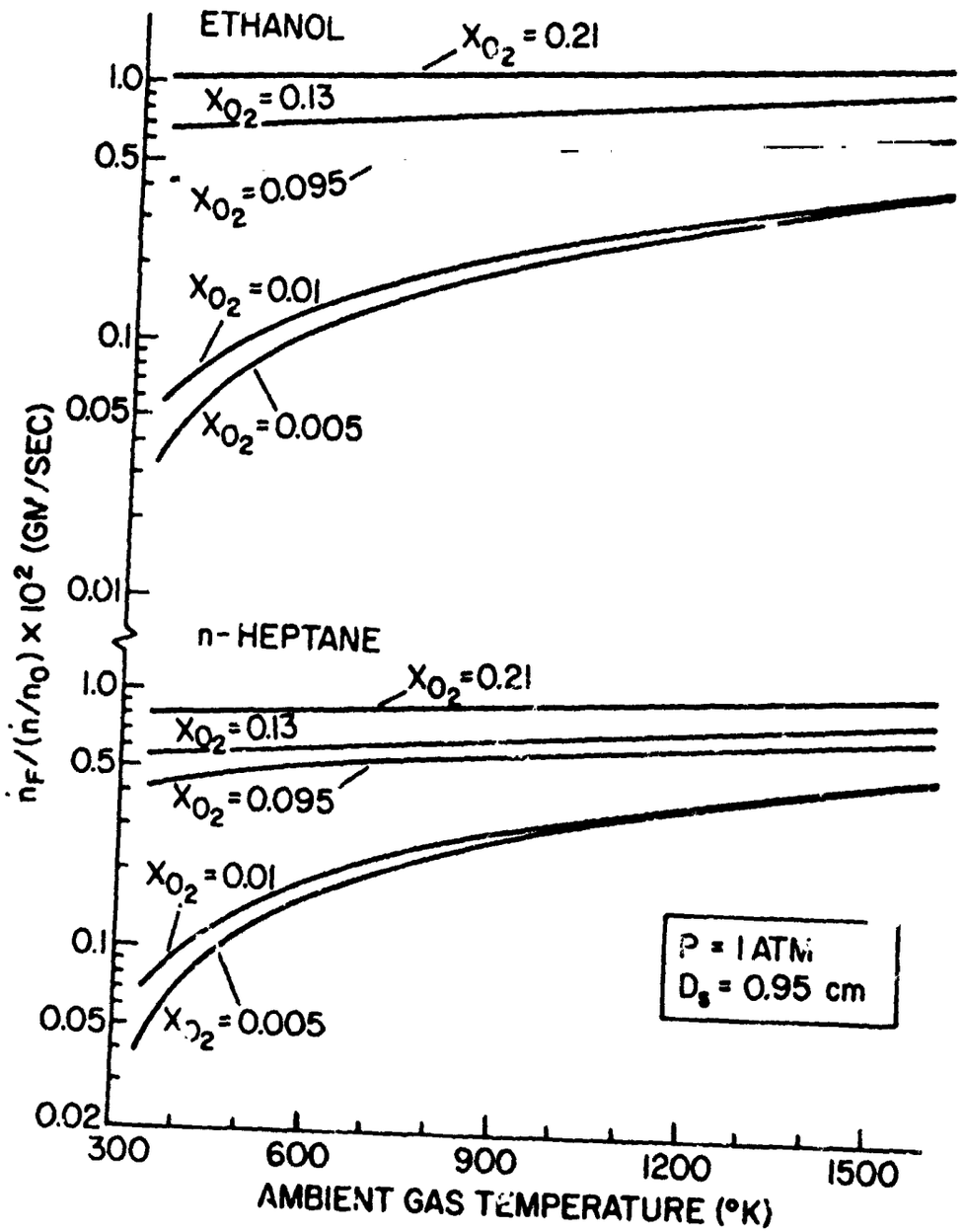

Figure 19 Theoretical Vaporization Rates

Liquid surface temperatures as a function of gas temperatures for ethanol and n-pentane are shown in Figure 20. The low pressure theory tended to predict lower droplet surface temperatures than the measured results. This was observed for both the combustion and evaporative cases, although the difference was more pronounced with respect to the evaporative case.

The effect of ambient oxygen concentration on the vaporization rate at a fixed ambient gas temperature of 1145°K is examined in Figure 21 for ethanol and n-heptane. There is fairly good agreement between theory and experiment at higher ambient oxygen concentrations. The poorer agreement between experiment and theory at low ambient oxygen concentrations was observed by other investigators [19] under similar test conditions.

4.3.3.2 High Pressure Test Results

Plots of the experimental burning rate versus pressure at various ambient oxygen concentrations are shown in Figures 22 and 23 for ethanol and n-heptane. The theoretical predictions of the variable property-variable specific heat versions of the low pressure and high pressure quaternary theories are shown along with the data. For these tests the ambient gas temperature was maintained around 1145°K (1600°F) for the two combustion cases and 1255°K (1800°F) for the evaporative case. The sphere size employed for these tests was 0.95 cm in diameter.

The theoretical curves are terminated at high pressures when the critical burning condition is reached (denoted by an asterisk).

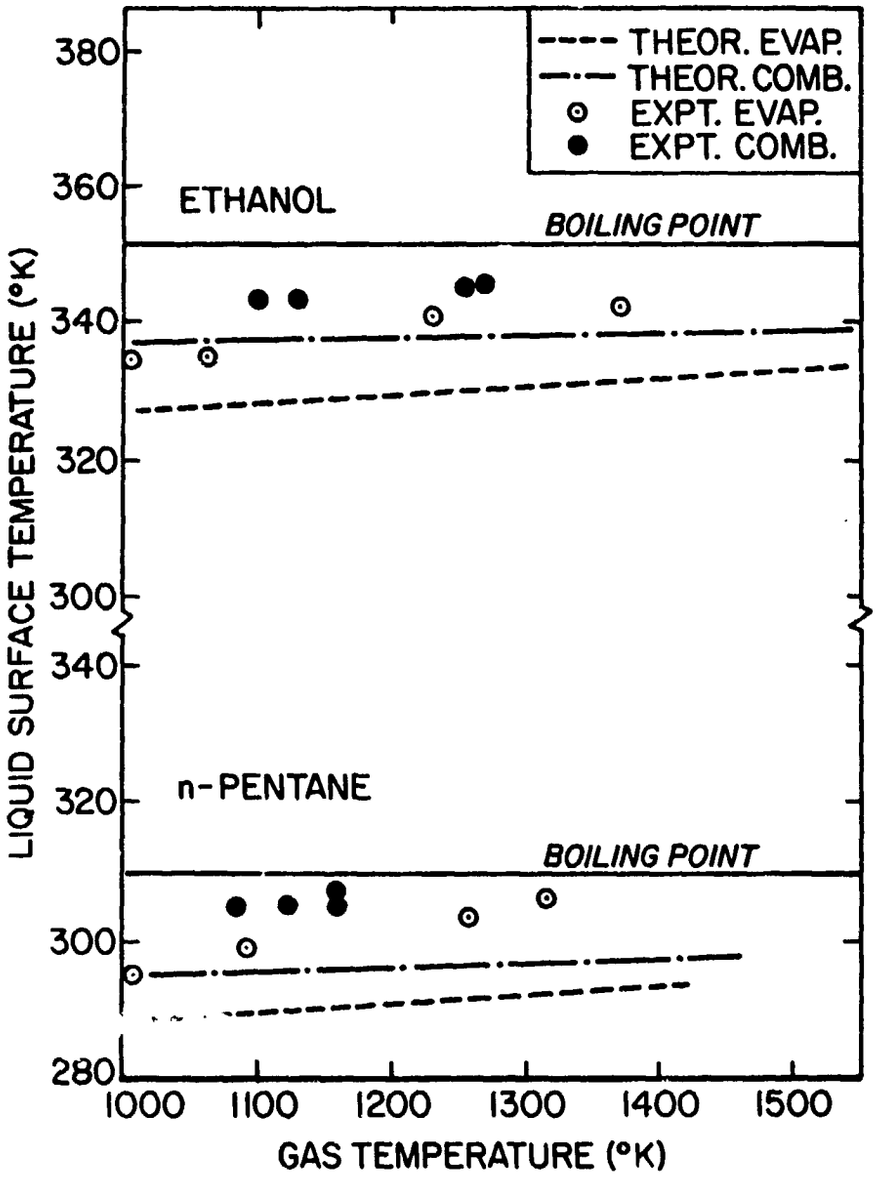

Figure 20 Liquid Surface Temperatures During Evaporation and Combustion for Ethanol and N-Pentane

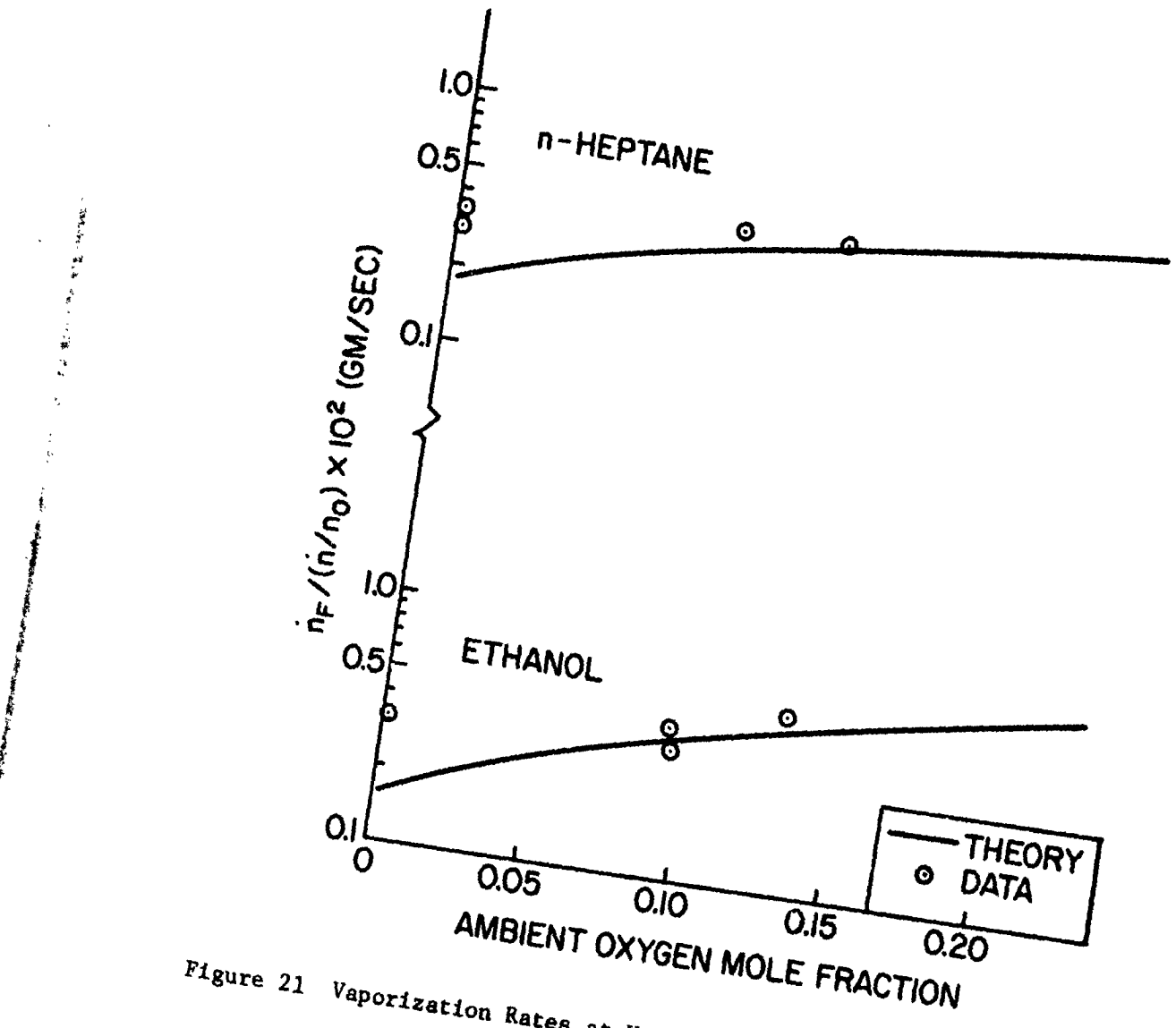

Figure 21 Vaporization Rates at Various Ambient Oxygen Concentrations

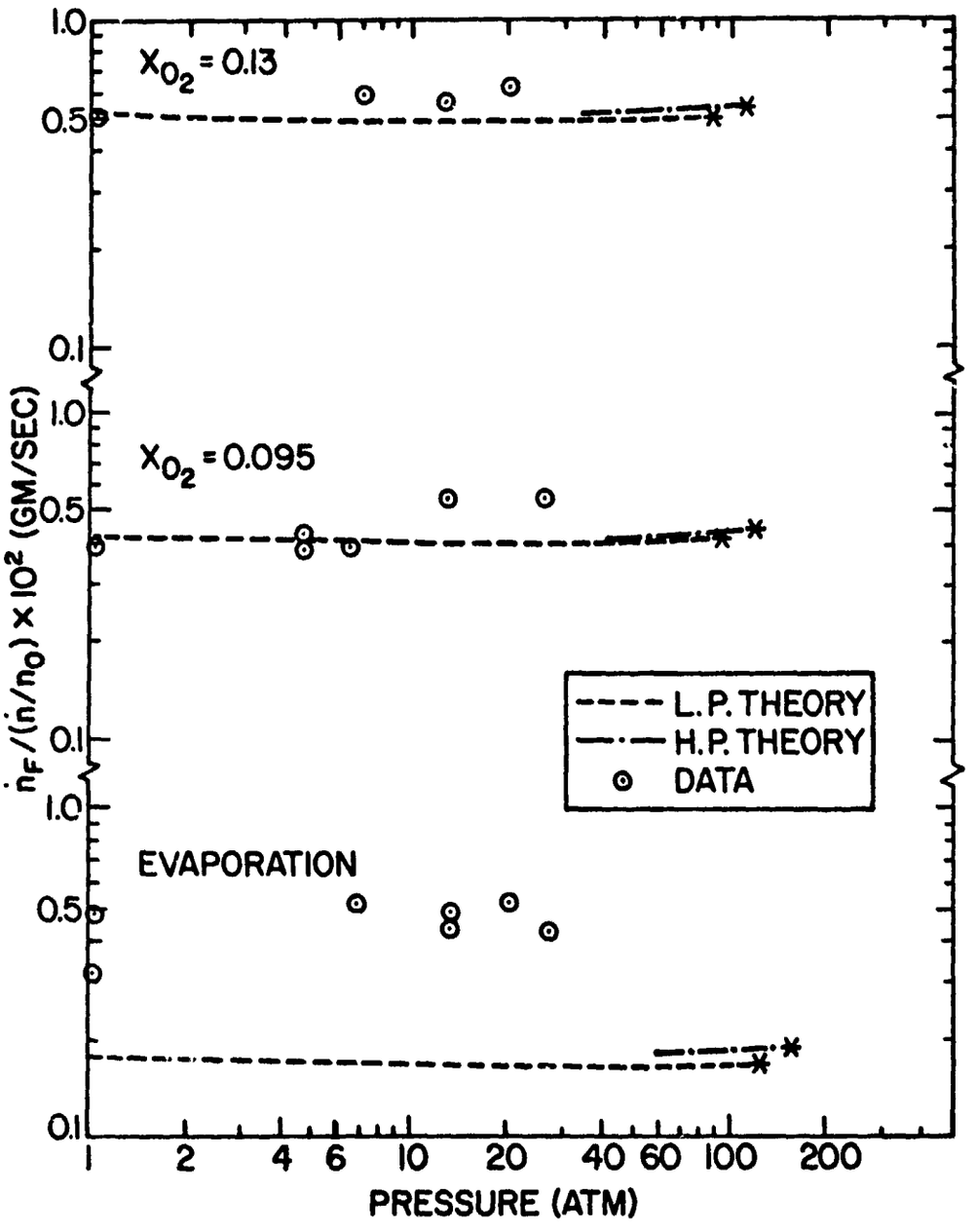

Figure 22 Ethanol Vaporization Rates

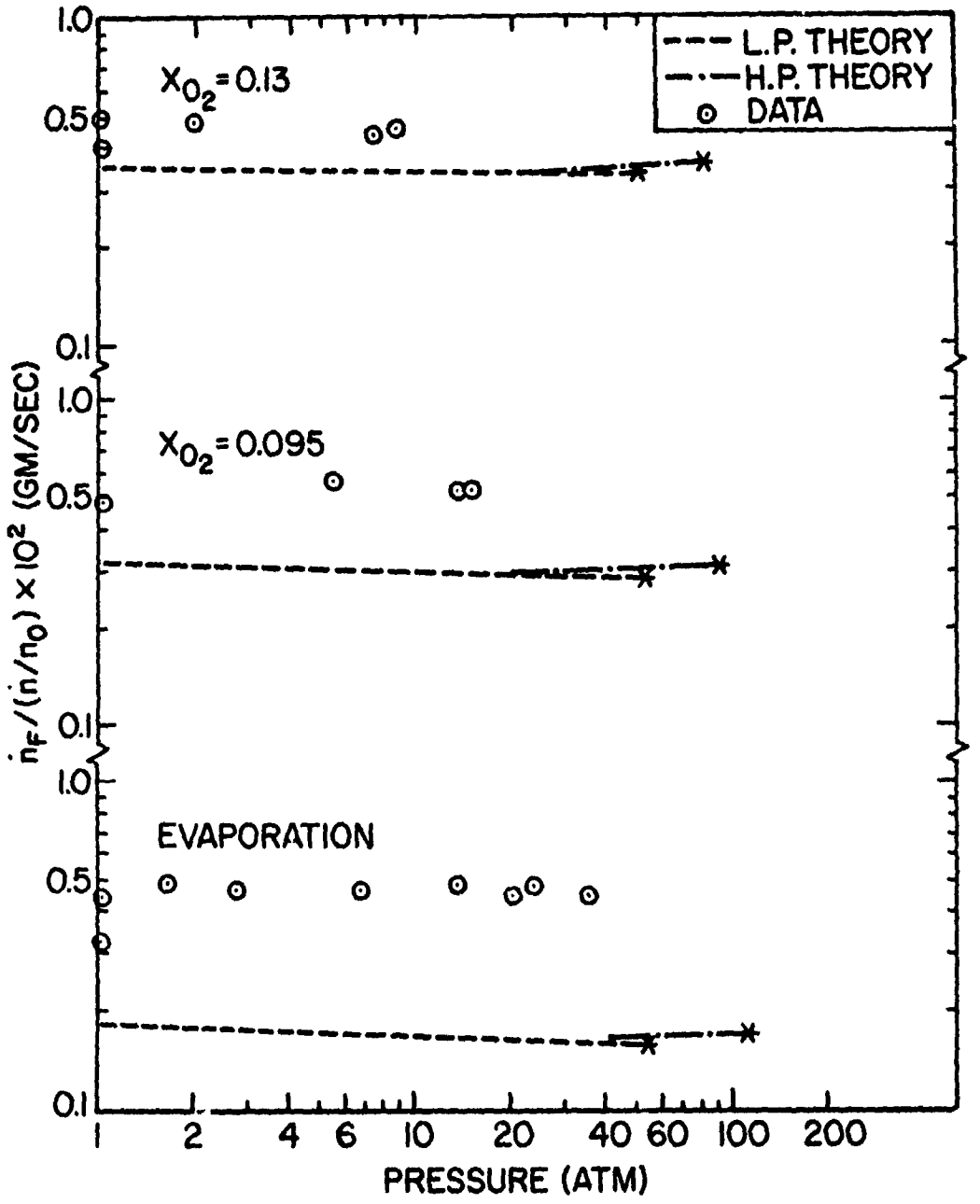

Figure 23 N-Heptane Vaporization Rates

The burning rate predictions of the two theories are in reasonable agreement with the experimental results at the higher ambient gas temperatures considered in these tests. These findings are consistent with the results of the natural convection, cold gas test results. The greatest difference between the two theories lies in the predicted critical burning condition. The low pressure theory predicts a significantly lower pressure for critical combustion, at a given ambient oxygen concentration, than the high pressure theory. The difference between the estimations of critical combustion pressures is greater in the case of n-heptane than for ethanol. Both theories predict an increase in the ambient pressure required for critical burning as the ambient oxygen concentration is reduced.

The experimental curves for n-heptane were termined due to the formation of soot for the two combustion cases. The combustion flame for the .095 molar oxygen concentration case was particularly smoky at pressures in the vicinity of 20 atmospheres. The experimental curve for the evaporative case was terminated due to experimental difficulties associated with maintaining a fully wetted sphere surface. At high pressures and high Reynolds numbers, there was a tendency for the sphere to dry off at the bottom stagnation point and then to progressively overheat.

The experimental curves for ethanol were terminated mainly due to difficulties in maintaining a fully wetted sphere at high pressures. There was no evidence of sooting over the ambient oxygen and pressure range considered in the tests. In both the ethanol and n-heptane combustion cases, the luminosity of the flame increased with increasing ambient oxygen concentration.

The vaporization rates shown in Figures 22 and 23 reveal a similar trend in burning rates with pressure noted for the normalized burning rates (Figure 10) for the natural convection tests. The present test results represent an adequate test of the burning rate correction for forced convection (Equation (2.51)) since the test results (which were taken over a Reynolds number range of 75 to 670) cover a significant portion of the Reynolds number range for which this correlation is applicable.

The liquid surface temperature results for ethanol and n-heptane are illustrated in Figures 24 and 25. The boiling point curve and the surface temperature predictions of both the low-pressure and quaternary high pressure theories are shown on the figures along with the data. The difference between the two theories is more obvious with regard to the prediction of surface temperatures.

For the liquid temperature results, the same general trends that were observed for the cold gas, natural convection tests can be seen for the high ambient gas temperature, forced convection tests. The n-heptane measurements tend to follow the low-pressure predictions, whereas the ethanol experimental results did not extend to high enough pressures to provide an adequate test of the theory. Over the experimental range shown, the low pressure theory appears to be adequate.

The theoretical predictions of the binary high pressure theory are examined in Table 5. This table considers the critical combustion pressures for ethanol and n-heptane at an ambient gas temperature of 1145°K. While both the high pressure binary and quaternary theories predict approximately the same liquid surface

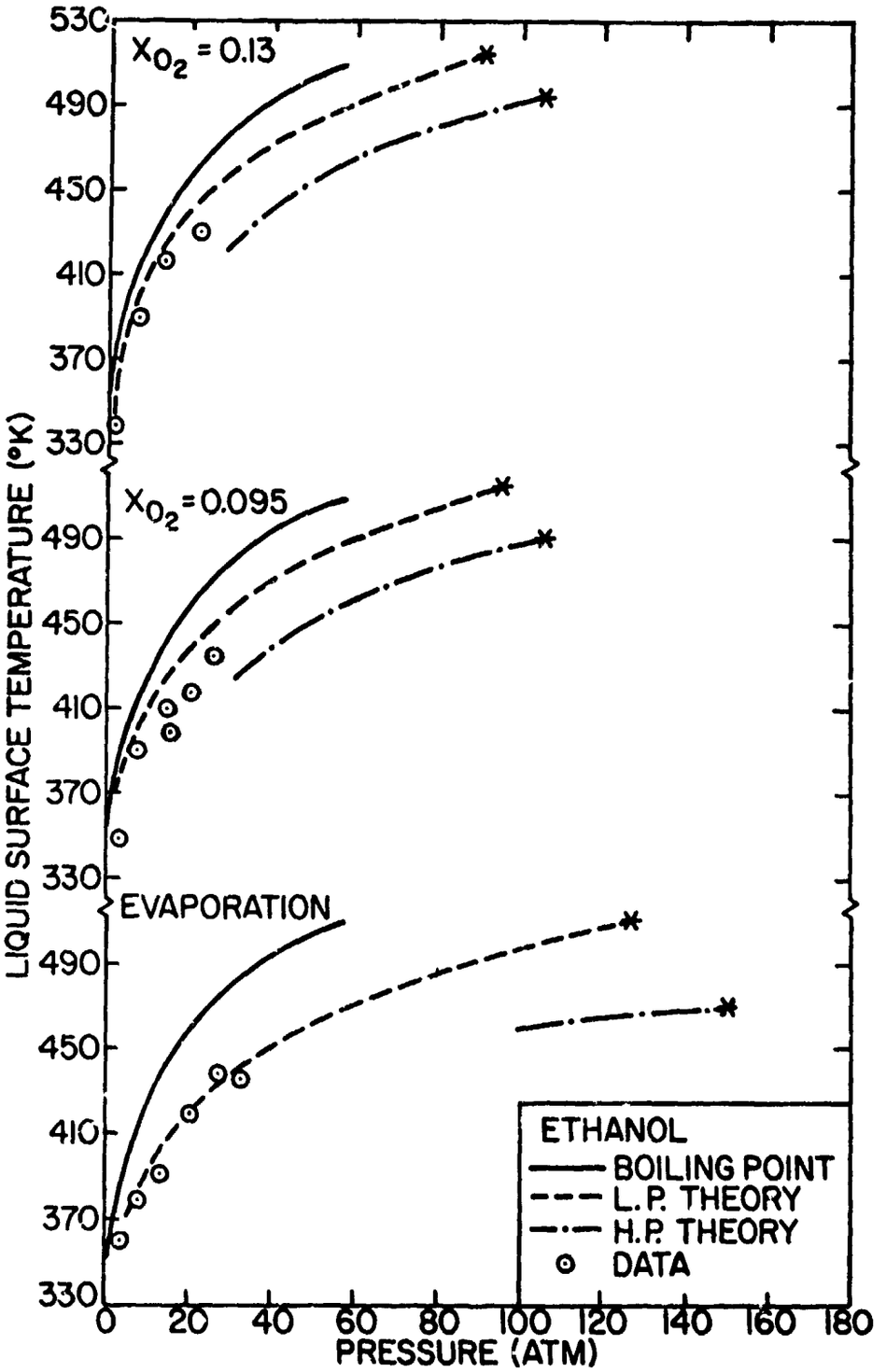

Figure 24 Ethanol Liquid Surface Temperatures

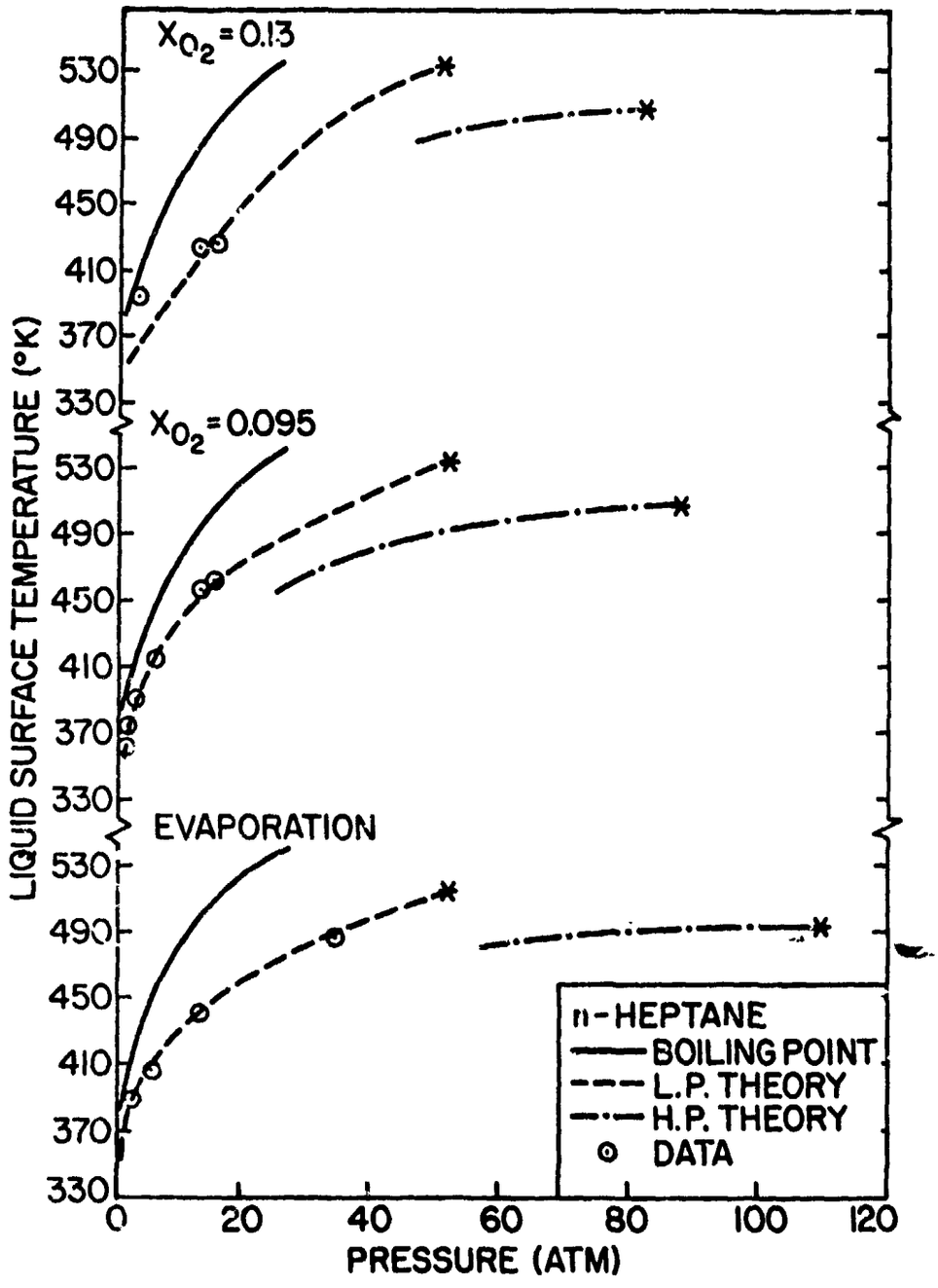

Figure 25 N-Heptane Liquid Surface Temperatures

temperatures, there is a significant difference in the predicted critical combustion pressures. The experimental tests in this investigation considered a four-fold variation in ambient gas temperatures (300°K to 1255°K) at high pressures. Over this ambient temperature and pressure range, there is a consistent tendency between the predictions of the two high pressure versions, with the binary theory generally predicting a much higher pressure for critical burning conditions.

Table 5

High Pressure Theoretical Predictions for Critical Burning Conditions

Fuel	Ethanol		N-Heptane	
	$X_{O_2} = .095$			
Theory	T_R	P_R	T_R	P_R
Binary	.949	2.22	.943	4.22
Quaternary	.946	1.83	.936	3.26
	$X_{O_2} = .13$			
Binary	.957	2.14	.945	3.89
Quaternary	.953	1.67	.939	3.04

The predicted reduced pressures for critical burning at various ambient oxygen concentrations and ambient gas temperatures using the low pressure variable property-variable specific heat model are shown in Table 6 for ethanol and n-heptane. The pressure required for critical burning decreases with increasing ambient oxygen concentration,

Table 6

Predicted Reduced Pressures for Critical Burning (L.P. Theory)
at Various Ambient Gas Temperatures

Fuel	$X_{O_{2\infty}}$	Ambient Gas Temperature (°K)					
		1145	1255	1365	1480	1645	1920
Ethanol	.210	1.37	1.35	1.35	1.33	1.32	1.30
	.130	1.49	1.48	1.46	1.44	1.41	1.38
	.095	1.51	1.51	1.51	1.51	1.51	1.51
	.005	1.97	1.97	1.97	1.97	1.97	1.97
n-Heptane	.210	1.78	1.74	1.74	1.70	1.70	1.67
	.130	1.85	1.85	1.85	1.81	1.81	1.74
	.095	1.85	1.85	1.85	1.85	1.85	1.81
	.005	1.85	1.85	1.85	1.85	1.85	1.85

although the difference is not appreciable considering the ambient gas temperature range involved.

4.3.3.3 Phase Equilibrium Results

Figures 26 and 27 illustrate computed gas an liquid phase compositions at the liquid surface for n-heptane and ethanol. The results in Figure 26 are for porous sphere combustion in air with a fuel inlet temperature of 300°K and an ambient gas temperature of 1145°K. There are no significant differences between the results for the two ambient oxygen concentrations shown in this figure.

The binary theoretical predictions for ethanol are shown in Figure 27. The predicted gas phase mole fractions for the fuel and nitrogen were more sensitive to ambient oxygen concentration than was the case for the quaternary theoretical results.

4.3.3.4 Discussion

The low pressure and high pressure theories gave essentially the same predictions of burning rates at high pressures in agreement with the cold gas, natural convection tests. The convection correction for forced convection gave adequate results for the Reynolds number range 70-672 over which the tests extended, although there is poorer agreement between theory and experiment for the evaporative case. Similar findings were reported in Reference [19] for low pressure tests. Despite the discrepancy between the theoretical and experimental results, both predict the same trends in evaporation rates with respect to ambient gas temperature and pressures.

Essentially the same general conclusions that were reached for the natural convection tests are applicable to the forced

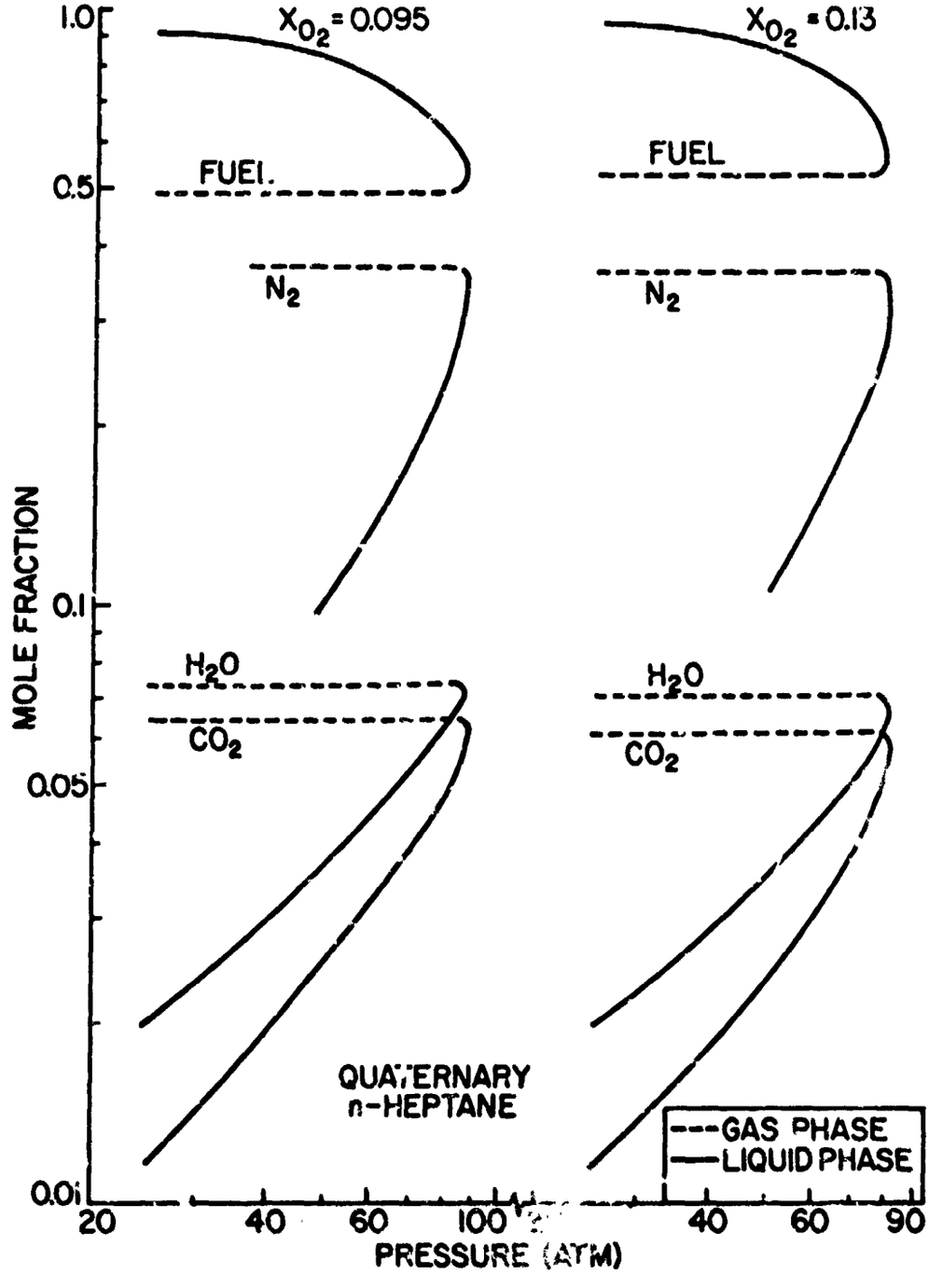

Figure 26 Predicted Liquid Surface Compositions for Porous-Sphere Combustion with a Fuel Inlet Temperature of 300°K and an Ambient Gas Temperature of 1145°K (Quaternary Theory)

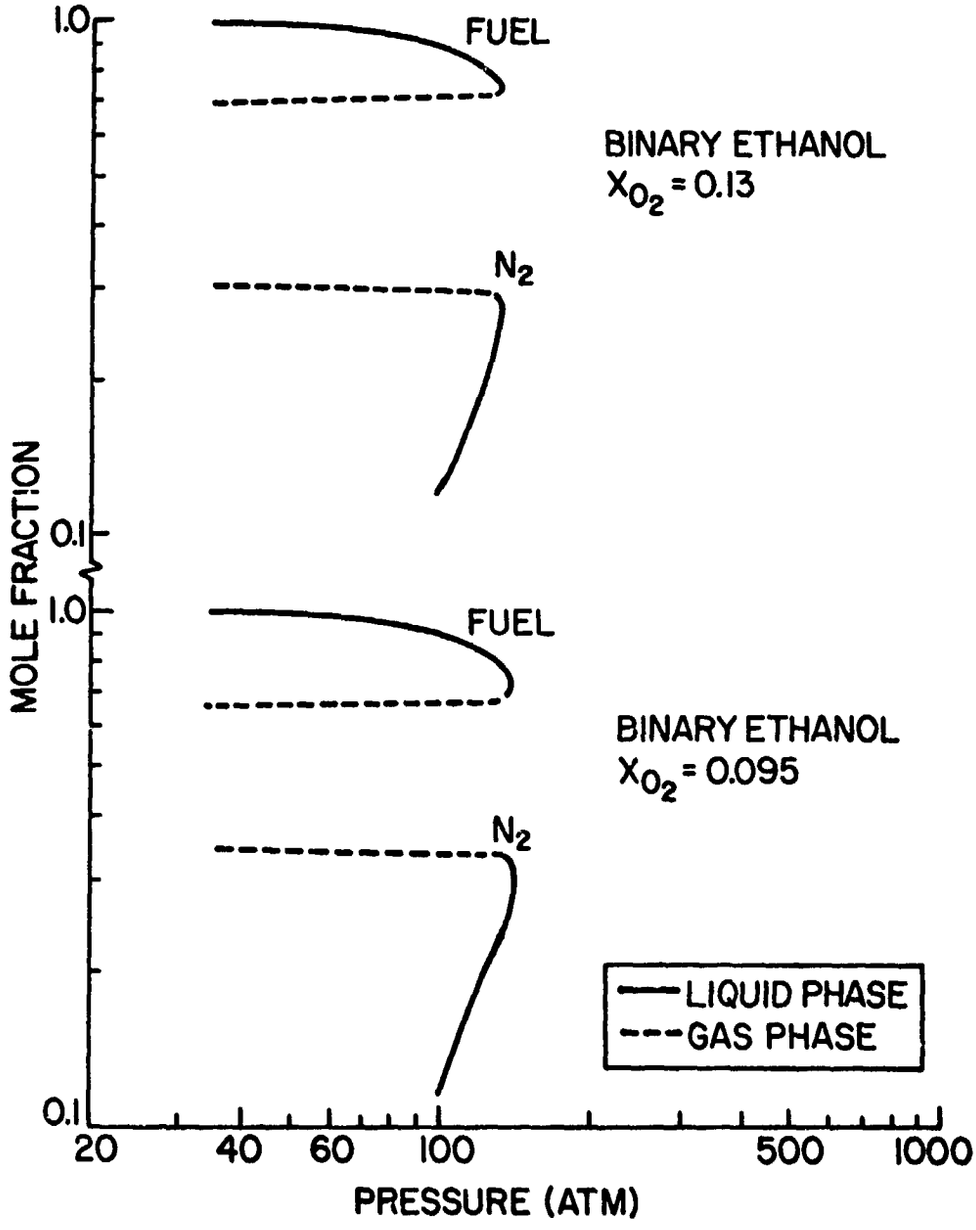

Figure 27 Predicted Liquid Surface Compositions for Porous-Sphere Combustion with a Fuel Inlet Temperature of 300°K and an Ambient Gas Temperature of 1145°K (Binary Theory)

convection tests. Even at the higher ambient gas temperatures, the low and high pressure models predicted the same trends that were noted for the cold gas tests. These included the lower liquid surface temperature predictions of the quaternary model as compared to those of the low pressure model.

Another similarity between the theoretical results of the natural and forced convection tests occurred in the predictions obtained using the variable property constant specific heat gas phase analysis. For the cold gas tests both the variable property-variable specific heat analyses gave essentially the same results as long as the respective constant properties were evaluated at average conditions inside and outside the flame. For the high ambient gas temperature tests both the quaternary and binary high pressure models gave essentially the same results for the variable and constant specific heat cases, although the binary model consistently predicted much higher pressures for critical burning than the quaternary theory.

On the other hand, the low pressure model gave identical predictions for both the variable specific heat and the constant specific heat cases at all ambient oxygen concentrations. Another interesting observation concerning the low pressure model is that over an ambient gas temperature range of 300°K to 1925°K, the predicted critical combustion pressure for ethanol at 21 per cent ambient oxygen molar concentration varied from only 88 to 82 atmospheres, respectively. The high pressure theories predicted a much wider range of pressures for critical combustion conditions at a given ambient oxygen concentration for a similar temperature range.

The sensitivity of the calculated results to errors in the properties was examined by parametrically varying χ_A ($\pm$20%) and the binary interaction parameter k_{ij} ($\pm$20%). The effect of varying the modified Lewis number (χ_A) for ethanol and n-heptane during combustion (X_{O_2} = .095) at an ambient gas temperature of 1145°K is examined in Figure 28. The theoretical results were obtained using the variable-property-variable specific heat low pressure model and the high-pressure quaternary model. In agreement with the cold gas test results the variations of χ_A ($\pm$20%) had the greatest effect on the predicted critical burning conditions. The low pressure predictions are virtually the same for n-heptane but the predicted critical pressures for ethanol vary an average of 15 per cent for the conditions shown.

The burning rate predictions obtained for the low and high pressure models were essentially the same as those predicted for the normal case.

The variation of the binary interaction parameter k_{ij} ($\pm$20%) had very little effect on the predicted critical burning liquid surface temperature. The temperature variation and reduced pressures for critical burning (X_{O_2} = .095) for ethanol and n-heptane is examined in Table 7. The percentage variation is less than 2% for the predicted liquid surface temperatures and less than 6% for the predicted critical burning pressures. The results shown were obtained using the high-pressure variable property-variable specific heat quaternary theory. A similar trend was noted using variable oxygen concentrations and employing the high pressure binary theory.

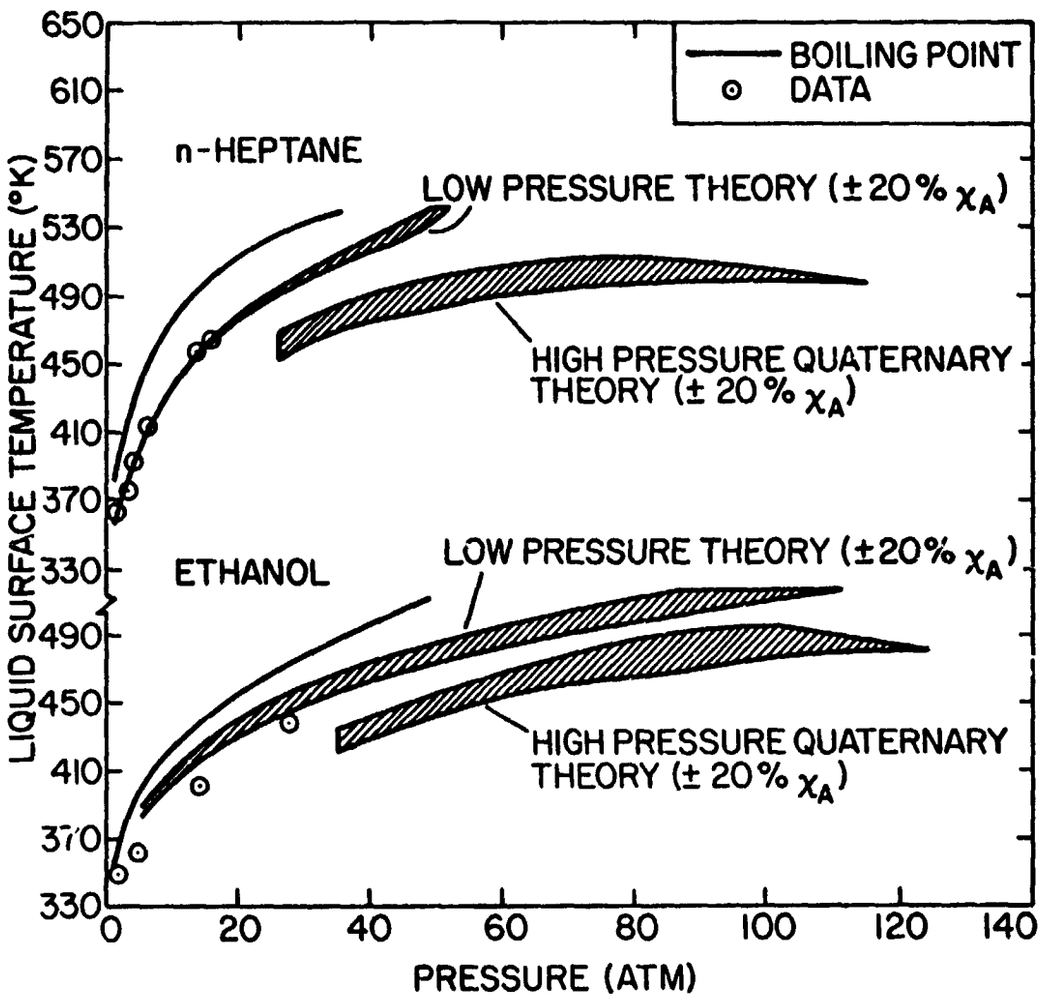

Figure 28 Effect of Variation of the χ_A Parameter on Droplet combustion (X_{O_2} = .095)

Table 7

Effect of Variation of the k_{ij} Parameter on Predicted Critical Burning Conditions (X_{O_2} = .095)

Fuel	Ethanol		n-Heptane	
Variation	T_R	P_R	T_R	P_R
Normal	.945	1.825	.936	3.26
+20% k_{ij}	.941	1.944	.934	3.33
-20% k_{ij}	.949	1.714	.925	3.02

CHAPTER V

SUMMARY AND CONCLUSIONS

5.1 Summary

The overall objective of the present investigation was to determine the characteristics of bipropellant droplet vaporization at high pressures under natural and forced convection conditions. The tests considered both cold gas and high ambient gas temperatures. The high pressure forced convection tests were conducted under simulated combustion chamber conditions. Porous spheres were used to simulate the fuel droplets in order to determine steady droplet burning rates and liquid surface temperatures. The tests considered various ambient oxygen concentrations and sphere sizes. Major emphasis was placed upon studying the effects of natural and forced convection on the combustion process.

The theoretical model that was used in the investigation was developed by extending the variable property, steady burning theory of Goldsmith and Penner [17]. The extensions included the effects of dissolved gas evaporation, allowance for variable specific heats of all species and the separate determination of the concentrations of the various gas phase species. The effect of convection was treated in the analysis through the use of a multiplicative correction of the theoretical burning rate computed for the case of no convection.

In the phase equilibrium analysis ambient gas solubility and high pressure effects were considered in the determination of conditions at the droplet surface. The calculations for these

conditions employed the modified Redlich and Kwong equation of state along with suitable mixing rules for application to multicomponent mixtures.

The measurements focussed upon droplet combustion under natural and forced convection conditions. The natural convection tests considered high pressure droplet burning in a cold ambient gas environment. A wide range of alochol and n-paraffin fuels were tested to provide further insight into the general applicability of the different models of combustion and the empirical corrections for natural convection.

The forced convection tests were conducted under conditions that were a realistic simulation of a combustion chamber environment. The atmospheric pressure baseline and high pressure tests provided burning and evaporation data for a wide range of fuels and considered various ambient oxygen concentrations and ambient gas temperatures. The tests also extended over a wide range of Reynolds numbers. The ambient oxygen concentration ranged from 0-13 per cent molar concentration and the ambient gas temperature ranged from 600°K to 1500°K. The Reynolds number range was sufficient to provide a fairly stringent test of the convection correction for forced convection.

The experiments indicated that methanol and ethanol were approaching critical combustion conditions at pressures on the order of 80-100 atm when burning in air under natural convection conditions. Both the low pressure and high pressure quaternary theories predicted critical burning in reasonable agreement with these results. Critical burning conditions could not be approached for the remaining fuels

due to the formation of soot deposits on the sphere. It was found that the rate of soot formation increased with increasing ambient pressures and ambient gas temperatures and decreasing ambient oxygen concentrations for the n-paraffin fuels.

The use of the variable property-variable specific heat, variable property-constant specific heat and constant property gas phase analyses gave essentially the same results as long as the respective constant properties were evaluated at average conditions inside and outside the flame. Parametric property variations caused variations in the computed results similar to those encountered in earlier high pressure combustion studies. [42, 55, 56] For porous spheres, the binary high pressure theory gave a poorer approximation of the quaternary high-pressure theory, than was the case for high pressure droplet combustion. [42] The theoretical predictions for the high pressure cold gas tests were consistent with the trends predicted for the high pressure, high ambient gas temperature tests.

Since many combustors are of the liquid spray or injection type, the results of this investigation will provide useful data concerning the effects of high pressures, temperatures, and convection on the phenomenon of combustion. Furthermore, the results of this investigation have provided fundamental burning rate data for a number of fuels and provided a fairly stringent test of the various high pressure models of combustion.

The results of previous investigations have revealed the need for a more fundamental understanding of high pressure combustion processes. There are several interesting extensions of this

investigation using the present experimental set-up that can be considered in future studies. One of these would be a detailed theoretical and experimental investigation into the phenomenon of soot formation during the combustion of n-paraffin fuels at elevated pressures. The present experimental facilities can be used to make a quantitative study of the effects of ambient oxygen concentration, pressure, and temperature on the mechanism of fuel pyrolysis and soot formation.

Another useful extension of the present work would be a study of the physical effects of ambient gas velocity and temperature on the flame stability of burning droplets at high pressures in a convective flow environment. Such phenomena as the transition from envelope to wake flames and the effect of gas velocity on the process in a combustion chamber environment require further investigation. The correlations that are presently being used for forced convection should be reexamined so that they may provide a better understanding of the physical processes that take place when a liquid fuel is burned in the form of droplets.

5.2 Conclusions

The major conclusions of this study are as follows:

1. Both low and high pressure theories gave essentially the same burning rate predictions (Figures 8, 9, 10, 22, and 23). The greatest difference between the theories lies in the predicted critical burning conditions (Tables 2 and 5). The low pressure theory predicts a significantly lower pressure for critical

combustion, at a given ambient oxygen concentration, than the high pressure theory. Furthermore, the low pressure theory predicted higher liquid surface temperatures at all pressures for critical combustion than the high pressure theory (Figures 11, 12, 24 and 25).

2. Discrepancies between theoretical and experimental burning rates were about the same as in earlier atmospheric pressure studies (Reference [19]).
3. The low pressure theory gave the best temperature prediction for methanol, as shown in Figure 11, whereas the high pressure theory was best for ethanol and propanol-1. Over the experimental range for n-heptane the low pressure theory was adequate. The experimental pressure range for n-pentane and n-decane was not high enough to be conclusive (Figure 12).
4. The experiments gave evidence of critical combustion for methanol and ethanol at pressures of 80-100 atm, in agreement with both theories.
5. Predicted dissolved gas concentrations reached values as high as 60% (n-decane) for the present test conditions.
6. The binary model was not a good approximation for the quaternary model in the present case of porous sphere combustion, unlike the previous findings of Lazar [43] for droplet combustion.

7. The various gas phase theories gave essentially the same results as long as any assumed constant property was evaluated at an average condition.
8. The effect of parametric property variations, as shown in Figure 28 and Table 7, was about the same as in the case of droplet combustion.
9. Based on approach conditions, the multiplicative correction for the natural convection correction for the burning rate appears adequate for Grashoff numbers in the range 10^4-10^8.
10. The multiplicative correction for forced convection appears adequate for droplet combustion, when based upon approach conditions, over the Reynolds number range 10-800.
11. Ambient air temperature has only a slight effect on the burning rates at finite ambient oxygen concentrations for the fuels considered in the tests (Figures 14 and 15). The burning rates are very sensitive to temperature for very low oxygen concentrations in the ambient gases (Figure 19).

BIBLIOGRAPHY

1. Godsave, G. A. E., "Studies of the Combustion of Drops in a Fuel Spray-The Burning of Single Drops of Fuel," Fourth Symposium (International) on Combustion, Williams and Wilkins, Baltimore, 1953, pp. 818-830.

2. Hall, A. R., and J. Diedrichsen, "An Experimental Study of the Burning of Single Drops of Fuel in Air at Pressures up to Twenty Atmospheres," Fourth Symposium (International) on Combustion, Williams and Wilkins, Baltimore, 1953, p. 837.

3. Goldsmith, M., "Experiments on the Burning of Single Drops of Fuel," Jet Propulsion, Vol. 26, 1956, pp. 131-144.

4. Isoda, H., and S. Kumagai, "New Aspects of Droplet Combustion," Seventh Symposium (International) on Combustion, Buttersworth Scientific Publications, London, 1959, pp. 523-531.

5. Wood, B. J., W. A Rosser and H. Wise, "Combustion of Fuel Droplets," AIAA Journal, Vol. 1, 1963, p. 1076.

6. Nuruzzman, A. S. M., A. B. Hedley, and J. M. Beer, "Combustion of Monosized Droplet Streams in Stationary Self-Supporting Flames," Thirteenth Symposium (International) on Combustion, The Combustion Institute, Pittsburgh, 1970.

7. Hottel, H. C., G. C. Williams, and H. C. Simpson, "Combustion of Droplets of Heavy Liquid Fuels," Fifth Symposium (International) on Combustion, Reinhold, New York, 1954, pp. 101-129.

8. Spalding, D. B., "Combustion of Liquid Fuel in a Gas Stream," Fuel, Vol. 29, 1950, p. 2.

9. Ingebo, R. D., "Vaporization Rates and Heat Transfer Coefficients for Pure Liquid Drops," NACA TN 2368, 1951.

10. Ranz, W. E. and W. R. Marshall, "Evaporation from Drops," Chemical Engineering Progress, Vol. 48, No. 3, pp. 141-146.

11. Borman, G. L., et al., "Graphs of Reduced Variables for Computing Histories of Vaporizing Fuel Drops and Drop Histories under Pressure," NACA TN 4338, September, 1958.

12. Torda, T. P. and R. Matlosz, "Liquid Droplet Evaporation in Stagnant High Pressure and High Temperature Environment," NASA CR-72373, 1968.

13. Savery, W. and G. L. Borman, "Experiments on Droplet Vaporization at Supercritical Pressures," AIAA Paper No. 70-6, January 1970.

14. Tarifa, C. S. and [illegible]spe, "Droplet Combustion at High Pressures with Un[illegible] Effects," Institute Nacional de Tecnica Aerospacial, "[illegible] Terrodas," Madrid, Spain, December, 1972.

15. Matlosz, R. [illegible], "Investigation of Liquid Drop Evaporation in High Temperature and High Pressure Environment," International Journal Heat Mass Transfer, Vol. 15, 1972, 831-852.

16. Rosner, D. E., "Transient Evaporation and Combustion of a Fuel Droplet Near Its Critical Temperature," Combustion Science and Technology, 1973, (Submitted).

17. Goldsmith, M. and S. S. Penner, "On the Burning of Single Drops of Fuel in an Oxidizing Atmosphere," Jet Propulsion, Vol. 24, 1954, pp. 245-251.

18. Bolt, J. A. and T. A. Boyle, "The Combustion of Liquid Fuel Spray," Transaction ASME, Vol. 78, 1956, p. 609.

19. Faeth, G. M. and R. L. Lazar, "Bipropellant Droplet Burning Rates and Lifetimes in a Combustion Gas Environment," NASA CR-72 622, 1969.

20. Harrje, D. T., "Liquid Propellant Rocket Combustion Instability," NASA SP-194, 1972.

21. Williams, A., "Combustion of Droplets of Liquid Fuels: A Review," Combustion and Flame, Vol. 21, No. I, August, 1973, pp. 1-32.

22. Williams, F. A., "On the Assumptions Underlying Droplet Vaporization and Combustion Theories," Journal of Chemical Physics, Vol. 33, July, 1960, pp. 131-144.

23. Brzustowski, T. A., "Chemical and Physical Limits on Vapor-Phase Diffusion Flame Droplets," Canadian Journal of Chemical Engineering, Vol. 43, February 1965, pp. 30-35.

24. Brzustowski, T. A. and R. Natarajan, "Combustion of Aniline Droplets at High Pressures," Canadian Journal of Chemical Engineering, Vol. 44, August, 1966, pp. 194-201.

25. Spalding, D. B., "Theory of Particle Combustion at High Pressures," ARS Journal, Vol. 29, November 1959, pp. 828-835.

26. Polymeropoulos, C. E. and R. L. Peskin, "Combustion of Fuel Vapor in a Hot, Stagnant Oxidizing Environment," Combustion Science and Technology, Vol. 5, 1972, pp. 165-174.

27. Chervinsky, A., "Supercritical Burning of Liquid Droplets in Stagnant Environment," AIAA Journal, Vol. 7, 1969, p. 1815.

28. Williams, F. A., "Theory of the Burning of Monopropellant Droplets," Combustion and Flame, Vol. 3, 1959, p. 529.

29. Rosser, W. A. and P. L. Peskin, "A Study of Decomposition Burning," Combustion and Flame, Vol. 10, 1966, p. 152.

30. Spalding, D. B., "Experiments on the Burning and Extinction of Liquid Fuel Spheres," Fuel, Vol. 32, 1953, pp. 169-185.

31. Wood, B. J., H. Wise and S. H. Inami, "Heterogeneous Combustion of Multicomponent Fuels," Combustion and Flame, Vol. 4, 1960, p. 235-242.

32. Udelson, D. G., "Geometrical Considerations in the Burning of Liquid Drops," Combustion and Flame, Vol. 6, 1962, pp. 93-102.

33. Agoston, G. A., H. Wise and W. A. Rosser, "Dynamic Factors Affecting the Combustion of Liquid Spheres," Sixth Symposium (International) on Combustion, Reinhold, 1956, pp. 708-717.

34. Sjorgen, A., "Soot Formation by Combustion of an Atomized Liquid Fuel," Fourteenth Symposium (International) on Combustion, The Combustion Institute, Pittsburgh, 1973, pp. 919-928.

35. Gollahalli, S. R. and T. A. Brzustowski, "Experimental Studies on the Flame Structure in the Wake of a Burning Droplet," Fourteenth Symposium (International) on Combustion, The Combustion Institute, Pittsburgh, 1973, pp. 1333-1344.

36. Michael, M. I. and M. M. El-Wakil, "On the Self Ignition of Hydrocarbon Mixtures," Eleventh Symposium (International) on Combustion, The Combustion Institute, Pittsburgh, 1971, p. 723.

37. Priem, R. J. and M. F. Heidmann, "Propellant Vaporization as a Design Criterion for Rocket Engine Combustion Chambers," NASA Technical Report R-67, 1960.

38. El-Wakil, M. M., P. S. Myers, and O. A. Uyehara, "Fuel Vaporization and Ignition Lag in Diesel Combustion," S.A.E. Transactions, Vol. 64, 1956, p. 712.

39. Gollahalli, S. R., "Studies on the Flame Structure in the Wakes of Burning Liquid Drops," Ph.D. Thesis, University of Waterloo, 1973.

40. Sami, H. and M. Ogasawara, "Study on the Burning of a Fuel Drop in Heated and Pressurized Air Stream," JSME Bulletin, Vol. 13, No. 57, 1970, p. 395.

41. Manrique, J. A., "Theory of Droplet Vaporization in the Region of the Thermodynamic Critical Point," NASA CR-72574, 1969.

42. Lazar, R. S. and G. M. Faeth, "Bipropellant Droplet Combustion in the Vicinity of the Critical Point," Thirteenth Symposium (International) on Combustion, The Combustion Institute, Pittsburgh, 1971, p. 801.

43. Lazar, R. S., "Bipropellant Droplet Combustion in the Vicinity of the Critical Point," Ph.D. Thesis, The Pennsylvania State University, 1970.

44. Williams, F. A., Combustion Theory, Addison-Wesley, Reading, Massachusetts, 1965.

45. Eisenklam, P., S. A. Arunachalam, and J. A. Weston, "Evaporation Rates and Drag Resistance of Burning Drops," Eleventh Symposium (International) on Combustion, The Combustion Institute, Pittsburgh, 1967, pp. 715-728.

46. Fendell, F. E, "Thin-Flame Theory for a Fuel Droplet in Slow Viscous Flow," Journal of Fluid Mechanics, Vol. 26, Pt. 2, 1966, pp. 267-280.

47. Frössling, N., "Uber die Verdunstung Fallender Tropfen," Beitraege zur Geophysik, Vol. 5, 1938, pp. 170-216.

48. Faeth, G. M., "The Kinetics of Droplet Ignition in a Quiescent Air Environment," Ph.D. Thesis, The Pennsylvania State University, 1964.

49. Penner, S. S., Chemistry Problems in Jet Propulsion, Macmillan, New York, 1957.

50. Allender, C., "Untersuchung des Absorptionvorganges in Absorbenlenschuhten mit Linearer Absorptionsisotherme," Transaction Royal Institute of Technology, No. 70, Stockholm, Sweden, 1953.

51. Prausnitz, J. M. and P. L. Chueh, Computer Calculations for High Pressure Vapor-Liquid Equilibria, Prentice-Hall, New Jersey, 1968.

52. Reid, R. C. and T. K. Sherwood, The Properties of Gases and Liquids, McGraw-Hill, New York, 1966.

53. Andersen, J. W. and K. Freidman, "An Accurate Metering System for Laminar Flow Studies," The Review of Scientific Instruments, Vol. 20, January 1949, p. 66.

54. Fristrom, R. and A. Westenberg, Flame Structure, McGraw-Hill, New York, 1965.

55. Spalding, D. B., "The Combustion of Liquid Fuels," Fourth Symposium (International) on Combustion, Williams and Wilkins, Baltimore, 1953, pp. 847-864.

56. Faeth, G. M., "High-Pressure Liquid Monopropellant Strand Combustion," Combustion and Flame, Vol. 18, No. 1, February, 1972, pp. 103-114.

57. Faeth, G. M. and R. S. Lazar, "Fuel Droplet Burning Rates in a Combustion Gas Environment," AIAA Journal, Vol. 9, 1971, p. 2165.

58. Li, T. S. and W. H. Gauvin, "Evaporation from Vertical Flat Plates in High-Temperature Surroundings," Chemical Engineering Progress Symposium Series, Vol. 62, No. 64, 1966, pp. 87-96.

59. Pei, D. C. T. and W. D. Gauvin, "Nacural Convection Evaporation from Spherical Particles in High-Temperature Surroundings," AIChE Journal, Vol. 9, No. 3, 1963, pp. 375-383.

60. Maxwell, J. D., Data Book on Hydrocarbons, Van Nostrand, New York, 1950.

61. Rossini, F. D., Selected Values of the Physical and Thermodynamical Properties of Hydrocarbons and Related Compounds, American Petroleum Institute, Carnegie, 1953.

62. International Critical Tables, McGraw-Hill, New York, 1926-1930.

63. Svelha, R. A., "Estimated Viscosities and Thermal Conductivities of Gases at High Temperatures," NASA Technical Report R-132, 1962.

64. Stull, D. R., "Vapor Pressure of Pure Substances, Organic Chemistry," Industrial and Engineering Chemistry, Vol. 39, No. 4, April, 1947, pp. 517-540.

65. Jones, W. H. (Chairman), JANAF Thermochemical Tables, Dow Chemical Company, Midland, Michigan.

APPENDIX A

CHECK OF ASSUMPTIONS OF THE ANALYSIS

A.1 Constant Total Pressure Assumption

Reference [48] gives the following approximate expression for estimating the pressure changes across the boundary layer surrounding a spherically symmetric droplet

$$\frac{P_\ell - P_\infty}{P} = -\frac{M}{2RT}\left[\frac{DX_{1\ell}}{r_\ell(1 - X_{1\ell})}\right]^2 \qquad (A.1)$$

The above equation was obtained by integrating the momentum equation for the flow field resulting from the binary diffusion of fuel vapor from the droplet. In addition to the assumption of a spherically symmetric system, it was assumed that the molecular weight of both species was the same and constant fluid properties in the boundary layer.

It was found in Reference [43] that for droplets as small as 10μ in diameter at one atmosphere pressure, that Equation (A.1) indicates that there is less than 5% change in pressure, providing $X_{1\ell} \leq 0.9$. Since the present investigation considered much larger droplet sizes (0.64-1.9 cm) and pressures much greater than one atmosphere, the pressure variation is negligible.

A.2 Radiation Assumption

A spherical model was used to estimate the contribution of radiant energy to the droplet from the flame. Such a model is obviously oversimplified since the distortion of the boundary layer

surrounding the droplet by convective forces will alter the assumed spherical symmetry of the system. Furthermore, the flames for most of the fuels used in the investigation were usually blue and non-radiant over the front half of the sphere, but yellow and highly radiant over the rear half.

Following the approximation suggested by Godsave [1] the system consists of a hot radiating surface (the flame) surrounding a cooler body (the droplet). Radiation from the vapours at intermediate temperatures between the flame front and the drop is neglected in view of the sharp temperature gradient. By neglecting the absorption of radiation by these intermediate vapors, the two approximations tend to cancel each other out and the final result is reasonably representative of the actual process.

For n-decane combustion at a flame temperature of 3000°K and for various pressures, Reference [43] indicates that thermal radiation accounts for a negligible portion of the energy required to vaporize droplets up to 1000μ in diameter at low and moderate pressures, but can become appreciable at very high pressures.

The present investigation considered the use of porous spheres to simulate the fuel droplets. If the radiation loss by the droplet is neglected, due to its relatively low temperature in comparison with that of the flame, the radiant energy flux absorbed by the droplet is:

$$\dot{Q}_R = 4\pi r_\ell^2 e_f a_d \sigma T_f^4 \qquad (A.2)$$

In this equation e_f is the emissivity of the thin zone of radiating gases, and σ is the Stefan-Boltzmann constant. The radiating gases

were assumed to be carbon dioxide and water vapor. The partial pressures of these gases were based upon the average concentrations of these species at the flame zone. For porous alundum spheres, the absorptivity, a_d, represents the combined effects of the liquid film and the surface absorptivities. It is known that the absorptivity of liquid films is a function of their thickness. Owing to the uncertainty concerning the exact thickness of the liquid film and the belief that the porous sphere surface may be an important factor in the absorption of radiation, other investigators [7, 58, 59] have used an average value of 0.8 for the surface absorbtivity.

For the case of insoluble ambient gases in the liquid phase, the total heat flux to the droplet for steady burning is

$$\dot{Q} = \dot{n}L \tag{A.3}$$

The low pressure variable property-variable specific heat theory was used to compute the molar burning rate and liquid surface temperatures. High pressure effects were considered in evaluating the heat of vaporization, L. For the combustion of n-heptane in air at a pressure of 50 atmospheres the thermal radiation was found to account for about 36 per cent of the energy required to vaporize the droplet.

APPENDIX B

GAS PHASE ANALYSIS

B.1 Variable Property-Variable Specific Heat Analysis

Under the assumption that compressibility effects are small in the gas phase, the ideal gas relationships are employed to evaluate the enthalpy difference terms appearing in the steady burning equations for conservation of energy. Substituting Equation (2.21)

$$(h-h_\ell)_i = \int_{T_\ell}^{T} (A_i + B_i T)dT = A_i(T-T_\ell) + \frac{B_i}{2}(T^2-T_\ell^2) \tag{B.1}$$

Substituting this expression Equation (2.8) becomes

$$\dot{n}\left[A_1(T-T_\ell) + B_1\left(\frac{T^2}{2} - \frac{T_\ell^2}{2}\right) + L_1\right] = 4\pi r^2 \lambda_A \frac{dT}{dr} \tag{B.2}$$

The burning rate, $\dot{n}$, is determined by applying Equation (2.20) and the boundary conditions, Equation (2.18), to Equation (B.2). Upon integration, the result is:

$$\frac{\dot{n}T_\ell B_1}{4\pi r_\ell \lambda_{A\ell}}\left(1 - \frac{r_\ell}{r_f}\right) = \ell n\left\{\frac{L_1 + \frac{B_1}{2}(T_f^2-T_\ell^2) + A_1(T_f-T_\ell)}{L_1}\right\} + \eta \tag{B.3}$$

where η is given by

$$\eta = \ell n\left[\frac{(A_1 + B_1T_f + \xi)(A_1 + B_1T_\ell - \xi}{(A_1 + B_1T_f - \xi)(A_1 + B_1T_\ell + \xi)}\right]^{A_1/\xi}, \quad \xi^2 > 0 \tag{B.4}$$

or

$$\eta = \frac{-2A_1}{\phi}\left[\tan^{-1}\left(\frac{A_1 + B_1T_f}{\phi}\right) - \tan^{-1}\left(\frac{A_1 + B_1T_\ell}{\phi}\right)\right], \quad \phi^2 > 0 \tag{B.5}$$

or

$$\eta = \frac{-2A_1B_1(T_f-T_\ell)}{(A_1 + B_1T_f)(A_1 + B_1T_\ell)}, \qquad \xi^2 = 0 \tag{B.6}$$

where

$$\xi^2 = -\phi^2 = A_1^2 - 2B_1[L_1 - A_1T_\ell - \frac{B_1}{2}T_\ell^2] \tag{B.7}$$

An expression for the fuel mole fraction at the droplet surface may be obtained by eliminating spatial deviatives between Equation (2.9) and (B.2), introducing Equation (2.18), and integrating. The solution has three branches which are as follows:

$$X_{1\ell} = 1 - \left[\frac{(A_1 + B_1T_f + \xi)(A_1 + B_1T_\ell - \xi)}{(A_1 + B_1T_f - \xi)(A_1 + B_1T_\ell + \xi)}\right]^{\chi_A/\xi}, \qquad \xi^2 > 0 \tag{B.8}$$

$$X_{1\ell} = 1 - \exp\left[\frac{2\chi_A}{\phi}\left(\tan^{-1}\left(\frac{A_1 + B_1T_\ell}{\phi}\right) - \tan^{-1}\left(\frac{A_1 + B_1T_f}{\phi}\right)\right)\right], \qquad \phi^2 > 0 \tag{B.9}$$

$$X_{1\ell} = 1 - \exp\left\{\frac{2\lambda_F B_1(T_\ell-T_f)}{(A_1 + B_1T_\ell)(A_1 + B_1T_f)}\right\}, \qquad \phi^2 = 0 \tag{B.10}$$

where

$$\chi_A = (\lambda/CD)_A .$$

To determine the concentration of any species in terms of the fuel mole fraction at the droplet surface and concentrations at the flame, Equation (2.9) is used. Eliminating spatial derivatives and introducing Equation (2.18) results in the following expression:

$$X_{i\ell} = X_{if}(1-X_{1\ell}), \qquad i=2, \ldots, N-1 \tag{B.11}$$

In order to determine conditions at the flame surface Region B must be considered. The mole fraction of any species at the flame may be expressed in terms of the ambient oxygen concentration through

the use of Equation (2.17) and integrating. The result is

$$\frac{\alpha' X_{if} - \alpha_i}{\alpha' X_{i\infty} - \alpha_i} = \frac{\alpha_N}{\alpha_N - \alpha' X_{N\infty}} \tag{B.12}$$

where

$$\alpha' = \sum_{i=2}^{N} \alpha_i \tag{B.13}$$

Substituting the specific heat relation Equation (2.21) into the energy equation leads to

$$\dot{n}[\sum_{i=2}^{N} \alpha_i \{A_i(T-T_\ell) + \frac{B_i}{2}(T^2 - T_\ell{}^2)\} - Q_\ell + L] = 4\pi r^2 \lambda_B \frac{dT}{dr} \tag{B.14}$$

Letting

$$a' = \sum_{i=2}^{N} \alpha_i A_i \tag{B.15}$$

$$b' = \sum_{i=2}^{N} \alpha_i B_i \tag{B.16}$$

Equation (B.14) becomes

$$\dot{n}[(T-T_\ell)\ a' + \frac{b'}{2}(T^2 - T_\ell{}^2) - Q_\ell + L] = 4\pi r^2 \lambda_B \frac{dT}{dr} \tag{B.17}$$

An expression for the combustion temperature in terms of the ambient oxygen concentration may be obtained by eliminating spatial derivatives between the conservation of energy and conservation of species equation for Region B and integrating between the limits

$$\begin{aligned} T &= T_f \quad & X_i &= X_{if} \\ T &= T_\infty \quad & X_i &= X_{i\infty} \end{aligned} \tag{B.18}$$

This results in the following expressions:

$$\frac{\alpha_N}{\alpha_N-\alpha' X_{N\infty}} = \left\{\frac{(b'T_\infty + a' + \gamma)(b'T_f + a' - \gamma)}{(b'T_\infty + a' - \gamma)(b'T_f + a' + \gamma)}\right\}^{\chi_B/\gamma\alpha'}, \qquad \gamma^2 > 0 \tag{B.19}$$

$$\frac{2\alpha'\chi_B}{\phi'} \exp\left\{\tan^{-1}\left(\frac{a' + b'T_f}{\phi'}\right) - \tan^{-1}\left(\frac{a' + b'T_\infty}{\phi'}\right)\right\} = \ell n\left(\frac{\alpha_N}{\alpha_N-\alpha' X_{N\infty}}\right), \qquad \phi'^2 > 0 \tag{B.20}$$

$$\ell n\left(\frac{\alpha_N}{\alpha_N-\alpha' X_{N\infty}}\right) = \frac{2\alpha'\chi_B b'(T_f-T_\infty)}{(a' + b'T_f)(a' + b'T_\infty)}, \qquad \phi'^2 = 0 \tag{B.21}$$

where

$$\gamma = -\phi'^2 = a'^2 - 2b'(L_1 - Q_\ell - a'T_\ell - \frac{b'}{2}T_\ell^2) \tag{B.22}$$

An expression for the combustion radius can be obtained through the use of Equations (B.17) and (2.19) and integrating.

There are again three branches to the solution depending on the value of γ. They assume the form

$$\frac{1}{r_f} = \frac{4\pi\lambda_{B\ell}}{\dot{n}T_\ell b'}\left[\ell n\left(\frac{(T_\infty-T_\ell)a' + b'/2(T_\infty^2-T_\ell^2) - Q_\ell + L_1}{(T_f-T_\ell)a' + \frac{b'}{2}(T_f^2-T_\ell^2) - Q_\ell + L_1}\right) + \eta'\right] \tag{B.23}$$

$$\eta' = \frac{a'}{\gamma}\ell n\left[\frac{(a' + b'T_f - \gamma)(a' + b'T_\infty + \gamma)}{(a' + b'T_f + \gamma)(a' + b'T_\infty - \gamma)}\right], \qquad \gamma^2 > 0 \tag{B.24}$$

$$\eta' = \frac{2a'}{\phi'}\left[\tan^{-1}\frac{(a' + b'T_f)}{\phi'} - \tan^{-1}\frac{(a' + b'T_\infty)}{\phi'}\right], \qquad \phi'^2 > 0 \tag{B.25}$$

$$\eta' = \frac{2a'b'(T_f-T_\infty)}{(a' + b'T_f)(a' + b'T_\infty)}, \qquad \gamma^2 = 0 \tag{B.26}$$

B.2 Variable Property-Constant Specific Heat Analysis

If B_i is set equal to zero in Equation (2.21) the solution corresponds to the constant specific heat version of the gas phase analysis. For this case the energy equation for Region A becomes

$$\dot{n}[A_1(T-T_\ell) + L_1] = \frac{\lambda_{A\ell}}{T_\ell} T 4\pi r^2 \frac{dT}{dr} \quad . \tag{B.27}$$

Integrating this expression between r_ℓ and r for $r < r_f$ leads to the following result for the combustion radius:

$$\frac{\dot{n} T_\ell A_1}{4\pi r_\ell \lambda_{A\ell}}\left[1 - \frac{r_\ell}{r_f}\right] = A_1(T_f-T_\ell) - (L_1-A_1T_\ell)\ \ell n\ \{1 + \frac{A_1}{L_1}(T_f-T_\ell)\} \tag{B.28}$$

An expression for the liquid surface mole fraction may be obtained by eliminating spatial derivatives between the equations of conservation of energy and species and integrating between the limits given in Equation (2.18). The result is

$$X_{1\ell} = 1 - \left[\frac{L_1}{L_1 + A_1(T_f-T_\ell)}\right]^{1/A_1\chi_A} \tag{B.29}$$

Equation (B.11) is unchanged for this case and remains

$$X_{1\ell} = X_{if}(1-X_{1\ell}) \qquad i=2, \ldots, N-1$$

Considering the outer region, Equation (B.17) with b'=0 becomes

$$\dot{n}[a'(T-T_\ell) - Q_\ell + L_1] = 4\pi r^2 \lambda_{B\ell} \frac{T}{T_\ell} \frac{dT}{dr} \tag{B.30}$$

When this equat'on is integrated between the limits

When this equation is integrated between the limits

$$r = r_f \qquad T = T_f$$
$$r = r_\infty \qquad T = T_\infty \tag{B.31}$$

the resulting expression for the burning rate is

$$\frac{\dot{n}'a'^2 T_\ell}{4\pi r_f \lambda_{B\ell}} = a'[T_\infty - T_f] - (L_1 - Q_\ell - a'T_\ell)\, \ell n \left[\frac{a'(T_\infty - T_\ell) - Q_\ell + L_1}{a'(T_f - T_\ell) - Q_\ell + L_1}\right] \tag{B.32}$$

An expression for the combustion temperature may be developed through the use of the conservation of energy and species equations. The result is

$$\frac{1}{\alpha'} \ell n \left[\frac{\alpha_N}{\alpha_N - \chi_{N\infty}\alpha'}\right] = \frac{\chi_B}{a'} \ell n \left[\frac{a'(T_f - T_\ell) - Q_\ell + L_1}{a'(T_\infty - T_\ell) - Q_\ell - L_1}\right] \tag{B.33}$$

B.3 Constant Property Analysis

In the assumptions that the fuel thermal conductivity and specific heat are independent of temperature are made along with the assumptions given in Chapter II, the analysis will correspond essentially to that of Reference [1]. With the exception of the combustion temperature, expressions for the unknowns must be rederived from the steady burning equations presented in Chapter II. Constant average specific heats are used for the fuel vapor, oxidizer and products, designated as Cp_F, Cp_o, and Cp_p, respectively. The derivation of the equations is developed in the same manner as presented in Section B.1 and the details are omitted here.

The resulting expressions for liquid phase mole fractions, combustion temperature, flame radius, and burning rate are:

$$X_{1\ell} = 1 - \left\{ 1 + \frac{Cp_F(T_f - T_\ell)}{L_1} \right\}^{-\lambda/CDCp_F} \tag{B.34}$$

$$X_{2\ell} = 1 - X_{1\ell} \tag{B.35}$$

$$\ell n \left[\frac{a'(T_f - T_\ell) - Q_\ell + L_1}{a'(T_\infty - T_\ell) - Q_\ell + L_1} \right] = \frac{a'}{\alpha'} \frac{CD_N}{\lambda_B} \ell n \left[\frac{\alpha_N}{\alpha_N - \alpha' X_{N\infty}} \right] \tag{B.36}$$

$$\frac{1}{r_f} = \frac{4\pi\lambda_b}{Cp_o \dot{n}} \ell n \left[\frac{a'(T_\infty - T_\ell) - Q_\ell + L_1}{a'(T_f - T_\ell) - Q_\ell + L_1} \right] \tag{B.37}$$

$$\left[\frac{1}{r_\ell} - \frac{1}{r_f} \right] \frac{\dot{n}}{4\pi\lambda_A} = \frac{1}{Cp_F} \ell n \left[1 + \frac{Cp_F(T_f - T_\ell)}{L_1} \right] \tag{B.38}$$

APPENDIX C

PHASE EQUILIBRIUM RELATIONS

C.1 Mixing Rules

The Redlich-Kwong equation of state is

$$P = \frac{RT}{V-b^\circ} - \frac{a^\circ}{T^{0.5}V(V+b^\circ)} \tag{C.1}$$

which is cubic in V. The largest positive root is used in calculations.

The mixing rules of Prausnitz and Chueh [51] are used to apply the above equation to mixtures. For a mixture of N components:

$$a^\circ = \sum_{i=1}^{N} \sum_{j=1}^{N} X_i X_j a^\circ_{ij} \tag{C.2}$$

where

$$a^\circ_{ii} = \frac{\Omega_{ai} R^2 T_{ci}^{2.5}}{P_{ci}} \tag{C.3}$$

and

$$a^\circ_{ij} = \frac{(\Omega_{ai} + \Omega_{aj}) R^2 T_{cij}^{2.5}}{2P_{cij}} \tag{C.4}$$

$$b^\circ = \sum_{i=1}^{N} X_i b^\circ_i \tag{C.5}$$

$$b^\circ_i = \frac{\Omega_{bi} RT_{ci}}{P_{ci}} \tag{C.6}$$

$$P_{cij} = \frac{Z_{cij} RT_{cij}}{V_{cij}} \tag{C.7}$$

$$V_{cij} = (V_{ci} + V_{cj})/2 \tag{C.8}$$

$$Z_{cij} = 0.291 - 0.04(\omega_i + \omega_j) \tag{C.9}$$

$$T_{cij} = \sqrt{T_{ci} T_{cj}}(1-k_{ij}) \tag{C.10}$$

C.2 Component Fugacities

Component fugacities were determined by substituting Equation (C.1) and the mixing rules, Equations (C.2) to (C.10), into Equation (2.54) and integrating. The result for a component i in a mixture of N components is given by the following expression:

$$\ell n(f_i / X_i P) = \ell n\left(\frac{V}{V-b^\circ}\right) + \frac{b_i^\circ}{v-b^\circ} - \frac{2\sum_{j=1}^{N} X_j a_{ji}^\circ}{RT^{3/2} b^\circ} \left[\ell n\left(\frac{V+b^\circ}{V}\right)\right] + \frac{a^\circ b_i^\circ}{RT^{3/2} b^{\circ 2}}$$

$$\left[\ell n\left(\frac{V+b^\circ}{V}\right) - \frac{b^\circ}{V+b^\circ}\right] - \ell n \frac{PV}{RT} \tag{C.11}$$

The molar volume, N, is determined from the equation of state which is cubic in V.

C.3 Heat of Vaporization

The heat of vaporization of a component i in a mixture, L_i, is the difference between the partial molar enthalpy in the vapor and liquid phases, i.e.,

$$L_i = \bar{h}_i^V - \bar{h}_i^L \tag{C.12}$$

The partial molar enthalpy of component i in a mixture is determined by the following thermodynamic relation:

$$\frac{\bar{h}_i^\circ - \bar{h}_i}{RT^2} = \frac{\partial}{\partial T}\left[\ell n \frac{f_i}{X_i P}\right] \tag{C.13}$$

In the above expression $\bar{h}_i^\circ$ represents the partial molar enthalpy in the ideal state. When Equation (C.12) is differentiated and the

resulting expression substituted into Equation (C.13) the following expression results:

$$\frac{\bar{h}_i^\circ - \bar{h}_i}{RT^2} = (\bar{A}-1)\frac{\bar{C}}{Z} + \frac{\bar{A}}{T} + \bar{B} \qquad (C.14)$$

where

$$\bar{A} = \frac{-b^\circ}{V-b^\circ} - \frac{b_i^\circ V}{(V-b^\circ)^2} + \frac{2\sum_{j=1}^{N} a_{ji}^\circ X_j}{RT^{1/5}(V+b^\circ)} - \frac{a^\circ b_i^\circ}{RT^{1.5}(V+b^\circ)^2} \qquad (C.15)$$

$$\bar{B} = \frac{3}{2RT^{2.5}b^\circ}\left[2\left(\sum_{j=1}^{N} X_j a_{ji}^\circ\right)\ell n\left(\frac{V+b^\circ}{V}\right) - \frac{a^\circ b_i^\circ}{b^\circ}\ell n\left(\frac{V+b^\circ}{V}\right) + \frac{a^\circ b_i^\circ}{V+b^\circ}\right] \qquad (C.16)$$

$$(3Z^2 - 2Z + \bar{D})\bar{C} = \frac{2\bar{D}Z}{T} + \frac{PZ}{(RT)^2}\left[\frac{a^\circ}{2T^{3/2}} + b^\circ R\right] - \frac{3.5a^\circ b^\circ P^2}{R^3T^{4.5}} \qquad (C.17)$$

$$\bar{D} = \left(\frac{a^\circ}{T^{1/2}} - b^\circ RT - b^{\circ 2}P\right)\frac{P}{(RT)^2} \qquad (C.18)$$

and

$$Z = \frac{PV}{RT} \qquad (C.19)$$

is the mixture compressibility factor.

By solving Equation (C.14) for each phase and substituting the results into Equation (C.12), the heat of vaporization for each component in the mixture is determined.

C.4 Physical Constants

The pure component constants P_c, T_c, V_c, and ω employed in the calculations are given in Table 8.

The binary interaction parameters, k_{ij}, for the alcohol and n-paraffin fuels used in the investigation are presented in Table 9.

Table 8

Pure Component Constants

Component	P_c (ATM)	$V_c\left(\frac{CC}{gm\text{-}mole}\right)$	T_c (°K)	ω	$M\left(\frac{gm}{gm\text{-}mole}\right)$
N_2	33.54	90.1	126.26	.040	28.016
CO_2	72.80	94.0	304.16	.225	44.01
H_2O	218.3	55.2	647.4	.344	18.02
CH_3OH	78.5	118.0	513.2	.556	32.04
C_2H_5OH	63.0	161.3	516.0	.635	46.07
C_3H_7OH	51.0	220.0	540.7	.600	60.09
C_5H_{12}	33.3	311.0	469.5	.252	72.15
C_7H_{16}	27.0	431.9	540.2	.349	100.20
$C_{10}H_{22}$	20.8	620.0	619.0	.479	142.28

Table 9

Binary Interaction Parameters

Component	N_2	CO_2	H_2O
Methanol	.10	.08	.15
Ethanol	.15	.11	.20
Propanol-1	.20	.16	.25
N-Pentane	.25	.20	.30
N-He tane	.35	.29	.40
N-Decane	.50	.43	.55

Note: $k_{ij} = k_{ji}$ and $k_{ii} = 0$

APPENDIX D

PHYSICAL PROPERTIES

D.1 References for Physical Properties

The sources of property data and correlations were the same as in earlier studies. [42, 43, 56] These sources are listed in Table 10. The specific correlations are given in the following sections.

For the low pressure theory calculations the combustion products were treated as a single species. The properties for this effective species was obtained by averaging the properties for an equimolar mixture of carbon dioxide, nitrogen and water vapor.

In calculations that required constant average values, the average temperature was used in the particular region. For Regions A and B these correlations assume the form

$$T_A = (T_\ell + T_f)/2 \tag{D.1}$$

and

$$T_B = (T_f + T_\infty)/2 \tag{D.2}$$

D.2 Liquid Phase Properties

The liquid molar density, vapor pressure, and heat of vaporization employed in the low pressure calculations were correlated with the following equations:

$$C_\ell = (C_1 - C_2 T_\ell)/M \left[\frac{gm/mole}{cc}\right] \tag{D.3}$$

The vapor pressure correlation for the alcohols assumed the form

$$P_v = \exp(C_3 - C_4/T_\ell) \tag{D.4}$$

Table 10

References for the Physical Properties

Property	References		
	Paraffins	Alochols	Ambient Gas
C_ℓ	61	62	--
C_p	61	52[a]	63
D	52[b]	52[b]	52[b]
L	52[c]	52[c]	--
P_v	61[d]	64	--
λ	60	63	63
μ	60	63	63

[a]Computed, Rihani and Doraiswamy Method

[b]Computed Fuller, Schettler, Giddings Method

[c]Watson Correlation

[d]Antoine Correlation

and for the n-paraffins

$$P_v = \exp\{C_5 - C_6/(T_\ell - C_7)\} \qquad (D.5)$$

The heat of vaporization correlation was

$$L = C_8(1 - T_\ell/T_c)^{0.38} \qquad (D.6)$$

The constants C_1 to C_8 are tabulated in Table 11. The molecular weight, M, and critical temperature, T_c, for each of the components considered in the calculations are also listed. In the above calculations the liquid temperature, T_ℓ, is in degrees Kelvin.

D.3 Gas Phase Properties

The specific heat of each species in the gas phase was represented by the equation:

$$C_p = A + BT \text{ (cal/m-mole °K)} \qquad (D.7)$$

The specific heat constants, A and B, for each species are tabulated in Table 12.

The thermal conductivity correlations employed for Regions A and B are as follows:

$$\lambda_A = \lambda_{A\ell}(T/T_\ell) \qquad (D.8)$$

and

$$\lambda_B = \lambda_{B\ell}(T/T_\ell) \qquad (D.9)$$

The constants $\lambda_{A\ell}$ and $\lambda_{B\ell}$ represent the thermal conductivities of the gas mixture, evaluated at the temperature, T_{avg}, for Regions A and B, respectively. The correlation used assumed the

Table 11

Constants in the Liquid Phase Property Equations

Component	C_1	C_2	C_3	C_4	C_5	C_6	C_7	C_8	$M\left(\frac{gm}{gm\text{-}mol}\right)$	T_c (°K)
Methanol	1.085	1.008	12.619	4241.52	--	--	--	12700	32.04	513.2
Ethanol	1.050	0.893	12.658	4400.48	--	--	--	14220	46.07	516.3
Propanol-1			12.268	4486.02	--	--	--	15380	60.09	536.7
N-Pentane	.903	.945	--	--	9.1445	2451.4	41.15	9020	72.15	469.5
N-Heptane	.941	.879	--	--	9.260	2919.95	56.25	11830	100.2	540.3
N-Decane	.962	.792	--	--	9.378	3456.90	78.67	15700	142.28	617.6

Table 12

Specific Heat and Thermal Conductivity Constants

Component	A	B	C_9	$C_{10} \times 10^3$	$C_{11} \times 10^3$
N-Pentane	31.75	28.86	--	--	215.00
N-Heptane	44.10	40.00	--	--	205.00
N-Decane	62.70	56.90	--	--	190.00
Methanol	11.00	9.00	--	--	340.00
Ethanol	17.60	13.20	--	--	305.00
Propanol-1	22.00	19.20	--	--	305.00
Water Vapor	7.90	1.80	-47.40	332.50	--
Carbon Dioxide	9.00	2.50	11.90	139.70	--
Nitrogen	6.90	.75	31.80	123.20	--
Oxygen	7.10	1.00	45.50	132.20	--

$$\lambda(\text{mix}) = \sum_{i=1}^{N} \frac{X_i \lambda_i}{\sum_{j=1}^{N} X_j \, \theta_{ij}} \qquad (D.10)$$

where

$$\theta_{ij} = \frac{1}{\sqrt{8}} \left(1 + \frac{M_i}{M_j}\right)^{-1/2} \left[1 + \left(\frac{\mu_i}{\mu_j}\right)^{1/2} \left(\frac{M_j}{M_i}\right)^{1/4}\right]^2 \qquad (D.11)$$

and

X_i = mole fraction of i

M_i = molecular weight of i

μ_i = viscosity of i

The species thermal conductivities, λ_i, were computed from the correlation

$$\lambda \times 10^6 = C_9 + C_{10} \times 10^{-3} \, T \qquad (D.12)$$

for the non-fuel species and from the correlation

$$\lambda \times 10^6 = C_{11}(T - 140) \qquad (D.13)$$

for the fuel species.

The constants C_9 to C_{11} are tabulated in Table 12 for all of the fuels considered in the investigation as well as the values for oxygen and the combustion products.

The gas phase molar density was computed from the ideal gas equation of state

$$C = P/RT \qquad (D.14)$$

The values for the viscosity of each species is given by the correlation

$$\mu_i = 10^{-6}(C_{12} + C_{13} \times 10^{-3}T) \quad \text{gm/cm-sec} \qquad (D.15)$$

The constants used in the above expression are listed in Table 13.

The binary diffusion coefficients for Regions A and B were computed according to the Fuller, Schettler, and Giddings [52] empirical correlation. This expression assumes the form

$$D_{ij} = \frac{10^{-3}T^{1.75}(1/M_i + 1/M_j)^{1/2}}{P[(\Sigma v)_i^{1/3} + (\Sigma v)_j^{1/3}]^2} \qquad (D.16)$$

with D in cm^2/sec and P and T in atm and °K, respectively. The values of the sums of atomic diffusion volumes for each of the gas species are listed in Table 13. The mixture diffusivities were obtained from the correlation

$$D_{i(mean)} = \frac{(1-X_i)}{\sum_{i=2}^{N}\left(\frac{X_j}{D_{ij}}\right)} \qquad (D.17)$$

D.4 Heat of Reaction

The standard heat of reaction for the six fuels used in the tests are tabulated in Table 14. The reference temperature was taken as 298°K.

D.5 Ambient Gas Properties

The Reynolds number and Prandtl number appearing in the convection correction, Equations (2.50) and (2.51) were evaluated for the ambient gas mixture. The properties appearing in these two dimensionless numbers were determined for a gas mixture of N component as follows:

Table 13

Viscosity Constants and Atomic Diffusion Volumes

Component	C_{12}	C_{13}	(Σv_i)
Methanol	65.00	235.00	29.90
Ethanol	60.00	190.00	50.36
Propanol	60.00	190.00	70.80
Pentane	80.00	125.00	106.26
Heptane	55.00	120.00	147.18
Decane	35.00	50.00	208.56
Carbon Dioxide	152.00	235.00	26.90
Water Vapor	136.00	260.00	12.70
Nitrogen	152.00	235.00	17.90
Oxygen	202.00	273.00	16.60

Table 14

Heats of Reaction

Component	Standard Heat of Reaction (kcal/g-mole)
N-Pentane	782.0
N-Heptane	1075.9
N-Decane	1516.6
Methanol	161.7
Ethanol	305.5
Propanol-1	452.2

Specific Heat

$$C_p = \sum_{i=1}^{N} X_i M_i \, C_{pi} / \sum_{i=1}^{N} X_i M_i \tag{D.20}$$

where

$$C_{pi} = C_{19} + C_{20} T_\infty \quad \text{(cal/gm °K)} \tag{D.21}$$

Viscosity

$$\mu = \sum_{i=1}^{N} X_i \sigma_i \tag{D.22}$$

where

$$\mu_i = C_{21} + C_{22} T_\infty \tag{D.23}$$

Thermal Conductivity

$$\lambda = \sum_{i=1}^{N} X_i \lambda_i \tag{D.24}$$

where

$$\lambda_i = C_{23} + C_{24} T_\infty \tag{D.25}$$

Density

$$\rho = P \sum_{i=1}^{N} X_i M_i / R T_\infty \quad \text{(gm/cc)} \tag{D.26}$$

The constants C_{19} to C_{24} used in the above correlations are tabulated in Table 15.

Table 15

Constants in the Ambient Gas Property Equations

Component	C_{19}	$C_{20} \times 10^{3}$	$C_{21} \times 10^{5}$	$C_{22} \times 10^{8}$	$C_{23} \times 10^{5}$	$C_{24} \times 10^{8}$
N_2	0.282	0.0121	15.2	23.5	3.18	12.32
O_2	0.248	0.0167	20.2	27.3	4.55	13.22
CO_2	0.298	0.0135	15.2	23.5	1.19	13.97
CO	0.292	0.0085	16.3	23.5	3.20	12.82
H_2O	0.583	0.0530	13.6	26.0	-4.74	33.25

APPENDIX E

EXPERIMENTAL RESULTS

Table 16

Experimental Burning Rates for Natural Convection Tests with Fuel Inlet and Ambient Air Temperature of 300°K

Fuel	D_s (cm)	P (atm)	$\dot{m}_F \times 10^2$ (gm/sec)	$X_{O_{2\infty}}$
Methanol	0.64	1.00	0.72	Air
		2.18	0.94	
		10.20	1.43	
		17.35	1.99	
		23.81	2.09	
		28.23	2.14	
		36.74	2.33	
		37.42	2.38	
Methanol	0.95	1.00	0.82	Air
		4.08	2.38	
		8.84	3.10	
		16.24	3.45	
		29.39	4.26	
		32.65	4.91	
		42.18	4.76	
		44.22	5.67	
		61.22	5.74	
		78.23	7.19	
Methanol	1.90	1.00	2.93	Air
		1.70	3.99	
		2.59	4.51	
		2.72	4.49	
		4.08	5.41	
		6.80	6.20	
		12.25	7.92	
		14.97	8.62	
		21.09	9.90	
		27.21	10.56	
		28.23	11.48	
		34.01	12.74	

Table 16 (Continued)

Fuel	D_s (cm)	P (atm)	$\dot{m}_F \times 10^2$ (gm/sec)	$X_{O_{2\infty}}$
Ethanol	0.95	1.00	1.10	Air
		1.76	1.48	
		3.40	1.88	
		4.08	2.28	
		4.76	2.73	
		6.80	3.15	
		8.11	3.28	
		16.32	3.62	
		33.33	7.17	
		41.49	8.31	
		71.42	9.86	
Propanol-1	0.95	1.00	1.34	Air
		1.36	1 42	
		2.17	1.69	
		3.40	1.96	
		4.08	2.03	
		5.44	2.11	
		8.02	2.38	
		11.56	2.57	
		12.92	2.59	
		20.40	3.57	
		27.21	3.82	
		31.97	4.72	
N-Pentane	0.95	1.00	1.83	Air
		1.29	2.22	
		2.72	3.27	
		6.80	3.68	
		13.60	4.42	
		27.21	4.98	
		51.02	5.64	
N-Heptane	0.64	1.00	0.73	Air
		1.50	0.74	
		2.85	1.06	
		5.60	1.35	
		8.20	1.45	
		10.50	1.49	
		14.39	2.52	
		21.77	2.94	

Table 16 (Continued)

Fuel	D_s (cm)	P (atm)	$\dot{m}_F \times 10^2$ (gm/sec)	$X_{O_{2\infty}}$
N-Heptane	0.95	1.09	1.56	Air
		2.04	1.69	
		4.08	2.06	
		8.16	2.66	
		10.88	2.71	
		18.71	3.04	
		27.21	3.57	
		54.42	3.79	
N-Heptane	1.90	1.00	3.94	Air
		1.91	4.53	
		2.38	4.59	
		3.06	5.43	
		4.08	5.66	
		6.12	6.46	
		8.16	8.09	
		9.52	8.29	
		12.93	10.65	
		17.00	13.16	
N-Decane	0.64	1.00	0.49	Air
		1.35	0.57	
		4.08	0.98	
		5.44	1.35	
		8.33	1.38	
		18.37	1.47	
N-Decane	0.95	1.09	1.21	Air
		1.36	1.41	
		2.72	1.96	
		6.26	2.17	
		13.61	3.29	
		32.65	3.98	
N-Decane	1.90	1.00	3.23	Air
		2.04	4.24	
		3.40	4.64	
		5.98	5.38	
		7.48	6.05	
		8.03	6.32	
		8.84	6.32	
		9.52	6.92	
		12.24	7.26	
		12.93	7.64	

Table 17

Experimental Liquid Surface Temperatures for Natural Convection Tests with Fuel Inlet and Ambient Air Temperature of 300°K

Fuel	P (atm)	T_ℓ (°K)	$X_{O_{2\infty}}$
Methanol	1.00	328	Air
	2.04	343	
	6.80	379	
	8.16	387	
	10.88	397	
	12.24	402	
	14.96	411	
	21.76	432	
	38.09	446	
	44.89	460	
	47.61	465	
	61.22	486	
	78.23	497	↓
Ethanol	1.00	341	Air
	2.72	359	
	4.08	372	
	5.44	384	
	6.80	391	
	8.16	397	
	10.84	407	
	13.60	410	
	18.70	415	
	34.01	426	
	48.97	442	
	61.22	453	↓
Propanol-1	1.49	342	Air
	2.04	367	
	3.53	370	
	3.80	389	
	6.80	397	
	7.48	409	
	20.40	447	
	29.53	461	
	43.53	468	↓

Table 17 (Continued)

Fuel	P (atm)	T_ℓ (°K)	$X_{O_{2\infty}}$
N-Pentane	1.00	298	Air
	2.38	337	↓
	3.40	339	
	6.12	341	
	6.80	342	
	9.52	353	
	11.22	356	
	13.60	402	
	20.40	413	
N-Heptane	1.00	360	Air
	2.38	378	↓
	3.06	383	
	5.10	422	
	6.12	436	
	7.48	444	
	8.84	431	
	11.56	448	
	12.92	453	
	13.60	454	
	15.64	475	
	17.00	469	
N-Decane	1.09	432	Air
	1.49	435	↓
	2.38	453	
	3.40	471	
	6.80	480	
	7.48	493	
	9.52	514	
	15.75	540	
	18.72	561	
	24.28	565	

Table 18

Experimental Vaporization Rates for Forced Convection Tests at Atmospheric Pressure

Fuel	T_∞ (°K)	Reynolds Number	$\dot{m}_F \times 10^2$ (gm/sec)	$X_{O_{2\infty}}$
Methanol	610	116	0.32	Evap.
	630	131	0.36	
	790	101	0.46	
	795	142	0.31	
	800	101	0.43	
	845	174	0.66	
	895	152	0.73	
	1090	52	0.85	
	1090	116	1.26	
	1130	112	1.38	
	1160	49	0.99	
	1180	64	1.20	
	1255	119	1.87	
	1270	46	1.46	
	1320	75	1.54	
	1350	141	2.40	
	1480	171	2.71	↓
Methanol	1150	110	2.13	0.095
	1160	55	1.83	
	1310	128	2.29	
	1340	100	2.17	↓
Ethanol	780	106	1.10	Evap.
	795	75	1.08	
	1000	114	1.00	
	1060	110	1.12	
	1230	99	1.63	
	1365	112	2.06	↓
Ethanol	1100	128	1.26	0.095
	1130	166	1.66	
	1265	78	2.04	
	1270	116	1.97	↓
Propanol-1	610	119	0.78	Evap.
	615	155	0.99	
	1045	52	0.62	
	1090	55	1.26	
	1145	82	0.83	↓

Table 18 (Continued)

Fuel	T_∞ (°K)	Reynolds Number	$\dot{m}_F \times 10^2$ (gm/sec)	$X_{O_{2\infty}}$
Propanol-1	1200	79	0.8∠	Evap.
	1265	50	1.52	↓
	1285	57	1.04	
	1310	115	2.19	
	1365	87	1.60	
	1395	92	2.10	
	1530	75	2.87	
Propanol-1	1215	67	1.71	0.095
	1255	54	2.17	↓
	1365	74	2.50	
	1380	97	2.62	
	1380	93	2.70	
	1450	182	3.55	
N-Pentane	980	118	1.00	Evap.
	1090	109	1.95	↓
	1255	99	2.31	
	1035	134	2.23	
	1090	115	2.95	
	1160	111	2.63	
	1255	118	3.55	
N-Heptane	885	71	0.92	Evap.
	910	137	1.16	↓
	1155	87	1.06	
	1200	99	1.46	
	1255	90	1.81	
	1255	115	2.10	
N-Heptane	1090	111	1.69	0.095
	1170	134	2.72	↓
	1245	119	2.86	
	1255	92	2.64	
	1255	79	1.93	
N-Decane	910	75	0.61	Evap.
	920	76	0.54	↓
	1000	152	1.19	
	1030	112	1.29	
	1255	79	1.03	
	1330	104	1.49	
	1365	143	2.03	

Table 18 (Continued)

Fuel	T_∞ (°K)	Reynolds Number	$\dot{m}_F \times 10^2$ (gm/sec)	$X_{O_{2\infty}}$
N-Decane	1130	126	1.42	0.095
	1220	80	1.62	↓
	1310	115	1.59	

Table 19

Experimental Liquid Surface Temperatures for Forced Convection Tests at Atmospheric Pressure

Fuel	T_∞ (°K)	Reynolds Number	T_ℓ (°K)	$X_{O_{2\infty}}$
Ethanol	1000	114	335	Evap.
	1060	110	335	
	1230	99	341	
	1365	112	342	↓
Ethanol	1100	128	343	0.095
	1130	166	343	
	1265	78	344	
	1270	116	345	↓
N-Pentane	795	160	293	Evap.
	820	160	293	
	920	107	294	
	1090	130	299	
	1255	117	303	
	1310	117	306	↓
N-Pentane	1085	86	305	0.095
	1130	127	306	
	1160	111	306	↓

Table 20

High Pressure Experimental Vaporization Rates and Liquid Surface Temperatures for Forced Convection Tests

Fuel	P (atm)	Reynolds Number	$\dot{m}_F \times 10^2$ (gm/sec)	T_ℓ (°K)	$X_{O_{2\infty}}$
		T_∞ = 1255°K			
Ethanol	1.00	99	1.63	335	Evap.
	2.99			361	
	6.80	167	2.16	381	
	6.80	167	2.07	381	
	13.61	312	2.36	395	
	20.40	315	2.74	424	
	27.20	406	2.54	443	
	30.61	416		440	
		T_∞ = 1145°K			
Ethanol	1.00	165	1.66	343	0.095
	1.36	82	1.75	347	
	4.76	145	1.53	381	
	4.76	145	1.67	361	
	6.80	243	2.39	391	
	13.61	325	3.03	399	
	20.40	461	3.15	417	
	27.20	617	3.92	439	
Ethanol	1.00	156	2.05	336	0.130
	7.10	276	3.00	390	
	13.00	437	3.43	418	
	20.40	657	4.50	430	
N-Heptane	1.00	129	1.06	350	Evap.
	1.63	188	2.12		
	2.72	66	1.86	388	
	2.72	188	2.03		
	6.80	236		404	
	6.80	236	2.00		
	13.70	236	2.30		
	13.70	314	2.52		
	14.28	314	2.30	441	
	20.40	448	2.61		
	23.20	534	3.24		
	27.55	640	2.36		
	34.01	672	3.24	486	

Table 20 (Continued)

Fuel	P (atm)	Reynolds Number	$\dot{m}_F \times 10^2$ (gm/sec)	T_ℓ (°K)	$X_{O_{2\infty}}$
		T_∞ = 1145°K			
N-Heptane	1.00	101	1.77	364	0.095
	2.12	188	2.12	372	↓
	3.40	157	3.02	390	
	5.44	251	2.72	413	
	6.80	236	2.03		
	13.61	314	3.16	457	
	14.28	314	3.16	459	
		T_∞ = 1145°K			
N-Heptane	1.00	150	2.52		0.130
	1.00	134	1.53		↓
	2.04	178	2.07	373	
	7.48	267	2.19	413	
	8.75	276	2.26	413	